Models for disordered phonons

Inaugural-Dissertation

zur
Erlangung des Doktorgrades
der Mathematisch-Naturwissenschaftlichen Fakultät
der Universität zu Köln

vorgelegt von
Sebastian E. Schmittner
aus Köln

Köln, 2015

Berichterstatter: Prof. Dr. Martin R. Zirnbauer

Prof. Dr. Alexander Altland

Tag der letzten mündlichen Prüfung: 12.01.2015

Abstract

We introduce novel models for disordered solids at very low temperatures with the goal of representing the physics of disorder causing local random fluctuations in the masses and inter-constituent forces. The basic model that provides the clean limit upon which the other models are built is a variant of the harmonic crystal. Neglecting the difference between longitudinal and transverse vibrational modes, known as *phonons*, we use a large number, n, of phonon bands. All models are constructed within a harmonic approximation for small oscillations about a *stable* ground state. That means that runaway dynamics are excluded, but interactions between phonons are neglected. Disorder is added by way of 14 suitable ensembles of local (hence sparse) random matrices. Each of these ensembles comes with a non-negative variance interpreted as the disorder strength. In principle, any of these disorder types can be combined, hence we obtain a model kit of disordered phonons.

To assess the building blocks in our kit, we study the average density of states in the large-n limit, known as the coherent potential approximation (CPA). It is determined self-consistently by means of illustrative diagrammatic as well as rigorous supersymmetric techniques. The validity of this mean-field type approximation in three dimensions is verified by comparison with exact numerical diagonalisation.

Two of our elementary models, one with pair potential (or "spring constant") and one with mass disorder, are particularly interesting. The model with strong spring constant and weak mass fluctuations is microscopically well motivated and leads to a phase transition (at finite disorder strength). A critical point terminates the weak-disorder (or Debye) phase, above which a strong-disorder phase is discovered. This novel phase features a finite density of states at zero energy. The two-parameter space of models combining both of these disorder types is called *interfering mass and spring constant disorder* (IMSC) model. Unlike the widely used two-level tunnelling system (TTLS) model, we do not make any *a priori* assumption about a finite density of scatterers at low energies. Hence we show that disorder alone is, in principle, sufficient to explain the experimental finding of the heat capacity of vitreous systems varying linearly with temperature below about 1 K, first observed in 1971.

The new strong-disorder phase is stable under the addition of most of the other disorder types. Assuming that the IMSC model is renormalisable and that critical points of the renormalisation group (RG) flow are correctly identified from the CPA, we predict a tentative RG flow diagram. Under these assumptions, the novel phase is also stable under the RG flow.

Kurzzusammenfassung

Wir konstruieren im Rahmen dieser Arbeit neuartige Modelle für ungeordnete Festkörper bei sehr tiefen Temperaturen. Diese beschreiben harmonische Schwingungen um einen *stabilen* Grundzustand, deren Normalmoden als *Phononen* quantisieren. Stabilität bedeutet hier, dass anfänglich kleine Auslenkungen aus der Gleichgewichtslage unter Zeitentwicklung klein bleiben, was eine notwendige Voraussetzung für die Vernachlässigung der Wechselwirkungen zwischen Phononen ist. Das zugrundeliegende Modell des harmonischen Kristalls stellt den sauberen Grenzfall verschwindender Unordnung in allen Modellen dar. Wir vernachlässigen den Unterschied zwischen longitudinalen und transversalen Schwingungsmoden und verallgemeinern den harmonischen Kristall zu einem Modell mit einer beliebigen Anzahl, n, lokaler Moden, resultierend in n Phononen-Bändern. Es werden 14 verschiedene Ensembles lokaler Zufallsmatrizen zur Modellierung der Unordnung benutzt, jedes mit einer nicht negativen Varianz (Unordnungsstärke). Durch Unordnung verursachte lokale Fluktuationen in den Massen und in den harmonischen Kräften werden durch diese Zufallsvariablen möglichst wirklichkeitsnah in die Modelle einbezogen. Alle Unordnungstypen in diesem Modellbaukasten ungeordneter Phononen können beliebig kombiniert werde.

Um die einzelnen Modelle hinsichtlich ihrer Realitätsnähe und Vorhersagekraft zu bewerten berechnen wir die Zustandsdichte asymptotische für große n. Dies entspricht einer als "*coherent potential approximation*" (CPA) bekannten Näherung. Die Berechnung mittels anschaulicher Diagrammatik liefert die selben Ergebnisse wie die rigorose supersymmetrische Methode. Die Anwendbarkeit der CPA in drei Dimensionen wird durch den Vergleich mit exakter Diagonalisierung verifiziert.

Besonders interessant ist ein Modell, dass schwache Unordnung in den Massen mit starker Unordnung in den Kräften kombiniert. Dieses Modell ist mikroskopisch gut motiviert und führen zu einem (Quanten-)Phasenübergang bei endlicher Unordnungsstärke. Die (Debye) Phase schwacher Unordnung endet an einem kritischen Punkt und bei stärkerer Unordnung finden wir eine neuartige Phase mit einer endlichen und positiven Zustandsdichte bei beliebig kleiner Energie. Anders als das weit verbreitete zwei-Level Systeme (TTLS) Modell wird eine positive Zustandsdichte an Streuzentren bei kleinen Energien in unserem Modell *nicht* von vornherein angenommen. Wir können somit zeigen, dass Unordnung prinzipiell ohne Weiteres ausreicht um die experimentell erstmals 1971 beobachtete lineare Temperaturabhängigkeit der Wärmekapazität amorpher Festkörper bei Temperaturen unterhalb von etwa 1 K zu erklären.

Die neue Phase starker Unordnung ist stabil unter Hinzunahme der meisten anderen Unordnungstypen. Unter Annahme der Renormierbarkeit und korrekt identifizierter kritischer Punkte treffen wir eine vorläufige Vorhersage für den Renormierungsgruppenfluss, welcher die neue Phase ebenfalls stabilisiert.

Contents

1 Introduction

1.1 Outline

This thesis is organised as follows. In the present Chapter 1, we review the relevant experimental findings as well as some existing models in order to motivate the construction of novel models for vitreous solids at low temperatures, or more specifically for disordered phonons. In Section 1.3 we review the harmonic crystal as the standard model of phonons in a not quite standard form. This is the basic deterministic model which we augment by disorder. In Section 1.5, we elaborate on bosonic random matrix models and in particular on stability. We consider this aspect as very important even though it has often been neglected in the literature.

In Chapter 2, we introduce most of our model classes, i.e. give the details of how the random matrix ensembles are constructed. The structural distinction between *additive* and *interfering* disorder is introduced in Section 2.1 before coming to the physical distinction between disorder of different types in the mass and spring sector in Section 2.2. We then explain the general idea of the diagrammatics to be used and settle our notation by deriving the self-consistency equations (SCE) for the case of additive disorder in Section 2.3. In Section 2.4, we immediately elaborate on our results for the average density of eigenfrequencies (DOS) in the coherent potential approximation (CPA, explained in Section 1.5.3) for the mass, spring length, and pinning disorder models in the additive as well as the interfering variant. The derivation of the SCE for the interfering models is postponed to Section 2.7 for pedagogical reasons. We highlight the interfering mass disorder model, which is the first one to feature the strong disorder phase with positive DOS at zero frequency, discussed in Section 2.4.2b.

The model building continues with a brief discussion of the class of *band mixing* disorder models before coming to the *spring constant* disorder models in Section 2.6. In particular, Section 2.6.2 is devoted to the interfering spring constant disorder model, which we consider as the summit of our disordered phonon model kit. This is the counter part to the interfering mass disorder model in that for strong spring and weak mass disorder it is microscopically better motivated but still features the strong-disorder phase.

In Chapter 3 we first introduce the remaining model classes. These are the time-reversal invariance breaking models, discussed in Section 3.1, as well as the models that implement spring length disorder without introducing pinning, studied in Section 3.2. Supersymmetry is used to derive the relevant self-consistency (or saddle-point)

equations describing the DOS of these new models as well as of some of the afore mentioned models. In particular, we compare the SCE derived by different techniques in Chapter 3, Chapter 2 and in [SZ10] to show that the different methods yield the same results. The detailed description of the supersymmetry techniques, in particular the Hubbard-Stratonovich transformation following [Zir98], are given in Section 3.3 after the discussion of the results. Chapter 4 contains an extensive summary and outlook.

1.2 Motivation

Starting with its discovery in 1971, the anomalous behaviour of strongly disordered, so-called vitreous or glassy, solids at low temperatures has been the subject of extensive experimental study, see [ZP71] for the seminal paper, [Ste73, Ste76] for more extensive experimental results and [TRV02, PLT02, HRK$^+$12] for some more recent experimental results and review. The power laws for the specific heat capacity, C, and the heat conductivity, Λ, as functions of the temperature at very low temperatures ($< 1\,\mathrm{K}$) show a striking universality. The very same laws are found in materials ranging from disordered crystals over a plethora of chemically different glasses to complex systems such as polymers. The essential observations are: a linear temperature dependence of C and a (roughly) quadratic temperature dependence of Λ to leading order in the temperature.

Our goal is to find a model for disordered solids which is generic enough to potentially explain these universal observations. Nevertheless, we will exclusively calculate the temperature dependence of the specific heat and use this one as the primary indicator for whether our models are in the right universality class. We will therefore compute the density of states of our models. As explained in Section 1.3.4, a density of states following a power law, $\rho \propto E^{\chi-1}$ for some $\chi \in \mathbb{R}$ to leading order in low energy, E, leads to the specific heat following a law with power increased by one, $C \propto T^{\chi}$. With this in mind, typical data plots showing C/T can be read as depicting directly the density of states, up to scale. For examples, see Figure 6 and 8 in [Ste76] and Figure 4 in [Ste73], which have been reproduced in Figure 1.1 for the convenience of the reader. The most prominent feature in these plots is $\rho \propto C/T > 0$ at $T = 0$.

To appreciate why these experimental findings are surprising, or "anomalous", we review the "normal" crystal in Section 1.3. In this so-called harmonic crystal model for lattice vibrations, the density of states follows $\rho(E) \propto E^{d-1}$ to leading order (known as the Debye approximation) in d dimensions. This means that one expects to find the heat capacity to scale like $C \propto T^3$ in experiments on 3-dimensional systems, as is indeed the case for clean crystals.

Notwithstanding some models which have been proposed for their explanation, the striking universality of the above-mentioned abnormal power laws in amorphous solids

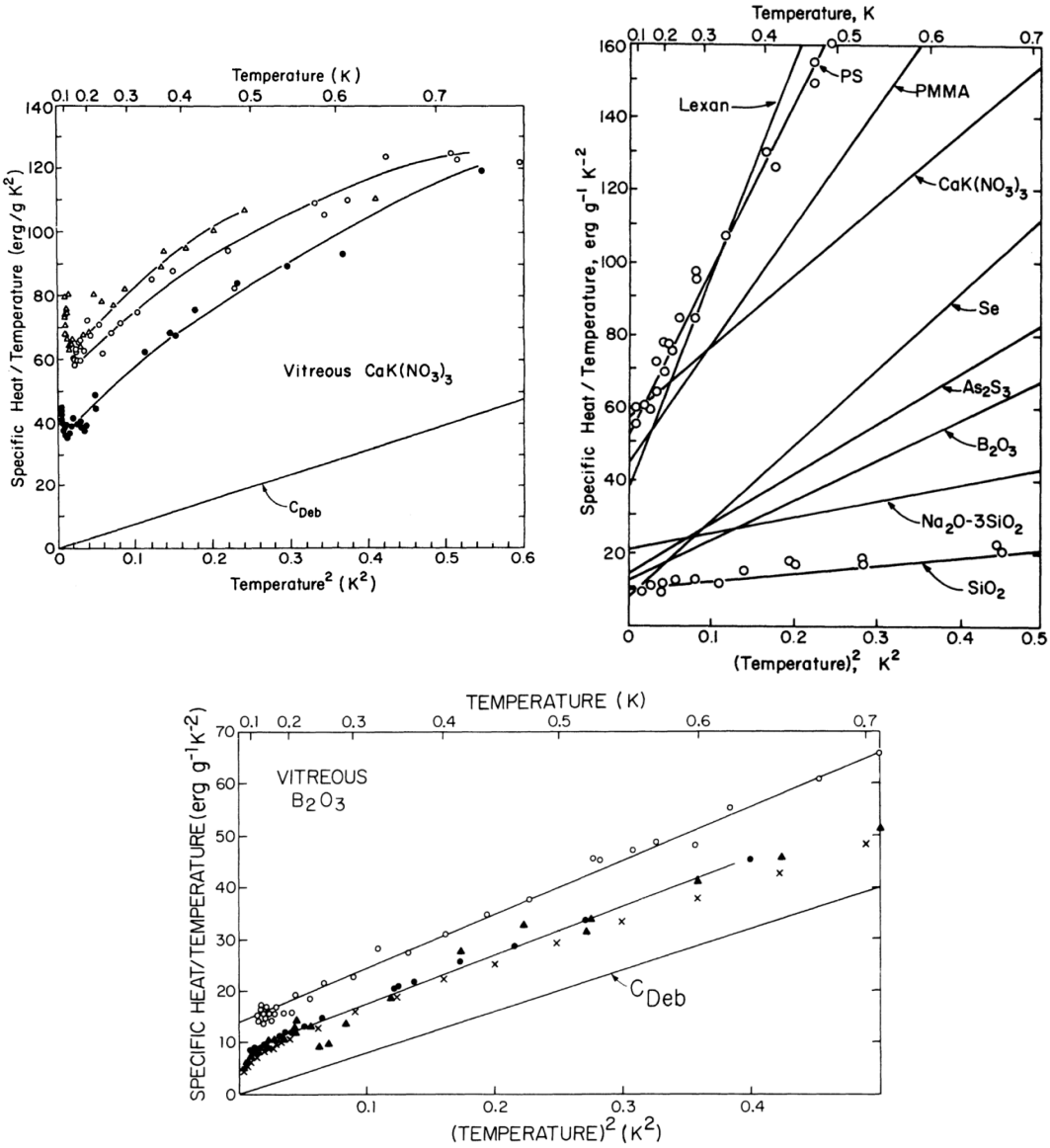

Figure 1.1: Comparison of specific heat divided by temperature for various samples of vitreous materials and the prediction of the Debye model. Notice the trend towards a finite value at zero temperature in the experimental data.[ab]

[a]Reprinted figures with permission from R. Stephens, Physical Review B, 13, 852, 1976. Copyright (1976) by the American Physical Society.

[b]Reprinted figure with permission from R. Stephens, Physical Review B, 8, 2896, 1973. Copyright (1973) by the American Physical Society.

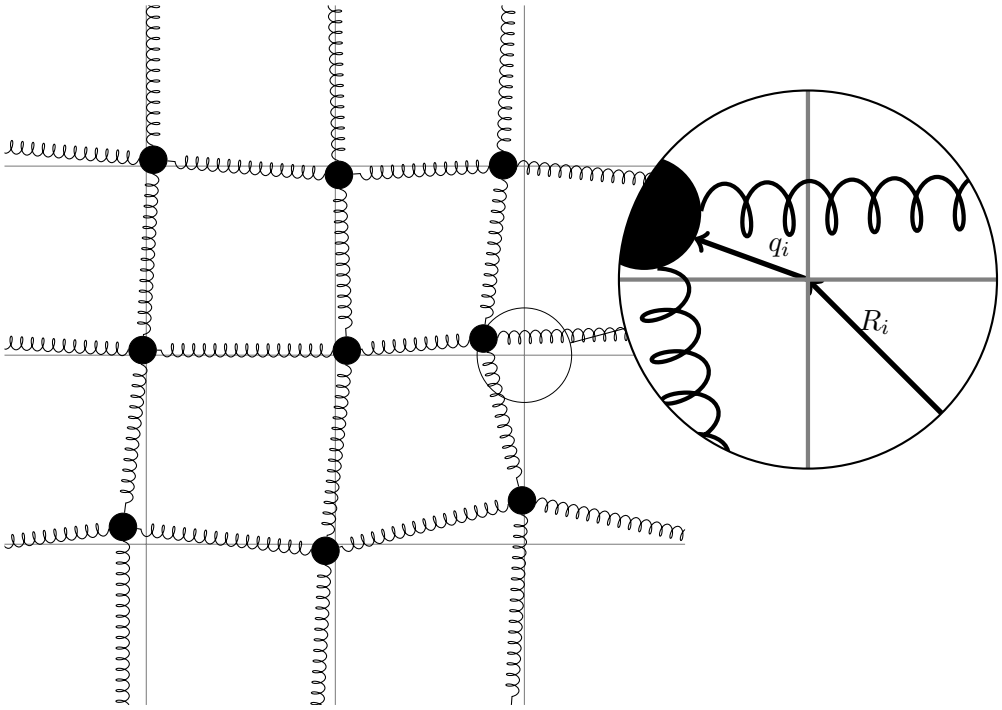

Figure 1.2: Schematic picture of the harmonic crystal as a model of masses and springs.

is "poorly understood", according to e.g. [FA86, PLT02, LV13]. In Section 1.4 we will review some of those models, in particular the most widely used tunnelling two level systems (TTLS) model.

1.3 Non-interacting phonons

In this section we review a deterministic model of a solid which is usually called the *harmonic crystal* in standard text books (see e.g. [JM73] or [AM76]). Its elementary excitations describe vibrations and quantise as bosons, called *phonons*. The phrase *harmonic* is used to stress that we do not take interactions between phonons into account. More precisely speaking, a harmonic Hamiltonian is of second order in positions and momenta (or equivalently in creation and annihilation operators) and hence the equations of motion are linear. In this sense, *all* models considered in this thesis are harmonic. The translation-invariant *crystal* described in this section will serve as the clean limit for all disordered systems constructed in this thesis.

The general idea is that the constituents (atoms or molecules) forming our solid are replaced by point masses and the inter-constituent forces are only treated in the

harmonic approximation. Hence the pair potential is specified by two parameters, the distance at which a pair of constituents rests force-free and the strength of the restoring force. At this level, the model becomes one of masses and springs, see Figure 1.2. Throughout, we will use this metaphor of springs to describe the pair potentials.

1.3.1 Harmonic crystal

For concreteness, we choose the *cubic lattice* of total side length $L \in \mathbb{N}$ in d dimensions with *periodic boundary conditions* as the spatial structure underlying our model. Although such "primitive cubic" crystals do exist in nature (e.g. sodium chloride), our main interest is in universal aspects rather than in modelling a concrete material.

The sites of the lattice and the directed links are denoted by[1]

$$\begin{aligned} C_0 &:= \mathbb{Z}^d / L\mathbb{Z}^d \\ \text{and } C_1 &:= \{(i, i+e_j) \in C_0^2 \,|\, j \in \{1, \dots, d\}\}, \end{aligned} \tag{1.1}$$

respectively, where e_j denotes the lattice vector in direction[2] j. While C_0 and C_1 specify the topology of the lattice, which we will keep fixed, the geometry can be encoded into an embedding $R : C_0 \hookrightarrow \mathbb{R}^d/(La)\mathbb{Z}^d$ (inducing an embedding of C_1), where a denotes the lattice spacing. In later sections, we set $a = 1$, i.e. the embedding to be the trivial one.

Rephrasing the last paragraph in less mathematical terms, we denote the equilibrium position of the mass at site $i \in C_0$ by $R_i \in \mathbb{R}^d$ and directed links between these positions by $R_{i,j} := R_i - R_j$. The elementary degrees of freedom of our models are the local displacements of each mass from its equilibrium position, denoted by $q_i \in \mathbb{R}^d$. Hence the actual positions of the masses are given by $Q_i := R_i + q_i$ as shown in Figure 1.2. To derive the Hamiltonian from this schematic picture, recall that Hooke's law for springs with spring constants $\kappa_{i,j}$ and relaxed lengths $l_{i,j}$ states that the potential energy of any configuration of the masses is to leading order in q given by

$$\sum_{(i,j)\in C_1} \frac{\kappa_{i,j}}{2} \left(|Q_i - Q_j| - l_{i,j}\right)^2 \tag{1.2a}$$

$$= \sum_{(i,j)\in C_1} \frac{\kappa_{i,j}}{2} \left(\left(|R_{i,j}| - l_{i,j}\right)^2 + 2\left(|R_{i,j}| - l_{i,j}\right) \frac{(q_i - q_j)\cdot R_{i,j}}{|R_{i,j}|} \right) \tag{1.2b}$$

$$+ \sum_{(i,j)\in C_1} \frac{\kappa_{i,j}}{2} \left(\frac{l_{i,j}}{|R_{i,j}|} \left(\frac{(q_i - q_j)\cdot R_{i,j}}{|R_{i,j}|} \right)^2 + \frac{|R_{i,j}| - l_{i,j}}{|R_{i,j}|} \left(q_i - q_j\right)^2 \right) . \tag{1.2c}$$

[1] Notice that C_0 and C_1 denote the *sets* of sites or links. The vector spaces to be associated with them are more complicated than the spaces of chains that are usually considered in algebraic geometry, hence we refrain from using that language here.

[2] Here the choice of the overall direction, $\pm e_j$, does not matter, what matters from Section 2.1.1 on is a consistent orientation of all links pointing in one direction.

If all $l_{i,j} = |R_{i,j}|$ then, in equilibrium, all springs are relaxed and oscillations in a given direction only couple to the neighbours in that direction. We call this model the *relaxed harmonic crystal*. Whilst looking very natural for the cubic lattice of masses and springs of equal length and strength, depicted in Figure 1.2, this model is unlikely to be the optimal one for describing a real solid. The feature of decoupled oscillations in different dimensions is rather special for the cubic lattice restricted to nearest neighbour interactions, which we only use for simplicity and do not consider as fundamental. Furthermore, a very small amount of disorder in κ and/or l (or even structural disorder) will almost surely rule out the relaxed crystal model, as each $l_{i,j}$ would need to be adapted to the equilibrium positions, which in turn depend on all other parameters.

Instead, we should generically expect $l_{i,j} \neq |R_{i,j}|$ in equilibrium, i.e. at least some of the springs are stretched or compressed. In this case, we can see in Equation (1.2b) that there is potential energy stored in these springs and each of them pulls or pushes its masses with some force. However, by the definition of equilibrium, these forces at each mass cancel, hence the overall sum in Equation (1.2b) is zero. In our periodic system, effectively living on a torus, it is easy to imagine that there can be an overall tension, since the crystal cannot contract. Also in the realistic situation of a real disordered crystal or glass, we should expect local stress and strain.

The opposite extreme to the relaxed crystal is given by $l_{i,j} = 0$. Here the inter-constituent forces are purely attractive. We will call this limit the *stressed harmonic crystal*. This model neglects the difference between transverse and longitudinal waves completely and hence is not perfectly realistic either. However, it is at least stable under spring constants disorder. It also has the appealing feature that the degrees of freedom are completely unrelated to dimensions. More concretely, every q_i^k is coupled to every neighbour q_j^k with the same coupling strength, independent of the direction of $R_{i,j}$. For simplicity, we will use this stressed crystal with its enhanced symmetry as the deterministic limit of all models and hence neglect the difference between longitudinal and transverse waves. We believe that this model is sufficient to capture the relevant physics, at least when it is assigned the role of the deterministic part in a strongly disordered situation or used for the Debye approximation of the clean case. We explicitly verify in Chapter 3 that spring length disorder of any strength does not change the mean-field density of states.

We would like to stress that the fundamental degrees of freedom are the *small* displacements from the equilibrium positions q_i, which justifies the harmonic approximation if the dynamics is stable. Although Equation (1.2) for $l_{i,j} = 0$ might look like one could use the absolute positions Q_i, just as well, this is a particularity of the stressed crystal model which has no universal significance.

1.3.2 Phonons

Since the crystal is invariant under discrete translations, we use Fourier transform in Equation (1.10) to obtain its eigenmodes, their quanta being called *phonons*. As mentioned above, the stressed harmonic crystal model can be easily generalised to feature any number $n \in \mathbb{N}$ of degrees of freedom per site, leading to n phonon bands and $N = nL^d$ degrees of freedom in total.[3] For the relaxed crystal model only $n = d$ (or a multiple thereof) would be realistic. The full Hamiltonian of the stressed harmonic crystal is given by

$$H = \sum_{b=1}^{n} \left(\sum_{i \in C_0} \frac{p_{i,b}^2}{2\mu} + \frac{1}{2}\kappa \sum_{(i,j)\in C_1} (q_{i,b} - q_{j,b})^2 \right) = \frac{1}{2}(q,p)h \begin{pmatrix} q \\ p \end{pmatrix} , \tag{1.3}$$

which is a quadratic form on the symplectic phase space,

$$V := V_s \oplus V_m \simeq \mathbb{R}^{2N} . \tag{1.4}$$

Here the $q_{i,b}$ and $p_{i,b}$ are linear coordinates dual to bases of V_s and V_m, respectively. Physically, expressed in quantum mechanical terms, V_s and V_m are spanned by the position and momentum operators, respectively. Those bases are fixed throughout. The parameters of the model are the effective mass, $\mu > 0$, and the spring constant, $\kappa > 0$. The geometric mean $\nu := \sqrt{\kappa/\mu}$ is known as the speed of sound which is the relevant scale for the eigenfrequencies.

In Chapter 2 we will introduce random coupling between the bands and we will study the $n \to \infty$ limit, which leads to the coherent potential approximation (CPA). By construction, the deterministic part does not couple bands and thus the clean density of states is not affected by this limit up to a trivial rescaling. As in Equation (1.3), we denote the matrix of H by

$$h = h_0 = \begin{pmatrix} -\kappa\Delta \otimes \mathbf{1}_n & 0 \\ 0 & \mu^{-1}\mathbf{1}_{L^d} \otimes \mathbf{1}_n \end{pmatrix} =: \begin{pmatrix} S_0 & 0 \\ 0 & M_0 \end{pmatrix} \tag{1.5}$$

where Δ is the standard lattice Laplacian with all diagonal matrix elements equal to $-2d$ and the off-diagonal matrix element between every pair of neighbouring sites equal to $+1$. Thus Δ is local in real space and diagonal in Fourier (or "momentum") space[4] with spectrum

$$\Delta_k = 2\sum_{i=1}^{d} \cos(k_i) - 2d = -|k|^2 + O\left(|k|^4\right) . \tag{1.6}$$

[3] We neither explain nor use general band theory, for which the reader may consult e.g. [AM76].

[4] The Fourier space dual to the underlying lattice C_0^* is not to be confused with the momentum sector V_m of the phase space.

As usual, momentum space is given by the dual lattice C_0^*, which is parametrised by $k \in [0, 2\pi/a)^d \cap \left(2\pi/(aL)\,\mathbb{Z}^d\right)$ above. In the infinite volume limit, $L \to \infty$, at constant lattice spacing, $a = 1$, momentum space is a torus parametrised by $k \in [0, 2\pi)^d$.

The equations of motion are Hamilton's equations given by the commutation relations of q and p with H, i.e. time evolution is generated by $X = Jh$ via

$$\partial_t \begin{pmatrix} q \\ p \end{pmatrix} = X \begin{pmatrix} q \\ p \end{pmatrix} , \tag{1.7}$$

where here and throughout

$$J := i\sigma_2 \otimes \mathbf{1}_N = \begin{pmatrix} 0 & \mathbf{1}_N \\ -\mathbf{1}_N & 0 \end{pmatrix} \tag{1.8}$$

denotes the symplectic unit. We stress that it is the spectrum of X (which is the same as that of $\sqrt{-M_0 S_0}$) rather than that of h which defines the eigenfrequencies of the normal modes. This becomes explicit by bringing H to harmonic oscillator form, i.e. by applying a Fourier transformation and introducing creation and annihilation operators:

$$a_k = \sqrt{\frac{m\omega_k}{2}} \left(q_k + \frac{i}{m\omega_k} p_k \right), \quad a_k^\dagger = \sqrt{\frac{m\omega_k}{2}} \left(q_{-k} - \frac{i}{m\omega_k} p_{-k} \right) \tag{1.9}$$

$$\Rightarrow H = \sum_k \frac{p_k p_{-k}}{2m} - \frac{1}{2} m\nu^2 \Delta_k \, q_k q_{-k} = \sum_k \frac{\omega_k}{2} \left(a_k^\dagger a_k + a_k a_k^\dagger \right) . \tag{1.10}$$

Here $\omega_k^2 = -\nu^2 \Delta_k$ are the eigenvalues of $M_0 S_0$. As explained in Section 1.5, it is very important to maintain the positivity of M and S when disorder is introduced, because this positivity is equivalent to the equations of motion (1.7) being Lyapunov-stable. If that was not the case, dynamics would run away to large values of our fields and the harmonic approximation would break down.

1.3.3 Debye approximation

The density of eigenfrequencies (DOS), $\rho(\omega)$, of the harmonic crystal is computed from the Green's function, $g(z)$, by

$$\rho(\omega) = \frac{1}{\pi} \lim_{\epsilon \searrow 0} \Re \left(g(\epsilon + i\omega) \right) , \tag{1.11}$$

$$g(z) = \int\limits_{[0,2\pi]^d} \frac{d^d k}{(2\pi)^d} \frac{z}{z^2 - \nu^2 \Delta(k)} . \tag{1.12}$$

Notice that the DOS is obtained from the *real* part of the Green's function for z approaching the cut on the *imaginary* axis, since the spectrum of X is purely imaginary. We derive the well-known result (1.12) along the way in Chapter 2. In one dimension, this integral can be calculated exactly (see Appendix A.1.1). We get

$$\rho(\omega) = \frac{1}{\pi\sqrt{4\nu^2 - \omega^2}}\,. \tag{1.13}$$

In higher dimensions more van Hove singularities [Van53] arise, which render the integral (1.12) intractable. Since these singularities are irrelevant for the low-energy properties, we neglect them in the following and replace the full lattice Laplacian by its Debye approximation, as indicated by the second equality sign in Equation (1.6). On the level of the density of eigenfrequencies, this approximation amounts to $\rho_{Debye}(\omega) \propto \omega^{d-1}\Theta(\nu\Omega - \omega)$ with appropriately chosen proportionality constant and wave number cutoff Ω such that ρ_{Debye} is normalised and resembles the full density of eigenfrequencies, ρ, to leading order in ω. A derivation is given in Appendix A.1.

1.3.4 Heat capacity

For all our models, we calculate the average density of eigenfrequencies, $\rho(\omega)$, which is directly related to the heat capacity. In a system of units with $\hbar = 1$ (which we are using throughout), the internal energy is given by

$$U = \int \rho(E)\left(e^{\frac{E}{kT}} - 1\right)^{-1} E dE\,. \tag{1.14}$$

Using $\rho(\omega) \propto \omega^{\chi-1}$ this leads to the specific heat following a power law, $C = \partial_T U \propto T^{\chi}$. For the clean system, we have $\chi = d$ as calculated in Equation (A.4d), consequently $C \propto T^3$ is expected for the harmonic crystal in three dimensions. This is indeed found to be the case in real crystals of sufficient purity. However, as mentioned in Section 1.2, strongly disordered solids behave in a markedly different way.

1.4 Existing models

1.4.1 Two level systems (TLS)

Already in 1972, Anderson, Halperin and Varma [AHV72] and Phillips [Phi72, Phi87] proposed a model of tunnelling two level systems (TTLS). This model received quite some attention ever since its discovery and is the most widely accepted explanation of the above, mentioned universal features of vitreous solids at very low temperatures.

The existence and in particular a finite density of states at zero energy of such TTLS is assumed *ad hoc*. Under some further assumptions about how phonons scatter from these TTLS, which were criticised to be unrealistic by [Ste76], the experimentally

found heat conductivity is explained. Although there have been many proposals for the microscopic origin and nature of the TTLS, see e.g. [Par94, SS09, LW03, Tur04], no clear consensus could be reached so far. In particular the "tunnelling" nature of the model and the explanatory power of more general "two level systems" beyond a phenomenological description have been challenged by [LV13]. Therein, the authors explicitly ask for a random matrix model of disorder to be coupled to the harmonic crystal model as a "convenient point of comparison" to the well established TTLS model. In this thesis, we construct models to provide exactly such a point of comparison.

1.4.2 Beyond TLS

The paper which we found to put forward ideas closest to ours is [JSS83]. There, a continuum version of the harmonic crystal is considered with the masses being random variables. The distribution of masses is unbounded (Gaussian) and therefore the ensemble contains realisations with negative masses with non-zero probability. The authors argue, based on a field theory, that this problem is irrelevant, i.e. a bounded distribution would not change their findings. In this thesis, we pay careful attention to only use stable models, as explained in Section 1.5. In particular, negative masses are forbidden. We do discuss models which are rather close to [JSS83], namely the additive mass disorder model in Section 2.4.1 and the interfering mass disorder model at weak disorder strength in Section 2.4.2, for which we can confirm their qualitative findings for the density of states. However, we found that mass disorder does not lead to a phase transition as long as the standard deviation of the *inverse* mass is smaller than the mean. Hence these model classes are precisely not the once which feature a transition to the strong-disorder phase discovered in our work.

In [CKR$^+$10] binary mass disorder is introduced into the harmonic crystal. That is, two different masses are placed at random on half of the sites of the lattice each. This model ensures that masses are positive and it is likely closer to the actual microscopical situation in certain experiments than our model for the mass disorder. The authors find numerically that the model stays in the Debye phase, i.e. the leading order power law of the density of states remains unchanged. This again fits to our observation of mass disorder not being the relevant type of disorder to drive the phase transition, unless it is allowed to fluctuate to extremely large local masses with high probability.

To our knowledge, so far no random matrix models have been considered which guarantee every realisation to be stable while at the same time including strong disorder for either the *inverse* mass or, with better physical motivation, for the spring constants. A notable exception is given by [LSZ06], which is a purely random and zero dimensional model. We will rediscover the latter as the random matrix limit of some of our models.

1.5 Random matrix theory

Instead of adding some "scatterers", such as TLS, to the harmonic crystal model, we will introduce disorder in the form of random matrices that modify the local couplings, i.e. masses and springs. In general, the term *random matrix* refers to a matrix which has random variables with some joint probability distribution as its matrix entries. We will not give an introduction to this subject here but refer to [ABDF11] for a broad and comprehensive overview of random matrix theory and in particular its applications to disordered metals. The application of random matrix theory to bosonic systems needs some extra care as compared to the well studied fermionic case. This was realised and a prototypical ensemble for disordered bosons was implemented in [LSZ06]. In this section, we review their ideas.

1.5.1 Positive cone of bosonic random matrix theory

The well known random matrix ensembles, such as the Gaussian ensembles, are usually used to produce the matrix of the single-particle Hamiltonian. So it might not be obvious why many-particle aspects like the exchange statistics need to be taken into account at all. The fundamental difference between bosons and fermions is that the transformations that preserve the anti-commutation relations for fermions form the (compact) orthogonal group, as opposed to the symplectic group of Bogoliubov transformations that preserve the bosonic commutation relations. The fermionic system is hence quite forgiving in the sense that any real symmetric matrix, h, of a bi-linear form can be diagonalised by acting with an orthogonal matrix g by $h \mapsto g^T h g = g^{-1} h g$. Furthermore, this action preserves the eigenvalues of h. It follows that one can use any ensemble of real symmetric matrices and directly compute the average eigenvalue density for a fermionic system with these single-particle Hamiltonians. Even negative eigenvalues do not spoil the underlying many-particle picture. Due to the Pauli principle, the many-particle Hamiltonian of a finite system of fermions is always bounded below and therefore positive up to a trivial shift in energy.

The situation for bosons is completely different. The symplectic group also acts on the matrix h of the Hamiltonian by $h \mapsto g^T h g \neq g^{-1} h g$. However, diagonalisability by this action is a non-trivial property and eigenvalues are not preserved.[5] In Section 1.3.2, we explain that one should consider the generator of time evolution $X = Jh$ as fundamental. Throughout, $J = i\sigma_2 \otimes \mathbf{1}$ denotes the symplectic unit. The spectrum of X, rather than the one of h, determines the eigenfrequencies of the decoupled harmonic oscillators as explained in Section 1.3.2, if one can bring X to harmonic oscillator form in the first place. It is of crucial importance that the eigenvalues of X are purely

[5] Notice that, although one can change to a basis of creation and annihilation operators as in Equation (1.10), it is still the (now twisted) symplectic group that acts and the argument above remains untouched.

imaginary for the time evolution to be stable. That means initially small displacements have to stay small under time evolution for the harmonic approximation to be justified. Or, in more physical terms, the eigenfrequencies, ω_i, necessarily need to be real for the system to oscillate instead of running away.

To provide a more geometric view on the space of admissible Hamiltonians for bosonic systems, denote the real symplectic group of Bogoliubov transformations over $\mathbb{R}^{2N}$ by $\mathrm{Sp} = \{g^{-1} = Jg^T J^{-1}\}$. It is a physical requirement that h be real symmetric and positive in order to provide a matrix of a bilinear form which leads to stable classical dynamics. In fact, these features are already sufficient for symplectic diagonalisablity.

More precisely, for all $h = h^T > 0$ there exist (unique up to ordering) eigenfrequencies $\omega \in (\mathbb{R}^+)^N$ and a $g \in \mathrm{Sp}(2N)$ such that $g^T h g = \Omega(\omega) := \mathrm{diag}(\omega_1, \ldots, \omega_N, \omega_1, \ldots, \omega_N)$. In physical terms, this means that we can change to a basis of quasi-particles for which the Hamiltonian is in harmonic oscillator form, $H = \sum_i \omega_i/2(a_i^\dagger a_i + a_i a_i^\dagger)$. More precisely,

$$[X, \mathrm{Ad}(J)(X)^T] = 0 \Rightarrow \exists g \in \mathrm{Sp} : g^{-1} X g = \begin{pmatrix} 0 & \mathrm{diag}(\omega) \\ -\mathrm{diag}(\omega) & 0 \end{pmatrix} \in \mathfrak{t}, \quad (1.15)$$

where $\mathfrak{t}$ denotes the standard Cartan subalgebra of $\mathfrak{sp}(2N) = \left\{x = -Jx^T J^{-1}\right\}$. Since $J \in \mathfrak{sp}$, this means that $g^T h g$ is indeed diagonal and positivity of h is preserved.

Now we have arrived at the geometrical picture of a positive cone, $\mathcal{E}$, of admissible time evolution generators:

$$X \in \mathcal{E} := \mathrm{Ad}(\mathrm{Sp}(2N)) \left(J\Omega\left((\mathbb{R}^+)^N\right)\right) \subset \mathfrak{sp}(2N)$$

within the symplectic Lie algebra $\mathfrak{sp}(2N)$. All realisations of time evolution generators drawn from ensembles constructed in this thesis lie in $\mathcal{E}$ in order to avoid runaway dynamics and to ensure the existence of a stable ground state.

1.5.2 Construction of ensembles

Since we have just established that taking h to be symmetric and positive ensures $X = Jh \in \mathcal{E}$, it is natural to write the former as a square. This is the essential idea of [LSZ06], where a Wishart ensemble was used for $h = R^T R$. An interesting point, which we make use of in Chapter 2, is that R might be non-square, i.e. we have the freedom to introduce an auxiliary Euclidean space, $W \simeq \mathbb{R}^{2(1+\alpha)N}$ for some $\alpha \geq 0$, to which R is mapping.

The pure random matrix model, without deterministic terms or an underlying lattice structure, with $\alpha = 0 + O(1/N)$, and broken time-reversal invariance, has been extensively studied in [LSZ06] and [Lüc09]. Using supersymmetry as well as

orthogonal polynomials, all correlation functions have been computed. The density of eigenfrequencies of this model has a $\rho \propto \omega^{-1/3}$ divergence for small ω, which is not compatible with the experimentally observed linear dependence of the heat capacity on temperature.

Thus it is our goal to construct more realistic models in order to explain the experimental results. To this end, we start from the clean harmonic crystal and do *not* add a full $2N$ by $2N$ random matrix, which would couple all degrees of freedom without accounting for their spatial distance. Instead we use *local* random matrix couplings of size of order $2n$ by $2n$. That means that the random matrices used in this thesis are very sparse, just as the matrix of the clean system h_0.

1.5.3 Coherent potential approximation

The coherent potential approximation (CPA), as introduced by [Sov67] and reviewed by e.g. [YM73], is an approximation of the average Green's function of self-consistent mean-field type. This means that fluctuating quantities, such as the random mass and springs matrices, are replaced by so-called *coherent* matrices which are constant in space but complex valued and energy dependent. Their value as a function of energy is determined by one or more so-called *self-consistency equations* (SCE).

As recognised by [Weg79], the average Green's function of certain n-orbital models is to leading order in $n \to \infty$ the same as the CPA average Green's function for $n = 1$. This version of the CPA is particularly well suited for the application to random matrix models. Furthermore, it is controlled by a large parameter which in principle makes it possible to calculate corrections to the leading order behaviour.

We use this approximation in the following, where n was already introduced to be the number of degrees of freedom per site, i.e. as the number of (phonon) bands. Although we do not calculate sub-leading terms in n, we compare our density of states to the one obtained by exact diagonalisation of finite-size matrices at $n = d$ to verify that the CPA results are accurate (see Section 2.4.2c).

2 Models

In this chapter, we introduce a number of models. To guide the reader through the gallery, we give an overview over the 4 physically distinct types of disorder that we are going to add to the harmonic crystal model, namely *mass*, *spring constant*, *spring length disorder*, and *random pinning* in Section 2.2. We have developed a (to our knowledge novel) way of implementing the disorder, which we call *interfering*. All types of disorder can either be implemented in the more standard way, which we call *additive*, or as interfering disorder, as explained in Section 2.1. This leads to a total of 8 different types of disorder which will be introduced in this chapter, together with two more variants of implementing spring length disorder which we call *band mixing*. The remaining 4 time-reversal invariance breaking types are left for Chapter 3.

Most of these disorder types do not lead to a phase with a finite density of eigenfrequencies in three dimensions. The purpose of discussing them is, apart from completeness, to introduce the ideas one by one which finally lead to the interesting (and possibly physically relevant) model classes. Further, all disorder types introduced here can be combined in order to investigate which aspects of the model are crucial for which phase and under which additional disorder types the phases are stable.

Let us briefly mention that time-reversal invariance forbids (random) couplings between positions and momenta and review the concrete definition of the density of eigenfrequencies before coming to disorder.

Time-reversal invariance. As long as our solids are not rotating rather quickly, it is hard to imagine how time-reversal invariance of lattice vibrations could be broken, since phonons are charge-less and do not couple to magnetic fields. For this reason, we consider the time-reversal invariant case to be the physically relevant one which deserves our primary focus. This means that the Hamiltonian, H, has to be of the form

$$H = \frac{1}{2}\left(p^T M p + q^T S q\right) , \tag{2.1}$$

with the inverse mass matrix $M = M^T = M^\dagger > 0$ and $S = S^T = S^\dagger > 0$, i.e. there must not be terms coupling p and q. It follows that we should add disorder to M and S separately as *mass disorder* and *springs disorder*. As discussed in detail in Section 1.5, every disordered realisation of M and S must be positive in order for the system to be stable and our harmonic (or random phase) approximation by a quadratic

Hamiltonian to make sense. We apply the idea of writing operators as squares (see Section 1.5.2) to ensure positivity for M and S individually.

Density of eigenfrequencies. Throughout this thesis, we calculate the Green's function within the coherent potential approximation (CPA, see Section 1.5.3) corresponding to the large-matrix limit of our random matrix models. When time-reversal invariance is preserved, we refer to this also as the *coherent mass* and *coherent springs* approximation. Concretely, we calculate the density of eigenfrequencies[1] from the Green's function as follows:

$$\rho(\omega) = \lim_{\epsilon\to 0^+} \frac{1}{\pi} \Re\, g(\epsilon + i\omega) = \lim_{N\to\infty} \left\langle \frac{1}{2N} \sum_{i\omega_0 \in \sigma(X)} \delta(\omega - \omega_0) \right\rangle , \tag{2.2}$$

$$\text{where} \quad g(z) := \lim_{N\to\infty} \frac{1}{2N} \left\langle \mathrm{Tr}(z - X)^{-1} \right\rangle \tag{2.3}$$

is the normalised trace of the resolvent operator. Here $\sigma(X)$ denotes the spectrum of $X = Jh$. Notice that, due to $\sigma(x) \subset i\mathbb{R}$, we are indeed interested in the *real* part of g. As mentioned in Section 1.3.4 and 1.2, $\rho(\omega)$ is a quantity of primary interest since it determines the heat capacity of the disordered solid and it is also an important ingredient in the calculation of other observables, such as the heat conductivity.

From Equation (2.3) one can proceed by expanding the geometric series, which reduces the calculation of g to a combinatorial task by Wick's theorem. To leading order in n, this can be handled diagrammatically. Throughout this chapter we will employ this technique which is rather simple and quickly produces the self-consistency equations. Thus it is well suited to scan through a large class of models to find the most promising one for further investigation. However, the validity of this expansion and re-summation may be questioned, in particular for small z. In Chapter 3 we set the mathematically rigorous (and also more powerful) machinery of supersymmetry into motion. There we will show in particular that the results of this chapter are correct (within their domain of validity).

2.1 Additive and interfering implementations of disorder

All disorder implementations are built from Gaussian distributed random matrix ensembles which are shifted by a deterministic part before or after being squared. In this way, we produce variants of Wishart ensembles, thereby staying in the realm of physically meaningful Hamiltonians for bosonic systems as introduced in Section 1.5.

[1] Throughout this thesis, we employ the usual physics notation of writing $\rho(\omega)$ and similar to denote the distribution $f \mapsto \int_{\mathbb{R}} \rho(\omega) f(\omega) d\omega$ without implying that the density exists as a function. On the other hand, all densities of eigenfrequencies in CPA encountered in this thesis do exist and are piece wise smooth.

In [SZ10] we added a positive and symmetric disorder term given by a Wishart ensemble to a deterministic hamiltonian: $h = h_0 + R^T R$. We can do the same on the level of $M = M_0 + R_M^T R_M$ and similarly for S to produce a time-reversal invariant version of the model considered there. This way of implementing the disorder will be called *additive*. An interesting variation is to also write the deterministic part as a square. This is always possible for a positive symmetric matrix. We will further demand the square roots to be local operators in an appropriate sense (as explained in Section 2.1.1). In this setting, we can add disorder to the square roots individually. One concrete variant is

$$\begin{aligned} M &= \mu^{-1}(D_m + R_m)^T(D_m + R_m) \\ \text{and} \quad S &= \kappa(D_s + R_s)^T(D_s + R_s)\,, \end{aligned} \tag{2.4}$$

where $\mu^{-1} D_m^T D_m = M_0$ and $\kappa D_s^T D_s = S_0$ are the deterministic parts, introduced in Section 1.3.1. We will refer to this implementation of disorder as *interfering* if R is locally square, i.e. if D and R have the same image. The name is motivated by the "interfering" terms, $D_m^T R_m + R_m^T D_m$, not already contained in the additive part, $M = M_0 + R_m^T R_m$.

Note that $M_0 = \mu^{-1}\mathbf{1}_N$ is taken to be scalar (i.e. proportional to the identity). Details of how to choose the square root of the Laplacian in the spring sector are given in Section 2.1.1, but let us mention right away that we choose the plain square root of M_0 to be scalar as well, i.e. $D_m = \mathbf{1}_N$. Consequently we can rewrite M in Equation 2.4 as

$$M = \mu^{-1}(\mathbf{1}_N + R_m)^T(\mathbf{1}_N + R_m)\,. \tag{2.5}$$

We stress that the crucial point about *interfering* disorder is that R is first shifted by a constant matrix and then squared, as opposed to the additive implementation, where R is first squared and then shifted. The square root of S is important for the physical interpretation of the disorder model, see Section 2.2, but not for the implementation being dubbed additive or interfering.

2.1.1 Auxiliary spaces and square roots

In this section, we explain the details of how the additive and interfering disorder types are implemented and in particular how both can be treated simultaneously. As was mentioned in Section 1.5.1 and is noticeable in Equation (2.4), we have the freedom to introduce auxiliary Euclidean target spaces for $R_m : V_m \to W_m$ and $R_s : V_s \to W_s$. For the interfering model, it is clear that we should first produce the square roots of the deterministic parts, which then determine the spatial structure of W and hence largely also R.

As mentioned above, we choose the square root of the inverse mass matrix to be the trivial one, i.e. D_m is, for each $i \in C_0$, proportional to an embedding of $V_m(i)$ into an auxiliary space $W_m(i) = (W_m^{\circledcirc}(i) \simeq \mathbb{R}^n) \oplus (W_m^{+}(i) \simeq \mathbb{R}^{\alpha_m n})$ at site i. Throughout, we use $\circledcirc$ to indicate quantities related to interfering and $+$ for quantities related to additive disorder. The parameter $\alpha_m \in \frac{1}{n}\mathbb{N}$ is used to tune the aspect ratio of R_m, i.e. it determines the number of additional *auxiliary* dimensions. The total auxiliary space for the mass sector is given by

$$W_m = \bigoplus_{i \in C_0} W_m(i) \simeq \mathbb{R}^{L^d(1+\alpha_m)n} \quad \text{and} \quad D_m = \mathbf{1}_{L^d} \otimes \left(\mathbf{1}_n \oplus \mathbf{0}_{(\alpha_m n)\times n}\right) . \tag{2.6}$$

Here and in the following we often show matrices. Therefore we fix the basis of V given by the original position and momentum operators and some orthonormal basis[2] of W. The notation $\mathbf{0}_{(\alpha_m n)\times n} : V_m(i) \to W_m(i)^+$ denotes the rectangular matrix of the constant zero map. Notice that additive and interfering disorder do not (directly) couple. We make this explicit by writing

$$R_m = R_m^{\circledcirc} \oplus R_m^{+} : V_m \to W_m^{\circledcirc} \oplus W_m^{+} . \tag{2.7}$$

Now we can take a closer look at the structure of Equation (2.4),

$$\begin{aligned} \mu M &= \begin{pmatrix} D_m + R_m^{\circledcirc} \\ R_m^{+} \end{pmatrix}^T \begin{pmatrix} D_m + R_m^{\circledcirc} \\ R_m^{+} \end{pmatrix} \\ &= (D_m + R_m^{\circledcirc})^T (D_m + R_m^{\circledcirc}) + (R_m^{+})^T R_m^{+} . \end{aligned} \tag{2.8}$$

By using different disorder strengths, i.e. different variances for the Gaussian probability distributions for the entries of $R^{\circledcirc}$ and R^{+}, we can consider an arbitrary mixture of interfering and additive disorder. While $R^{\circledcirc}$ is naturally square, the aspect ratio α_m of R_m^{+} can be tuned.[3]

The square root D_s of the lattice Laplacian is implemented by placing the auxiliary spaces, $W_s(l) = W_s^{\circledcirc}(l) \oplus W_s^{+}(l) \simeq \mathbb{R}^{(1+\alpha_s)n}$, on the *links*, $l \in C_1$, as introduced in Equation (1.1). This means that we implement

$$W_s = \bigoplus_{l \in C_1} W_s(l) \simeq \mathbb{R}^{dL^d(1+\alpha_s)n} . \tag{2.9}$$

On the level of bands, the story is the same as in the M sector. We split $R_s = R_s^{\circledcirc} + R_s^{+}$ with the aspect ratio of R_s^{+} being called $\alpha_s \geq 0$. The spatial part of $D_s + R_s : V_s \to W_s$

[2] More precisely, we only fix the orthogonal decomposition of W into the additive and interfering sector. Given this decomposition, all matrices are invariant (in distribution) under orthogonal basis change.

[3] Notice that α_m changes the index of the linear operator R_m, which turns out to be of minor importance as long as D_m or $R_m^{\circledcirc}$ are non-zero.

mapping from sites to links is zero unless the site and link under consideration are adjacent. If so, D_s acts as $\pm\mathbf{1}_n$, the sign depending on whether the site is at the start or end point of the oriented link. This action squares to the appropriate multiple of the lattice Laplacian (see Figure 2.1 for a schematic picture).

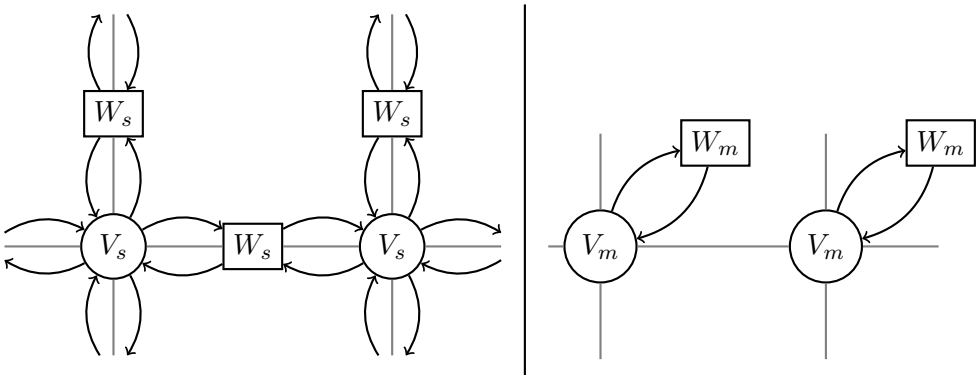

Figure 2.1: Left: action of the square root $D_s : V_s \to W_s$ of the spring constants S. Up and to the right D_s acts by $+\mathbf{1}_n$, down and to the left by $-\mathbf{1}_n$. Right: action of D_m.

2.2 Physical types of disorder

To make the situation more transparent, especially in the springs sector, we drop the Euclidean structure of $W_s^{\circledcirc}$. This means that $W_s^{\circledcirc}$ does *not* come with a scalar product. Instead, spring constants should really be considered as the matrix of the isomorphism $\kappa : W_s \to W_s^*$. Complementing the local picture in Figure 2.1, we give a more conceptual sketch of the situation in Figure 2.2.

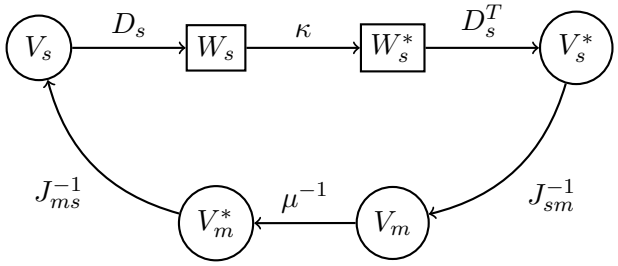

Figure 2.2: The structure of $\ddot{q} = J_{ms}^{-1}\mu^{-1}J_{sm}^{-1}D_S^T\kappa D_S\, q$ reveals the physical meaning of the individual matrices.

Here, all maps and spaces have a clear physical meaning. V_s contains local displacements. These are translated into spring elongations in $W_s^{\circledcirc}$ via D_s. The clean D_s reflects the geometry of the stressed harmonic crystal. In terms of masses and springs (see Equation (1.2)), adding a random part to D_s means disordering the relaxed spring lengths. In particular, each realisation is no longer of the form of a stressed crystal since terms distinguishing between longitudinal and transverse modes are randomly generated. We call this *spring length disorder*. Here the interfering disorder type, as indicated in Equation 2.4 is very natural.

The isomorphism $\kappa : W_s^{\circledcirc} \xrightarrow{\sim} (W_s^{\circledcirc})^*$ maps spring elongations to spring tensions, which is the role of spring constants. Ergo, randomness in κ will be called *spring constant disorder*. As in Equation (2.5), κ and its square root can be chosen to be scalar if some fixed isomorphism proportional to κ is understood. Being additive or interfering here has a similar meaning as in the mass sector, i.e. the distinction is between $\kappa + R^T R$ and $(\sqrt{\kappa} + R)^T(\sqrt{\kappa} + R)$. Also for springs, additive disorder randomly increases the local spring constants while interfering disorder might also lower them. Spring constants locally fluctuating down to zero effectively removes some springs from the model at random. This is as close to *structural* disorder as we get in this thesis.

The spring part of Figure 2.2 is completed by the dual of D, which maps spring tensions to forces, $D^T : W_S^* \to V_S^*$. In total, $S = D^T \kappa D$ describes how displacements cause forces.

The symplectic structure, J, provides a non-degenerate pairing of V_s and V_m and hence isomorphisms $J_{sm} : V_s \to V_m^*$ and $J_{ms} = -J_{sm}^T : V_m \to V_s^*$. In quantum terms, these are given by (i times) the commutator, or in classical terms by the Poisson bracket of phase space. The second part of Hamilton's equations (1.7) is given by $\dot{p} = J_{sm}^{-1} S\, q$, which is represented in Figure 2.2 by the chain of maps from V_s, containing q, to V_m, containing p. Notice that the matrix of $J_{sm}^{-1} = -\mathbf{1}_N$ is the same as that of J_{sm}.

In the mass sector, μ^{-1} translates momenta into velocities. Similar to the spring sector, J_{ms}^{-1} completes Hamilton's equation, $\dot{q} = J_{ms}^{-1}\mu^{-1}p$. Due to the site-diagonal structure of μ^{-1}, there is only one type of disorder to be added, namely mass disorder, similar to spring constant disorder. Overall, the diagram[4] in Figure 2.2 generates accelerations as in $\ddot{q} = J_{ms}^{-1}\mu^{-1}J_{sm}^{-1}D_S^T\kappa D_S\, q = -MS\, q$ and similarly for $\ddot{p}$.

The upshot of this section is that the "auxiliary" space in the interfering spring length sector, $W_s^{\circledcirc}$, has a physical meaning as does the corresponding square root D_s. The scalar product on this space is determined by the spring constants κ. The other spaces introduced in Section 2.1.1 are actually auxiliary for the definition of the Wishart ensembles. They are introduced together with scalar products, equivalent to isomorphisms $W_s^+ \simeq (W_s^+)^*$ and $W_m \simeq W_m^*$.

[4]Notice that this diagram is in particular *not* commuting.

2.2.1 Probability distributions

Now we have all definitions in place to specify the physically different types of disorder to be studied. The simplest one is mass disorder. Here the space of local square roots, $L_m \subset \{V_m \to W_m\}$, is given by operators mapping from physical to auxiliary spaces, both associated with sites. "Local" here means site diagonal, i.e. all $R_m \in L_m$ are required to act by zero, unless the origin and target sites are the same. As explained above, R_m is split into an additive and an interfering part, $R_m = R_m^+ + R_m^\circledcirc$, for which we define Gaussian probability measures

$$\left\langle f(R_m^\circledcirc, R_m^+)\right\rangle \propto \int\limits_{L_m} f(R_m^\circledcirc, R_m^+)\, e^{-\frac{n}{2b_m^\circledcirc}\,\mathrm{Tr}(R_m^\circledcirc)^T R_m^\circledcirc - \frac{\alpha_m n}{2b_m^+}\,\mathrm{Tr}(R_m^+)^T R_m^+}\, dR_m^\circledcirc\, dR_m^+ \qquad (2.10)$$

with normalisation $\langle 1\rangle = 1$. Here the appropriately rescaled variances, $b_m^\circledcirc$ and b_m^+, measure the disorder strength of interfering and additive disorder, respectively.

When adding disorder to S, it is important to note that the springs introduced in Section 1.3 only couple to $(q_i - q_j)^2$, i.e. the resulting contributions to the total energy are invariant under global shifts of all displacements, which are the Goldstone modes of broken translation invariance. In addition to disordering the length and spring constants of these original springs, we also introduce a third type of disorder in the S sector, namely terms proportional to $(q_i + q_j)^2$. These terms represent a random pinning to a background (substrate), which can be visualised by springs that attach each mass to its equilibrium position. However, we reserve the term *springs* to the original springs and will denote the translation invariance breaking terms as *pinning*. Let $L_{sp} \subset \{V_s \to W_s\}$ be the space of operators mapping from each site only to adjacent edges. Let Π act on L_{sp} by swapping all pairs of blocks associated with the same edge. I.e. the matrix block $\Pi(R)|_{V_s(i)\to W_s(l)}$ is defined to be equal to $R|_{V_s(j)\to W_s(l)}$ for $l = (i,j) \in C_1$. This formalises the notion of pinning and spring length disorder to be the operators in

$$L_{p/s} := \{R \in L_{sp} : \Pi(R) = \pm R\}\,, \qquad (2.11)$$

respectively. In particular, $D_s \in L_s$. Notice that L_s and L_p are orthogonal with respect to $\mathrm{Tr}_V\left(R_s^T R_p\right) = 0$ for $R_{p/s} \in L_{p/s}$. This leads to factorisation of the Gaussian probability measure:

$$\langle f(R_s, R_p)\rangle_{s,p} \propto \int\limits_{Ls}\int\limits_{L_p} f(R_s, R_p) e^{-\frac{n}{b_s}\,\mathrm{Tr}\,R_s^T R_s} e^{-\frac{n}{b_p}\,\mathrm{Tr}\,R_p^T R_p}\, dR_s\, dR_p\,, \qquad (2.12)$$

where, again, $\langle 1\rangle_{s,p} = 1$.

In this chapter, spring length disorder is only discussed in combination with the less well motivated random pinning because we want to keep the diagrammatics as

simple as possible and hence do not consider diagrams that connect different points in space, which would arise otherwise. This will be remedied in Chapter 3 with the help of supersymmetry. Section 2.6 offers the spring constant disorder model as a type of disorder in the S sector which can be handled diagrammatically without introducing pinning. At least in three dimensions, such models without pinning are certainly more relevant to describe experiments. For now we choose $b_s = b_p =: b_{sp}$, which leads to

$$\langle f\left(R_s + R_p\right)\rangle_{s,p} = \langle f\left(R_{sp}\right)\rangle_{sp} \propto \int\limits_{L_{sp}} f(R_{sp}) e^{-\frac{n}{b_{sp}} \operatorname{Tr} R_{sp}^T R_{sp}} \, dR_{sp} \,. \tag{2.13}$$

While ignoring the difference between spring length and pinning disorder for now, we will right away use different disorder strengths, b_{sp}^{+} and $b_{sp}^{\circledcirc}$, for the additive and interfering parts,

$$\left\langle f(R_{sp}^{\circledcirc}, R_{sp}^{+})\right\rangle \propto \int\limits_{L_s} f(R_{sp}^{\circledcirc}, R_{sp}^{+}) \, e^{-\frac{n}{b_{sp}^{\circledcirc}} \operatorname{Tr}(R_s^{\circledcirc})^T R_s^{\circledcirc} - \frac{\alpha_m n}{b_{sp}^{+}} \operatorname{Tr}(R_s^{+})^T R_s^{+}} \, dR_{sp}^{\circledcirc} \, dR_{sp}^{+} \,. \tag{2.14}$$

In this form, spring length and pinning disorder can be treated diagrammatically.

2.3 Additive disorder diagrams

In this section, we explain the diagrammatic derivation of the self-consistency equations (SCE) for the CPA DOS of the *additive* mass and spring length disorder model, postponing the more general case to Section 2.7 for pedagogical reasons. That is, we specialise to $b_m^{\circledcirc} = b_p^{\circledcirc} = b_s^{\circledcirc} = 0$ from Section 2.3.2 on. As mentioned in Section 2.2.1, we will restrict ourselves to[5] $b_s = b_p = b_{sp}$ throughout this chapter, i.e. we do never treat spring length and pinning disorder separately, in order to keep the diagrammatics tractable.

In summary, the specific model to be studied in this section has the form:

$$\mu M = \mathbf{1} + R_m^T R_m \tag{2.15}$$

$$\text{and} \quad \kappa^{-1} S = -\Delta + R_{sp}^T R_{sp} \,, \tag{2.16}$$

with the probability distribution of R_m and R_{sp} given in Equation (2.10) and (2.14).

[5] Whenever sub- or superscripts are omitted, the corresponding equation is understood as a template and all specialisations of the template obtained by inserting admissible labels are to be true. For example, $b_s = b_p$ is to say that $b_s^{+} = b_p^{+}$ *and* $b_s^{\circledcirc} = b_p^{\circledcirc}$.

2.3.1 Geometric series and self-energy

We start from Equation (2.3) with the aim of expanding the geometric series and then averaging term by term. The first step of the derivation is to use time-reversal invariance to rewrite the resolvent operator as

$$(z - Jh)^{-1} = \begin{pmatrix} z & -M \\ S & z \end{pmatrix}^{-1} = \begin{pmatrix} z(z^2 + MS)^{-1} & M(z^2 + SM)^{-1} \\ -S(z^2 + MS)^{-1} & z(SM + z^2)^{-1} \end{pmatrix} . \quad (2.17)$$

Here and in the following, we omit the unit matrix $\mathbf{1}_N$. As advertised in Section 1.3.1, it is MS (or equivalently SM) which determines the Green's function g from the reduced resolvent operator G. The latter tends to the clean G_0 for $b \to 0$:

$$g(z) = \frac{1}{2N} \operatorname*{Tr}_V (z - Jh)^{-1} = -\frac{z}{N} \operatorname*{Tr}_{V_q} G \quad (2.18)$$

$$\text{with} \quad G := -(z^2 + MS)^{-1} = (1 - G_0 \mathtt{R})^{-1} G_0 = \sum_{l=0}^{\infty} (G_0 \mathtt{R})^l G_0 \quad (2.19)$$

$$\text{and} \quad G_0 := -(z^2 + M_0 S_0)^{-1} . \quad (2.20)$$

In this section, $M_0 = \mu^{-1} D_m^T D_m = \mu^{-1}$ is considered as a scalar and a fixed isomorphism $V_m \simeq V_m^*$ is understood. Similarly $S_0 = \kappa D_s^T D_s = -\kappa\Delta$, where the isomorphism $W_s^{\circledcirc} \to (W_s^{\circledcirc})^*$ is understood and κ is treated as scalar. We also identify $V_s \simeq V_m$ via the non degenerate pairing provided by the symplectic form and the above isomorphisms. All random variables have been gathered into

$$\mathtt{R} := MS - M_0 S_0 = M_0 R_S^T R_s + R_m^T R_m S_0 + R_m^T R_m R_s^T R_s . \quad (2.21)$$

Calculating the average of $(G_0 \mathtt{R})^l$ over our Gaussian measures introduced in Section 2.2.1 reduces to a combinatorial task due to the elementary identity

$$\int f(x) e^{-\frac{1}{2b} x^2} = f(\partial_y)\big|_{y=0} e^{\frac{b}{2} y^2} , \quad (2.22)$$

leading to Wick's theorem. In our setting, this means that we draw all symbols representing matrices (see Figure 2.3) in the order corresponding to the matrix polynomial we want to average. Then we sum over all diagrams obtained from this string of shapes by joining triangles with the same labels by double lines in all possible ways. To leading order in large n we show below that only non-crossing diagrams contribute. Similar diagrammatics for non-crossing averages of matrix polynomials have been pioneered by [tH74].

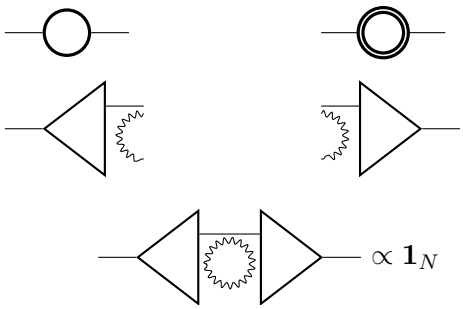

Figure 2.3: Graphical notation for the elementary matrices. The upper left single circle denotes a deterministic matrix (such as G_0, M_0, etc.) and the upper right double circle a coherent matrix (such as $\mathcal{G}$, $\mathcal{M}$, etc.). The left triangle stands for a transposed random matrix (R_m^T or R_{sp}^T) and the right one for R_m or R_{sp}. The elementary average $\langle R^T R \rangle$ is depicted in the lower line.

The first observation is that higher order terms in the expansion of $\langle g \rangle$ contain copies of lower order terms joined by G_0, which implies that we can re-sum

$$\mathcal{G} = \left\langle \sum_l (G_0 \mathtt{R})^l G_0 \right\rangle = (G_0^{-1} - \Sigma)^{-1} \tag{2.23}$$

where the "self energy" Σ consists of irreducible diagrams. Here "irreducible" means that diagrams cannot be cut by removing one G_0. The next observation is that only non-crossing diagrams contribute to leading order in n (see Section 2.7 for some examples). Throughout, it is more convenient to work with the coherent inverse mass matrix $\mathcal{M}$ (called coherent mass for short) and the coherent springs (matrix) $\mathcal{S}$ than with the self-energy, because the irreducible diagrams have the following structure:

$$\Sigma = \mathcal{M}\mathcal{S} - M_0 S_0 \tag{2.24}$$

$$\Rightarrow -\mathcal{G}^{-1} = z^2 + \mathcal{M}\mathcal{S}\,. \tag{2.25}$$

Comparing Equation (2.25) with (2.19) and (2.20), the meaning of these coherent matrices becomes clear. The CPA amounts to replacing the fluctuating matrices M and S with the coherent ones. The latter have to be determined self-consistently and will in general be complex and z-dependent and tend to M_0 and S_0 in the clean limit.

Whilst this section has been general in that it also applies to the diagrammatics of the interfering and combined model, we will now specialise to the purely additive case.

2.3.2 Re-summation

The series of irreducible diagrams for $\mathcal{M}$ is shown in Figure 2.4. The diagrams in the spring sector look exactly the same with all variants of M and S symbols exchanged.

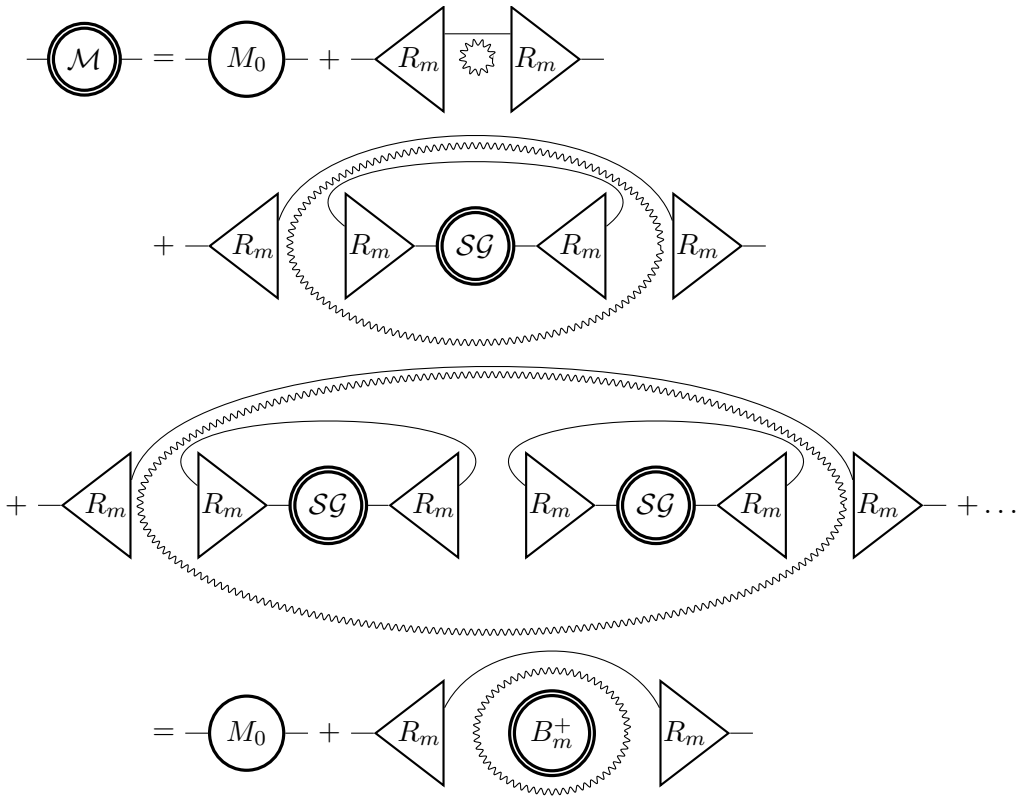

Figure 2.4: Diagrammatic derivation of the coherent mass of the additive mass disorder model.

Re-summing the geometric series of bubble diagrams called B_m^+ in Figure 2.4, we obtain

$$\mathcal{M} = M_0 + \mu^{-1} b_m^+ B_m^+ \tag{2.26a}$$

$$B_m^+ = 1 + B_m^+ \frac{b_m^+}{\mu \alpha_m} \frac{1}{n} \operatorname{Tr}(\mathcal{SG}) \tag{2.26b}$$

$$\mathcal{S} = S_0 + d\kappa b_{sp}^+ B_{sp}^+ \tag{2.26c}$$

$$B_{sp}^+ = 1 + B_{sp} \frac{\kappa b_{sp}^+}{\alpha_s} \frac{1}{n} \operatorname{Tr}(\mathcal{MG}) \ . \tag{2.26d}$$

The factor of d in the spring sector is due to the free summation indicated by the wiggly loop contributing a factor $n\alpha_s^+ d = \dim(\oplus_{l \in C_1} W(l))$, where the direct sum runs over edges adjacent to some site $i \in C_0$.

The solutions of these self-consistency equations are discussed in Section 2.4.1.

2.4 Mass, spring length, and pinning disorder models

2.4.1 Additive disorder

The model of *additive mass, spring length and pinning* disorder, $b^{\circledcirc}_{sp} = b^{\circledcirc}_{m} = 0$, is a time-reversal invariant version of [SZ10]. A similar model has been studied in [JSS83]. The authors of the latter also consider additive mass disorder and argue that spring constant disorder does not change the qualitative picture. We present the detailed assessment of this claim for our model below. Notice, however, that our model ensures positivity of the mass matrix and is thus dynamically stable. More importantly, we take the *inverse* mass to be fluctuating. On the level of the DOS, this is equivalent to fluctuations in $\nu^2 = \kappa/\mu$, which might locally become very small in our case. In contrast, [JSS83] take μ to fluctuate with finite variance around a finite value, hence ν is bounded away from zero.

The diagrammatics for the additive model are presented in Section 2.3. The resulting self-consistency equations (2.26) can be rewritten as

$$\left(B^+_{sp}\right)^{-1} = 1 + \frac{b^+_{sp}}{\alpha_s}\frac{\tilde{g}}{\tilde{z}}\mu\mathcal{M} \tag{2.27a}$$

$$(\mu\mathcal{M} - 1)\frac{b^+_m}{\alpha_m}\tilde{g}\tilde{z} = (\mu\mathcal{M})^2 + \mu\mathcal{M}\left(\frac{1-\alpha_m}{\alpha_m}b^+_m - 1\right) - \frac{b^+_m}{\alpha_m} \tag{2.27b}$$

$$\kappa^{-1}\mathcal{S} = -\Delta + d\, b^+_{sp} B^+_{sp} \tag{2.27c}$$

$$\text{and} \quad \tilde{g} = \frac{1}{n}\,\mathrm{Tr}\,\frac{\tilde{z}}{\tilde{z}^2 + \mu\mathcal{M}\kappa^{-1}\mathcal{S}}\,, \tag{2.27d}$$

where we have eliminated the parameter B^+_m stemming from the geometric series of bubble diagrams in the mass sector. Further we measure frequency in units of ν, i.e. $\tilde{z} = z/\nu$ and consequently $\tilde{g} = \nu g$ is measured in the same units. Equations (2.27) can be combined into a single equation that is to be solved for the (complex) coherent mass as a function of (complex) frequency, $\mathcal{M}(z)$, which in turn determines $g(z)$ via Equation (2.27b).

2.4.1a Debye phase

In Equation (2.27b), the left hand side vanishes for $z = 0$. Hence we must have one of two solutions for the coherent inverse mass at zero frequency, but only the positive one, $\mu\mathcal{M}(z=0) = 1 + b^+_m + O((b^+_m)^2)$, connects continuously to the clean case, $M_0 = \mu^{-1}$. For $b^+_m > 0$, the second solution would lead to a negative density of states and will be disregarded. This means that a small amount ($b^+_m \ll 1$) of Mass disorder *increases* the inverse mass and hence the *speed of sound* by a factor $1 + b^+_m$. Notice that M in Equation (2.15) was defined to be the sum of two independent[6] positive (semi) definite

[6] More precisely speaking, M_0 and $R^T_m R_m$ are *free* in the sense of free probability.

operators, hence the eigenvalues are necessarily shifted up. The two solutions for $\mathcal{M}$ do not meet for any $b_m^+ \geq 0$. As a consequence, continuity forbids the additive mass disorder model to have a transition to any strong disorder phase and the Debye phase persists for any disorder strength. This is in agreement with the findings of [JSS83].

To leading order in small $-z^2 = \omega^2$, b_{sp}^+, and b_m^+, spring length and pinning disorder leads to a shift in the denominator of g:

$$-\tilde{\omega}^2 \mapsto d b_{sp}^+ (1 + b_m^+) - \tilde{\omega}^2 \,. \tag{2.28}$$

This shift has a drastic effect, since the Debye DOS is proportional to

$$\rho(\omega) \propto \Re \left(i\omega\sqrt{x} \log\left(\frac{1-\sqrt{x}}{1+\sqrt{x}} \right) \right) \tag{2.29}$$

$$\text{for} \quad x = \frac{\nu^2 \Omega^2}{\tilde{\omega}^2 - d b_{sp}^+ (1 + b_m^+)} \,, \tag{2.30}$$

in odd dimensions and $\rho(\omega) \propto \Re(i\omega \log(1-x))$ in even dimensions, as can be seen from Equations (2.27c), (2.27d), (A.2), and (A.8) or (A.9). The Green's function is rendered purely imaginary and consequently the density of states to be zero for

$$|\omega| < \sqrt{d b_{sp}^+ (1 + b_m^+)} \,, \tag{2.31}$$

opening a gap at small frequencies. We will show in Chapter 3 that this gap is actually due to *pinning* rather than spring length disorder.

In Figure 2.5 we confirm that the numerical solution of the self-consistency equations (SCE) stays in the Debye phase, even for very strong additive mass disorder and that indeed a gap of width of the order of $\sqrt{b_{sp}}$ is opened up by pinning disorder.

2.4.1b Strong disorder limit

For $\mu^{-1}, \kappa \to 0$ at constant $\mu^{-1} b_m^+$ and κb_{sp}^+, the Green's function is determined by

$$\frac{\hat{z}}{\alpha_m \alpha_s} \hat{g}^3 + \frac{2 - \alpha_m - \alpha_s d}{\alpha_m \alpha_s} \hat{g}^2 + \left(\hat{z} + \frac{1 - \alpha_m - \alpha_s d + \alpha_m \alpha_s d}{\hat{z} \alpha_m \alpha_s} \right) \hat{g} = 1 \tag{2.32}$$

for $\hat{g} = \nu g \sqrt{b_m^+ b_{sp}^+}$ and $\nu \hat{z} \sqrt{b_m^+ b_{sp}^+} = z$. For $d = \alpha_s = \alpha_m = 1$ this is the self-consistency equation for the Green's function found in [LSZ06], which in particular leads to $\rho(\omega) \propto \omega^{-1/3}$ to leading order in small frequencies. This also holds true in higher dimensions if $\alpha_m = 1 = \alpha_s d$. If exactly one of these two conditions holds then

$$\hat{g}(z = 0) = \frac{\alpha_s \alpha_m}{\alpha_s d + \alpha_m - 2} \tag{2.33}$$

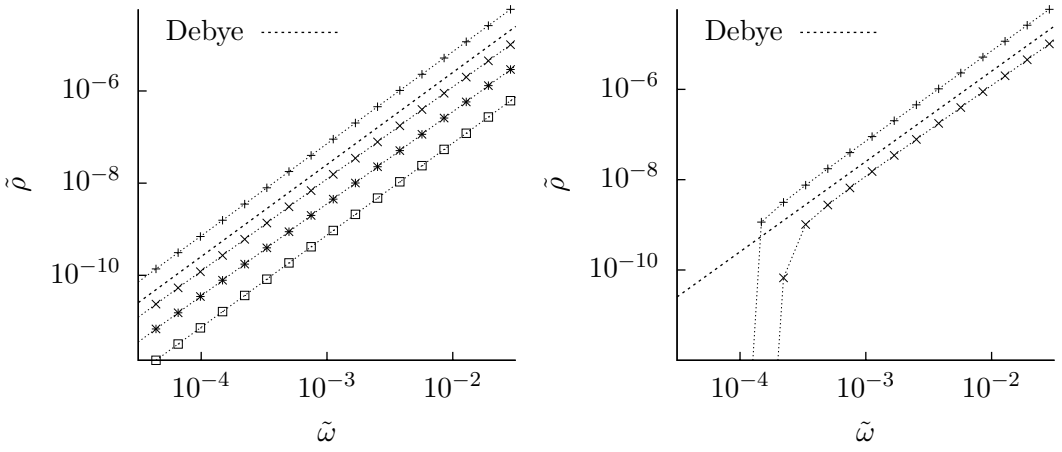

Figure 2.5: CPA DOS in *three dimensions*. Left: *interfering* compared to *additive mass disorder*. Top to bottom: interfering disorder model in the Debye phase ($b_m^{\circledcirc} = 0.5$, marked with +), clean Debye model (dashed line), and additive disorder model ($b_m^{+} = 1$, $b_m^{+} = 10$, and $b_m^{+} = 100$, marked with x, $*$ and boxes, respectively). Right: a small amount of *pinning* is added to the interfering mass disorder model ($b_m^{\circledcirc} = 0.5$, $b_s^{\circledcirc} = 10^{-8}$, top, marked with +) and additive mass disorder model ($b_m^{+} = 1$, $b_s^{+} = 10^{-8}$, bottom, marked with x).

is finite. Notice that this is the case for the most natural values $\alpha_m = \alpha_s = 1$, if $d > 1$. If Equation (2.33) yields a negative number then the time evolution operator cannot have full rank and it follows that there is a δ-peak of zero modes. For $\hat{g}(z = 0) > 0$ in Equation (2.33), however, we find that the DOS of this purely random model is positive and finite at zero frequency. This is the first promising hint at a phase which could explain the experimentally observed linear heat capacity. In Section 2.4.2 we discuss the interfering disorder model, which features a transition to this new phase at finite disorder strength.

The generic case of full rank $\alpha_m > 1 < \alpha_s d$ leads to $g \propto z$ being purely imaginary to leading order, similar to the clean case. Also the second order contribution to g vanishes and the DOS follows the law $\rho \propto \omega^4$.

2.4.2 Interfering disorder

We focus on the *interfering* mass, spring length and pinning disorder model in this section, i.e. $b_{sp}^{+} = b_m^{+} = 0$. This also renders α_m and α_s irrelevant. Apart from the deterministic scale, there are only two parameters left. These are the strength of

interfering mass disorder $b_m^\circledcirc$, as well as $b_{sp}^\circledcirc$, which tunes interfering spring constant and pinning disorder simultaneously.

The diagrammatic derivation of SCE for this model is technically a little more involved, but conceptually very similar to the one presented in Section 2.3. For this reason, we postpone the detailed derivation to Section 2.7. Here, we start from the resulting Equation (2.75) (restricted to $b^+ = 0$), which yields

$$b_m^\circledcirc \tilde{g}\tilde{z} = B_m^\circledcirc (B_m^\circledcirc + b_m^\circledcirc - 1) \tag{2.34a}$$

$$\mu\mathcal{M} = B_m^\circledcirc (B_m^\circledcirc + b_m^\circledcirc) = \frac{1 - B_{sp}^\circledcirc}{b_{sp}^\circledcirc B_{sp}^\circledcirc} \frac{\tilde{z}}{\tilde{g}} \tag{2.34b}$$

$$\kappa^{-1}\mathcal{S} = -B_{sp}^\circledcirc \Delta + b_{sp}^\circledcirc (d - 1 + \tilde{g}\tilde{z}) \tag{2.34c}$$

$$\text{and} \quad \tilde{g} = \frac{1}{n} \operatorname{Tr} \frac{\tilde{z}}{\tilde{z}^2 + \mu\mathcal{M}\kappa^{-1}\mathcal{S}}\,, \tag{2.34d}$$

where again $\tilde{z} = \frac{z}{\nu}$ and $\tilde{g} = \nu g$. Again, we can combine Equations (2.34) into a single self-consistency equation that determines the (complex) value of the vacuum bubble series $B_m^\circledcirc(z)$, which in turn determins the other parameters and in particular the Green's function. Note, however, that this equation generally has more than one solution. We determine which is the correct one by demanding $B_m^\circledcirc$ to be continuous in all parameters, ρ to be non-negative, and $g(z)$ to decay like $1/z$ for large z. (The latter is actually not discriminating.)

2.4.2a Weak disorder

The effects of weak disorder are (qualitatively) similar to those found in Section 2.4.1. Here, Equation (2.34a) at $z = 0$ is solved by either $B_m^\circledcirc(z = 0) = 0$ or $B_m^\circledcirc(z = 0) = 1 - b_m^\circledcirc$. The latter is the relevant solution for small $b_m^\circledcirc$ since it connects continuously to the clean limit (and it leads to a finite and positive density of states). To leading order in small frequencies, the effect of *interfering* mass disorder of strength $b_m^\circledcirc$ is to rescale

$$M_0 = \mu^{-1}\mathbf{1} \mapsto \mathcal{M} = \mu^{-1}\left(1 - b_m^\circledcirc\right)\mathbf{1} \tag{2.35}$$

i.e. mass disorder effectively increases the mass or *decreases the speed of sound* by a factor of $1 - b_m^\circledcirc$. This is the first hint to the interfering model being more interesting than the additive model as it indicates that low energy modes are being generated by disorder. The power law of the DOS at small frequencies is the same as in the clean case, i.e. $\rho \propto \omega^{d-1}$, see Equation (A.3). Equation (2.35) is correct in Debye approximation and to first order in z but for all $0 \leq b_m^\circledcirc < 1$, i.e. this is not just a perturbative result. We have confirmed this effect also in the numerical solution of the SCE. See for example Figure 2.5.

At this point, we would like to mention that, on the perturbative level (see Equation (2.65)), pure spring length disorder has a similar effect on the speed of sound as mass disorder. However, this effect is precisely cancelled by the random pinning of equal strength that we are currently considering. In contrast, to leading order in small z and for $b_m^{\circledcirc} < 1$ pinning leads to a shift,

$$-\tilde{\omega}^2 \mapsto b_{sp}^{\circledcirc}(d-1)(1-b_m^{\circledcirc}) - \tilde{\omega}^2 \,. \tag{2.36}$$

As mentioned in Section 2.4.1a, this leads to a gap at small frequencies. Here, it is of half-width $\sqrt{b_{sp}^{\circledcirc}(d-1)(1-b_m^{\circledcirc})}$ to leading order in small $b_{sp}^{\circledcirc}$.

2.4.2b Interfering mass disorder model

The above considerations for small $b_m^{\circledcirc}$ and $b_{sp}^{\circledcirc}$ motivate setting $b_{sp}^{\circledcirc} = 0$ for now. At small frequencies, this *interfering mass disorder* model looks very similar to the clean Debye model with an increased mass as long as mass disorder is weak, $b_m^{\circledcirc} < 1$. At the critical value $b_m^{\circledcirc} = 1$, the regime of weak disorder terminates. For critical disorder, the unique solution of Equation (2.34a) is $B_m^{\circledcirc}(z=0) = 0$. Also for strong ($b_m^{\circledcirc} > 1$) disorder, this solution is the only one that leads to a non-negative density of eigenfrequencies.

For $b_m^{\circledcirc} = 1$, we have $(B_m^{\circledcirc})^2 = \tilde{g}\tilde{z}$. Using the Debye approximation (see Section 1.3.3 and A.1) and integrals computed in Appendix A.1.1, we determine the solution of Equations (2.34) to leading order[7] in $\tilde{z}$:

$$\tilde{g} \propto \begin{cases} \tilde{z}^{\frac{1}{3}} & d \geq 3 \\ \tilde{z}^{\frac{1}{3}} \log^{\frac{2}{3}}(\tilde{z}) & d = 2 \\ \tilde{z}^{-\frac{1}{5}} & d = 1\,. \end{cases} \tag{2.37}$$

For strong disorder, $b_m^{\circledcirc} > 1$, we find to leading order[7]

$$\tilde{g} = \begin{cases} \frac{\sqrt{b_m^{\circledcirc}-1}}{b_m^{\circledcirc}\Omega}\sqrt{\frac{d}{d-2}} & d \geq 3 \\ \frac{\sqrt{b_m^{\circledcirc}-1}}{b_m^{\circledcirc}\Omega}\sqrt{-\log(\tilde{z})} & d = 2 \\ \left(\frac{(b_m^{\circledcirc}-1)^3}{4(b_m^{\circledcirc})^4}\right)^{\frac{1}{5}} \tilde{z}^{-\frac{3}{5}} & d = 1\,. \end{cases} \tag{2.38}$$

Notice that $0 < g(z=0) < \infty$ for all $b_m^{\circledcirc} > 1$ in three dimensions and maximal for $b_m^{\circledcirc} = 2$ (see Figure 2.8). In two dimensions, the density of states of this model diverges, but only at a logarithmic rate.

[7] In two dimensions, the next-to-leading order terms come with $\log\log(z)$ instead of $\log(z)$. In all other dimensions, the next-to-leading order terms are of higher power in z.

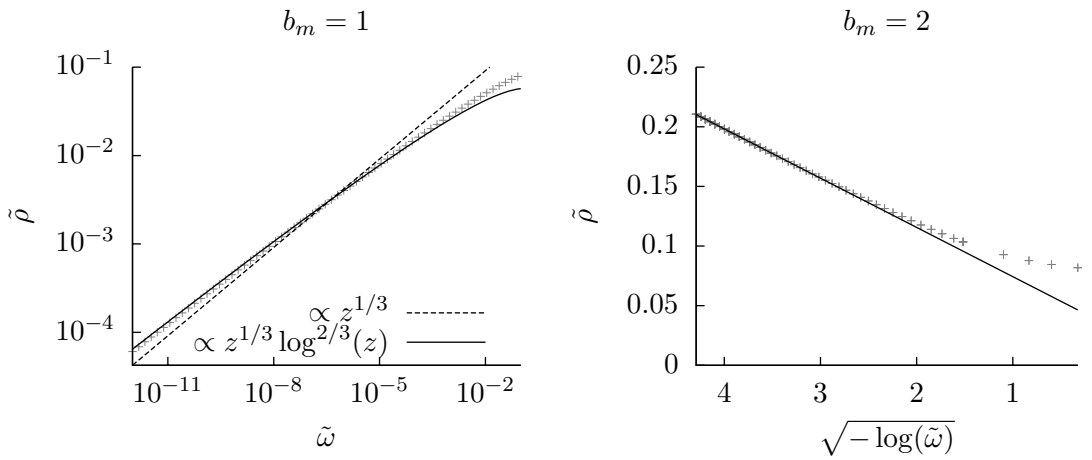

Figure 2.6: Coherent potential approximation of the density of eigenfrequencies (CPA DOS) of the *interfering mass disorder model* in *two dimensions*. Left: critical disorder strength. Right: Large disorder. The right plot shows $\tilde{\rho}$ as a function of $\sqrt{-\log(\tilde{\omega})}$ and we have reversed the x-axis such that small frequencies are again on the left. The fitted slope agrees with the predicted value of $\pi^{-3/2}/4$ within numerical accuracy.

These power laws are well observable in the numerical solution of the self-consistency equation in three dimensions. In particular, the unusual power law $\rho \propto \omega^{1/3}$ at $b_m^{\circledcirc} = 1$ is clearly visible and for $b_m^{\circledcirc} > 1$ the density of eigenfrequencies stays constant at low energies, as shown in Figure 2.7. Also in two dimensions, the numerical solution fits the analytic predictions very well. It takes careful examination to spot the logarithmic contribution at criticality, but for strong disorder, the logarithmic divergence is easier to find as shown in Figure 2.6.

Since S is purely deterministic in the currently considered mass disorder model, there is no meaningful random matrix limit. Sending $\kappa \to 0$ leads to the spectrum of X being exactly zero, which is correctly reproduced by the self-consistency equations (2.34) leading to $g \propto 1/z$ and hence $\rho \propto \delta(\omega)$ in this limit. In the limit of $\mu^{-1} \to 0$ at finite κ and $\mu^{-1} b_m^{\circledcirc}$, the strong disorder phase persists (as can be seen from inserting $\tilde{g} = (\kappa\mu^{-1})^{1/2} g$ back into Equation (2.38)).

2.4.2c Numerically averaged finite size spectra

Together with Artur Swiech, we numerically calculated the integrated density of states (also known as cumulative distribution function) for the interfering random mass model by pseudo-random sampling and exact diagonalisation for small system size L. Since

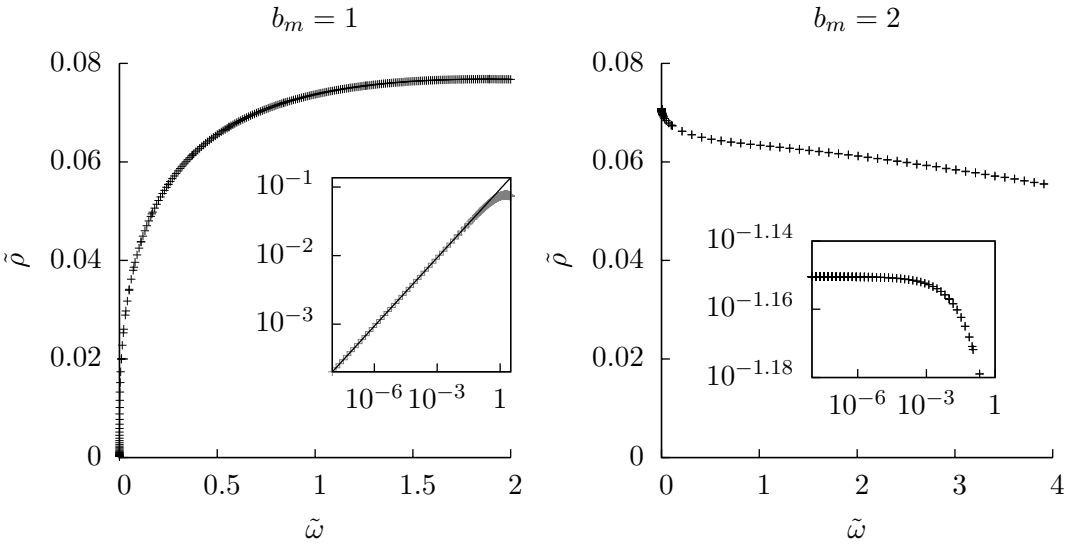

Figure 2.7: CPA DOS of the *interfering mass disorder model* in *three dimensions*. At the critical value of disorder (left), the inset reveals the power law at criticality, where the slope is 1/3. For large disorder (right), $\tilde{\rho}(\tilde{\omega})$ is constant to leading order.

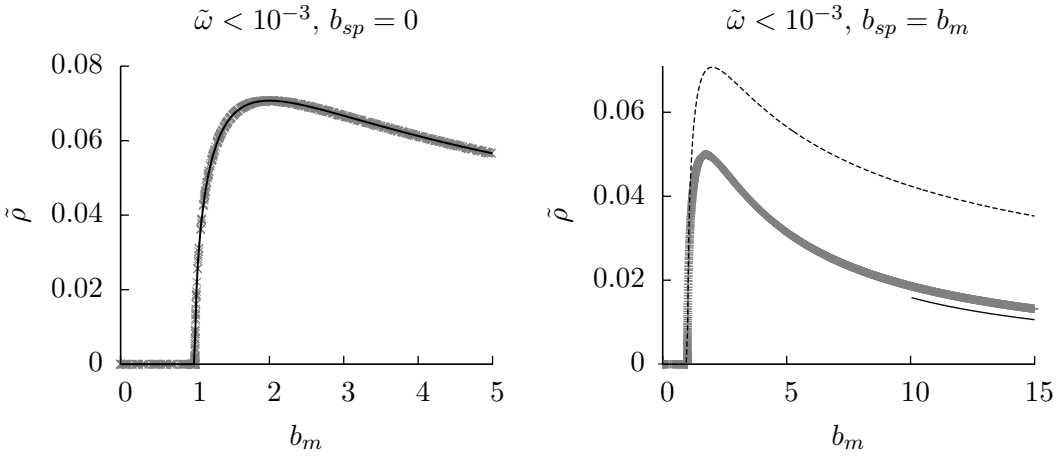

Figure 2.8: Left: CPA DOS for the *interfering mass disorder model* at very small frequencies in *three dimensions* as a function of disorder strength. The solid line is our prediction, $(\sqrt{3}/2/\pi^2)^{1/3}\sqrt{b_m - 1}/b_m$, as given in Equation (2.38). Note that there are no fitting parameters. Right: Spring length disorder and pinning do not change the qualitative picture. The dashed line is again the $b_{sp} = 0$ result and the solid line the asymptotic behaviour.

h is a sparse matrix, the Lanczos algorithm is used to find the smallest eigenvalues for larger system size. All simulations were done for $n = d$ bands and finite lattice size L in two and three dimensions for the full Laplacian (i.e. without Debye approximation). By comparison with these results, we confirm that the CPA results for the leading-order power laws of the DOS are applicable to the physically relevant case of $n = d$ bands, although the CPA becomes exact only for $n \to \infty$.

The effect of weak disorder is best observed in two dimensions, where we can go to large lattice size. In Figure 2.9, we can see the expected Debye power law with increased mass as long as frequencies are high enough to escape finite size effects. More interestingly, Figures 2.10 and 2.11 confirm the existence of the critical transition to the strong-disorder phase in three dimensions with the predicted leading order power laws. In particular, the finite density of states at zero frequency in three dimensions is confirmed.

In two dimensions, the simulation results at strong disorder look similar to those in three dimensions. That is, we do not find logarithmic divergences, but a finite density of states at zero. This is not completely unexpected. Even if the mean-field results in such low dimension were still trustworthy, the logarithmic terms only become visible at frequencies well below the finite-size limit. Notice that for example a very small amount of random pinning added to the interfering mass disorder model also removes the logarithmic factors within our CPA.

We notice that, in particular for strong disorder, the numerical averaging already converges after rather few (meaning 10 to 50) samples. Even for a single sample, the integrated density of states hardly deviates from its average value.

2.4.2d Spring length disorder and pinning

Taking also spring length disorder and random pinning of equal strength into account, the most notable result is that $b_m^{\circledcirc} = 1$ still marks a critical phase, independent of $b_{sp}^{\circledcirc}$. This is because Equation (2.34a) is independent of $b_{sp}^{\circledcirc}$ and so are the solutions $B_m^{\circledcirc}(z)$ and also $\mathcal{M}(z = 0)$, which in turn leads to the phase transition upon vanishing. Spring length disorder does not lead to similar phenomena for $\mathcal{S}$. More precisely, $B_{sp}^{\circledcirc}(z = 0)$ stays finite for any $0 \leq b_{sp}^{\circledcirc} < \infty$. Consequently, spring length disorder only influences the pre-factor of ρ to leading order in ω, not the law. However, the additive term $\propto \mathbf{1}$ in Equation (2.34c) does remove the logarithmic factors in two dimensions. This term is due to pinning, as we hinted at several times but prove only in Chapter 3.

More concretely, for critical mass disorder ($b_m^{\circledcirc} = 1$) in any dimension larger than one and any $0 < b_{sp}^{\circledcirc} < \infty$, we find $\tilde{g} \propto \tilde{z}^{1/3}$. As mentioned in Section 2.4.2a, the width of the gap in the Debye phase goes to zero as $\sqrt{1 - b_m^{\circledcirc}}$ and there is no gap for $b_m^{\circledcirc} \geq 1$.

For strong mass disorder $b_m^{\circledcirc} > 1$ the DOS at zero frequency is finite. Also here, the logarithmic factor in two dimensions is removed. The value of $\rho(0)$ is now determined by a transcendental equation (see Figure 2.8). For $b_{sp} > 0$ we can send $\mu^{-1} \to 0$ and

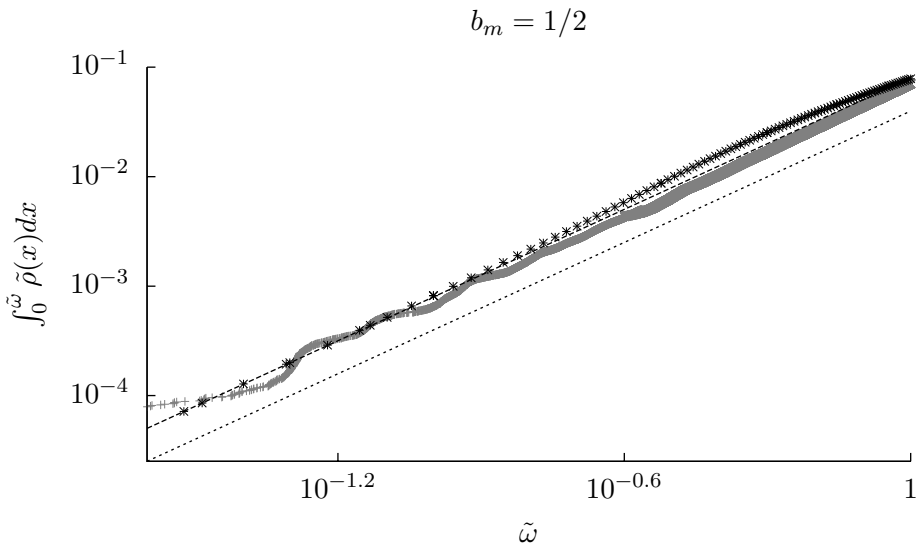

Figure 2.9: The integrated density of states of the *interfering mass disorder model* computed from exact diagonalisation (marked with grey +) for a lattice of 100×100 sites (in *two dimensions*), compared to our CPA prediction (marked with black x, low frequency prediction marked with dashed line) and the integrated Debye density of states (dotted line). Note that there are no fitting parameters.

$\kappa \to 0$ at constant $\mu^{-1} b_m^{\circledcirc}$ and $\kappa b_{sp}^{\circledcirc}$ and obtain a non-trivial purely random lattice model. In the rescaled units $\hat{g} := \nu g \sqrt{b_m b_{sp}}$ and $\nu \hat{z} := z/\sqrt{b_m b_{sp}}$ we find

$$1 = \hat{z}\hat{g} + (d-1)\hat{g}^2 + \hat{z}\hat{g}^3 \,. \tag{2.39}$$

Since for the purely random model there is no distinction between additive and interfering disorder, Equation (2.39) is the same as Equation (2.32) for $\alpha_m = \alpha_s = 1$. It was discussed in Section 2.4.1b.

2.4.3 Combined additive and interfering disorder

Before closing this section, we would like to mention some results for the model of combined additive and interfering mass, spring length and pinning disorder. In this model, there are already six parameters. The corresponding SCE are derived in Section 2.7. Yet we have learnt in the previous sections that the leading order power law of $\rho(\omega)$ is already determined by the leading order laws of $\mathcal{M}(z)$ and $\mathcal{S}(z)$. As was always the case throughout this chapter, the coherent springs matrix at zero frequency

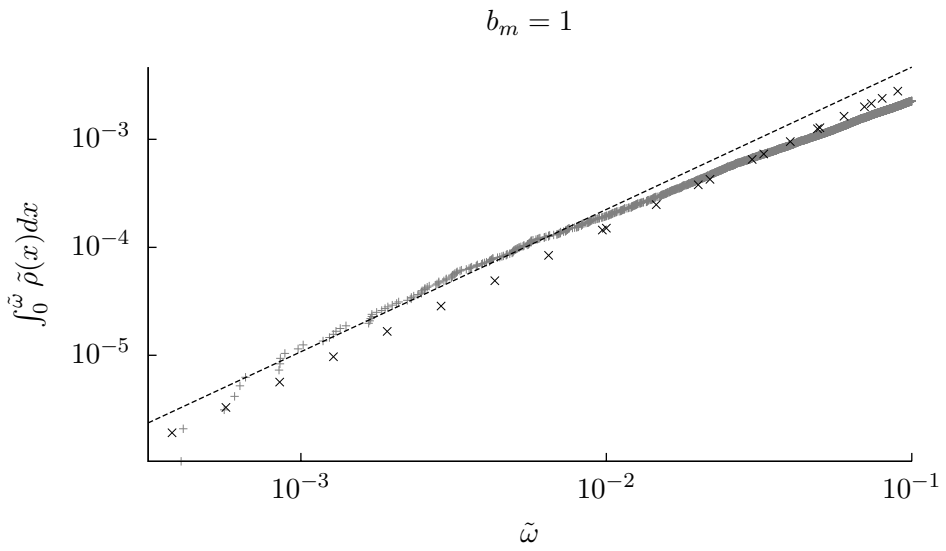

Figure 2.10: Integrated density of states from exact diagonalisation (20^3 sites, grey +) for the *interfering random mass model* compared to our CPA prediction (black x) at critical disorder strength in *three dimensions*. The slope of the dotted line is about 4/3.

is non-vanishing, also in the combined model and the phase of the system is determined by the law of the coherent mass. $\mathcal{M}(z=0)$ in turn is now determined by a third order polynomial. One of the roots is

$$\mu\mathcal{M}(z=0) = 0\,, \tag{2.40}$$

witch corresponds to the strong disorder phase that we found in Section 2.4.2b. The other two solutions lead to non-trivial functions of the three parameters of the M sector, but from their perturbative form we can identify

$$\mu\mathcal{M}(z=0) = 1 + b_m^+ + b_m^\circledcirc \left(\frac{2\alpha_m}{b_m^+} + 1 + 2\alpha_m - 2b_m^+ \right) + O(b_m^2)\,, \tag{2.41}$$

to be the additive solution, i.e. the one found in Section 2.4.1. Notice that for $b_m^\circledcirc > 0$ this solution does not connect to the clean case for $b_m^+ \to 0$. The third solution,

$$\mu\mathcal{M}(z=0) = 1 + (2b_m^+ - 1)b_m^\circledcirc + O(b_m^2)\,, \tag{2.42}$$

is the interfering solution, i.e. it connects continuously to the weak-disorder phase found in Section 2.4.2b. This is the one solution, which also connects to the clean

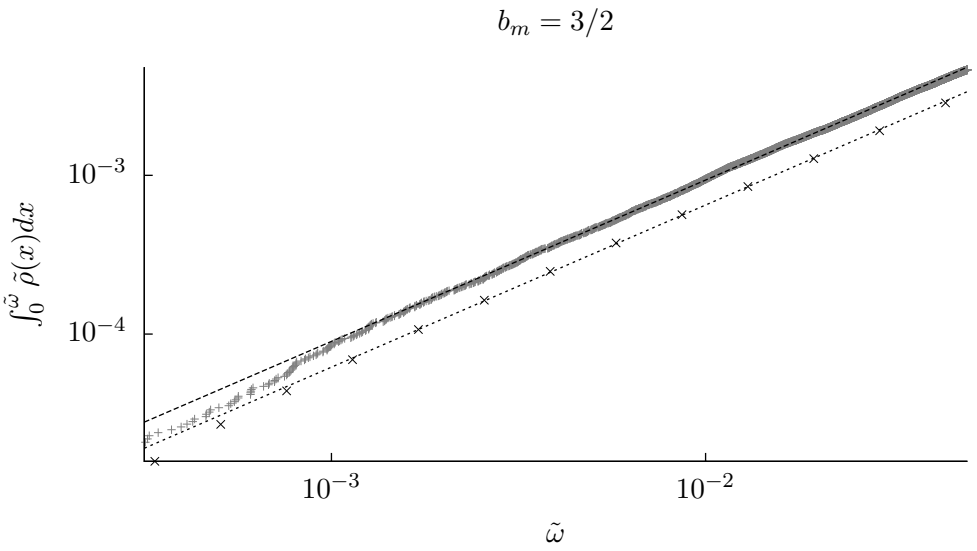

Figure 2.11: Integrated density of states from exact diagonalisation (20^3 sites, grey +) for the *interfering random mass model* compared to our CPA prediction (black x) at strong disorder in *three dimensions*. The slopes are both equal 1 (within numerical accuracy).

case for any small $0 < b_m^+, b_m^\circledcirc \ll 1$ and is hence the generic weak-disorder solution. As discussed above, it leads to a Debye phase with a rescaled mass. Already on this perturbative level, we can see how additive disorder works against a transition to the strong disorder phase. In fact, this solution does not meet the other solutions for any value of the parameters. As a consequence, there is no phase transition and the Debye phase persists also for strong disorder, similar to the additive disorder model (see Figure 2.12 for a numerical verification). All plots are for $\alpha_m = \alpha_s = 1$, but varying α does not change the qualitative picture.

Since the combined model, like the additive model, is always in the Debye phase, random pinning of any type opens a gap. In Figure 2.12 we see the gap caused by pinning, the Debye contribution due to additive disorder and a constant region remnant of the stronger interfering disorder phase.

We would like to stress that the DOS as a function of b_m^+ and ω at $b_m^\circledcirc > 1$ is smooth everywhere, except for $\omega = b_m^+ = 0$, where it is discontinuous in b_m^+. A caricature of the situation is given by the function $(\omega, b) \mapsto \omega/(\omega + b)$ on $\mathbb{R}^{\geq 0} \times \mathbb{R}^{\geq 0}$.

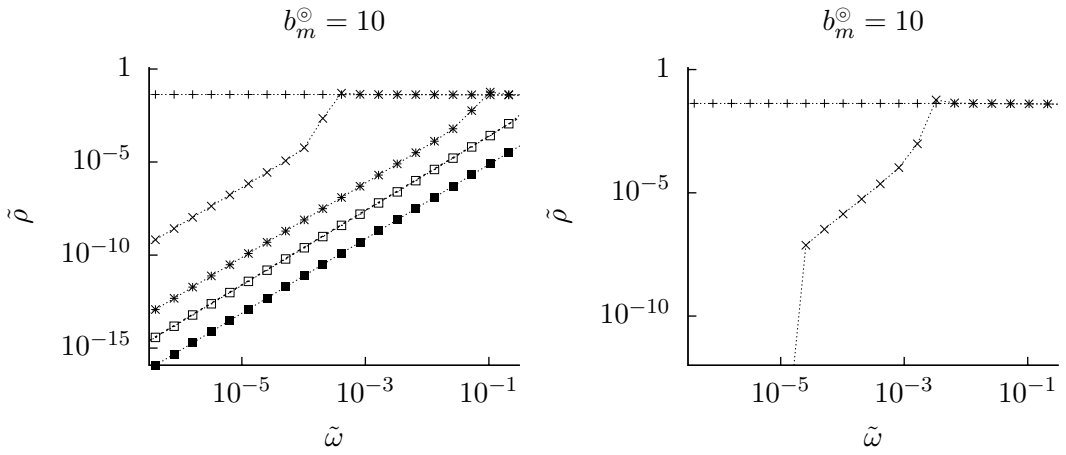

Figure 2.12: Left: CPA DOS for *combined additive and interfering mass disorder in three dimensions*. Top to bottom: $b_m^+ = 0$ (+), $b_m^+ = 10^{-8}$ (x), $b_m^+ = 10^{-3}$ ($*$), $b_m^+ = 0.1$ (empty boxes), and $b_m^+ = 10$ (filled boxes). Right: interfering mass(+) and combined model with $b_m^+ = 10^{-6}$ and $b_s^+ = b_s^{\circledcirc} = 10^{-8}$ (x).

2.4.4 Conclusions from the mass, spring length, and pinning disorder models

From the additive and interfering disorder models studied in this section, we have learnt the following:

- Interfering mass disorder effectively increases the mass, i.e. decreases the speed of sound, by a factor $1 - b_m^{\circledcirc}$ for weak ($b_m^{\circledcirc} < 1$) disorder. It leads to a critical transition at $b_m^{\circledcirc} = 1$ to a strongly disordered phase with a finite density of states at $\omega = 0$ in three dimensions.

- In coherent potential approximation (CPA), logarithmic divergences of the density of states of the interfering mass disorder model in *two dimensions* are found for critical and strong disorder.

- In the critical and strong-disorder phase in two dimensions, random pinning removes these logarithmic factors. In ≥ 3 dimensions at critical or strong disorder, the qualitative features of $\rho(\omega)$ are not changed by adding random pinning.

- In the weak-disorder (Debye) phase, random pinning leads to a gap in the spectrum.

- Additive mass disorder decreases the mass, i.e. increases the speed of sound, by a factor $1 + b_m^+$ and does not lead to a critical transition to a strong-disorder phase.
- Combining additive and interfering mass disorder also leads to a model without strong disorder phase, similar to the purely additive case. To get a transition to a non-Debye phase at finite disorder strength, it is crucial to implement the disorder such that the speed of sound can fluctuate down to zero, locally. For our mass disorder model this means that we must disorder in the interfering way.
- In particular, $\rho(\omega = 0)$ discontinuously drops to zero when an infinitesimal amount of additive mass disorder is added to the interfering mass disorder model in the strong-disorder phase. The size of the Debye-region which is created in the band centre however depends smoothly on $b_m^+ > 0$.
- For the interfering mass disorder model, we confirm the power laws that are predicted within coherent mass and Debye approximation by comparison to exact spectra for finite lattices with $n = d$ phonon bands.

Strictly speaking, the techniques used in this chapter do not allow us to disentangle the effect of random pinning spring and length disorder on the self-consistent level. The above formulations are supported by perturbative arguments in this chapter, but are confirmed in Section 3.2.

2.5 Band mixing disorder models

From our experience with the disorder models studies so far, we learn that the coherent springs matrix, $\mathcal{S}$, replacing the fluctuating S, must be proportional to the Laplacian in order to avoid the gapped phase. That is, disorder must not lead to an additive (scalar) contribution to $\mathcal{S}$, or, in other words, we are looking for a model with $\mathcal{S} \propto S_0$. This is another definition of the *spring constant* disorder model (see Section 2.2). We will show that both agree, i.e. that the model outlined in Section 2.2 does lead to $\mathcal{S} \propto S_0$ in Section 2.6. To get a feeling for how to implement spring constant disorder, we briefly describe a model, which might look promising at first but does nevertheless lead to pinning.

An admissible way (i.e. preserving positivity and symmetry of M and S) of implementing disorder is the following:

$$M = M_0 + R_m^T M_0 R_m \tag{2.43}$$

$$\text{and} \quad S = S_0 + R_s^T S_0 R_s \,. \tag{2.44}$$

The construction of this *band mixing disorder model* is even simpler than for the spring length disorder model considered above. There are no auxiliary intermediate spaces

and both $R_m : V_m \to V_m$ and $R_s : V_s \to V_s$ should be site diagonal. The effect of this kind of disorder is to mix and weight bands randomly. Of course, all disorder models considered in this thesis mix bands at some point, but here the structural aspects (compare to Figure 2.1 and 2.2) are provided by the deterministic part alone.

Using Gaussian disorder distributions once more, this model can be handled diagrammatically:

$$\langle f(R_x)\rangle \propto \int_{Loc} f(R_x) e^{-\frac{n}{2b_x}\operatorname{Tr} R_x^T R_x}\, dR_x\,. \tag{2.45}$$

In fact, the mass sector of this model is exactly the same (up to rescaling b_m) as for the additive mass disorder model and also the combined band mixing disorder diagrams are similar to the additive ones. We obtain:

$$\mathcal{M} = M_0 + \frac{b_m}{n}\operatorname{Tr}\left(\frac{M_0}{1 - M_0\frac{b_m}{n}\operatorname{Tr}(\mathcal{G}\mathcal{S})}\right) \tag{2.46a}$$

$$\mathcal{S} = S_0 + \frac{b_s}{n}\operatorname{Tr}\left(\frac{S_0}{1 - S_0\frac{b_s}{n}\operatorname{Tr}(\mathcal{G}\mathcal{M})}\right) \tag{2.46b}$$

$$\mathcal{G}^{-1} = z^2 + \mathcal{M}\mathcal{S}\,. \tag{2.46c}$$

Notice that both, coherent mass and coherent springs, have gained an additive term and $\mathcal{S}$ is *not* proportional to S_0. From the discussion in Section 2.4.1a and 2.4.2a, we learn that a scalar summand in $\mathcal{S}$ leads to a gap in the Debye phase. In fact, we can see already in Equation (2.44) that $S = S_0 + R_s^T S_0 R_s$ breaks global translation invariance, i.e. the zero modes of S_0 are not preserved. Also on the local scale, it is easy to spot that terms like $(\xi_i q_i - \xi_j q_j)^2$, for random ξ, break the invariance under global shifts of all q_i and lead to random pinning.

From Equations (2.46) we see that both types of disorder increase the speed of sound to leading order in small disorder strength. This is due to the additive nature of the model. We could now also study an interfering version, but in the mass sector this would be the same as the interfering mass model considered in Section 2.4.2b and in the spring sector it seems impossible to implement local band mixing without causing random pinning. For this reason, we refrain from developing the band mixing model further and rather turn to actual spring constant disorder.

2.6 Spring constant disorder models

The interfering mass disorder model with deterministic springs, studied in Section 2.4.2b, features a strong disorder phase that could explain the experimentally observed linear temperature dependence of the heat capacity. However, the inverse

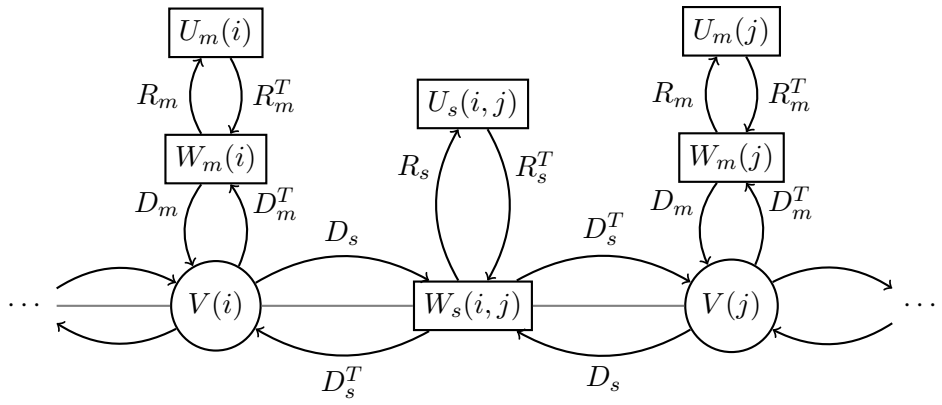

Figure 2.13: Sketch of two neighbouring physical spaces, $V(i)$ and $V(j)$, together with the auxiliary spaces located at the same sites or the shared edge as well as the action of R and D in the *mass and spring constant disorder* model.

mass fluctuating down to zero means that there are extremely heavy particles in the model, or that certain points are fixed, i.e. can not be accelerated. This is not likely generic the physical cause of the low energy modes. A more realistic model of a disordered solid should take randomness in the properties of the springs into account. We found that pinning leads to a gap in the weak-disorder phase, which is not observed in experiment. Moreover, it is hard to imagine pinning disorder in the bulk of a three dimensional material and a model of interfering spring *length* disorder without pinning is not studied diagrammatically to avoid technical difficulties. This will be remedied by supersymmetry in Chapter 3 but the aim of this section is to construct a model for spring *constant* disorder that does not lead to random pinning and can still be handled diagrammatically with ease.

2.6.1 Additive spring constant disorder

The discussion in Section 2.5 in view of Figure 2.2 indicates that we should locally multiply spring *constants* by random variables to produce a model, which preserves the invariance under global displacements. Schematically, $(\xi_{ij}(q_i - q_j))^2$ should be used instead of $(\xi_i q_i - \xi_j q_j)^2$. This leads us to construct the *additive spring constant disorder* model, which can be handled diagrammatically and does *not* introduce pinning. It is given by

$$M = M_0 + D_m^T R_m^T R_m D_m \tag{2.47a}$$

$$\text{and} \quad S = S_0 + D_s^T R_s^T R_s D_s \,. \tag{2.47b}$$

We recall that the target space for $D_s : V_s \to W_s$ has the physical meaning of spring elongations, explained in Section 2.2. In the spring constant disorder models, we have the freedom to introduce a new auxiliary target space for $R_s : W_s \to U_s$. As before, the mass sector is equivalent to the other versions of mass disorder introduced above, but to stress the duality of mass and spring constant disorder in this model, we use similar formulas for M and S in Equation (2.47a). We may also use two auxiliary spaces for the M sector, which will be associated with the sites. For the S sector, the auxiliary spaces are located on the links. D_m and D_s are as introduced in Section 2.1.1 with $W_i \simeq W_l \simeq V_i \simeq \mathbb{R}^n$ for $i \in C_0$ and $l \in C_1$. The new spaces are $U_m(i) \simeq \mathbb{R}^{\alpha_m n}$ and $U_s(l) \simeq \mathbb{R}^{\alpha_s n}$. Notice that the formal meaning of α in this model is slightly changed as compared to the spring length disorder model. See Figure 2.13 for a schematic picture of the spatial arrangement of auxiliary spaces. The appropriate spaces of local operators are given by site and link-diagonal operators:

$$L_m := \bigoplus_{i \in C_0} \{R_m(i) : W_m(i) \to U_m(i)\} \tag{2.48}$$

$$\text{and} \quad L_s := \bigoplus_{l \in C_1} \{R_s(l) : W_s(l) \to U_s(l)\} \tag{2.49}$$

and the probability measures are (as usual) Gaussian,

$$\langle f(R_s, R_m) \rangle = \int_{L_s} \int_{L_m} f(R_s, R_m) e^{-\frac{n}{2b_m} \operatorname{Tr} R_m^T R_m} \, dR_m \, e^{-\frac{n}{2b_s} \operatorname{Tr} R_s^T R_s} \, dR_s \,. \tag{2.50}$$

The diagrammatics for this model is the same as for the additive spring length and mass disorder model (see Section 2.3) with slightly changed meaning of the symbols. Now triangles include a factor of the corresponding square root of the deterministic part. The resulting SCE are

$$\mathcal{M} = M_0(1 + \alpha_m b_m B_m) \tag{2.51}$$

$$B_m^{-1} = 1 - \frac{b_m}{n} \operatorname{Tr}(M_0 \mathcal{G} \mathcal{S}) \tag{2.52}$$

$$\mathcal{S} = S_0(1 + \alpha_s b_s B_s) \tag{2.53}$$

$$B_s^{-1} = 1 - \frac{b_s}{n} \operatorname{Tr}(S_0 \mathcal{G} \mathcal{M}) \,. \tag{2.54}$$

These can be rewritten in a more compact form:

$$gz = 1 + (1 + \alpha_m b_m B_m) \frac{B_m - 1}{b_m B_m} = 1 + (1 + \alpha_s b_s B_s) \frac{B_s - 1}{b_s B_s} \tag{2.55a}$$

$$\text{and} \quad g = \frac{1}{n} \operatorname{Tr} \frac{z}{z^2 - \nu^2 (1 + \alpha_m b_m B_m)(1 + \alpha_s b_s B_s) \Delta} \,. \tag{2.55b}$$

Comparing Equation (2.55b) with (2.34d) and the discussion in Section 2.4.2a, we see that the spring constant disorder model is indeed gapless. The leading order effect of *additive* disorder is, as usual, to increase the speed of sound by $1 + b_s$. This can be seen directly by solving Equation (2.55a) for $z \to 0$, or by realising that *coherent* spring constant and mass disorder are equivalent. More precisely, there is an exact duality of exchanging b_s and b_m and relabeling B_s and B_m in Equations (2.55). The phenomenology of additive spring constant disorder is therefore the same as for the additive mass disorder in Section 2.4.1. Also the conclusion of Section 2.4.1 applies, namely the additive internal disorder model stays in the Debye phase and there is no strong disorder phase.

2.6.2 Interfering spring constant disorder

Gathering our experience from Section 2.4.4 and 2.6.1, it becomes clear that we should forge an *interfering spring constant disorder model* in order to combine the existence of a strong-disorder phase with the absence of pinning and the corresponding gap in the weak-disorder phase. This is done as follows:

$$M = D_m^T(\mathbf{1}_n + R_m)^T(\mathbf{1}_n + R_m)D_m \tag{2.56a}$$

$$S = D_s^T(\mathbf{1}_n + R_s)^T(\mathbf{1}_n + R_s)D_s\,, \tag{2.56b}$$

where we choose the dimensions to match, i.e. $\mathbb{R}^n \simeq V_m(i) \simeq W_m(i) \simeq U_m(i)$ and also $\mathbb{R}^n \simeq V_s(i) \simeq W_s(l) \simeq U_s(l)$ and $\mathbf{1}_n$ in Equations (2.56) stands for latter of these isomorphisms. Notice that all realisations of M and S are symmetric and positive, hence also this model is Lyapunov-stable. As mentioned in Section 2.6.1, the development focuses on the spring sector. M is written in a similar way only for convenience but is equivalent (up to rescaling b_m) to the interfering mass disorder model considered above.

We could combine additive and interfering disorder, as explained in Section 2.1.1, by choosing $U_m(i) \simeq \mathbb{R}^{(1+\alpha_m)n}$ and similarly for S. Although we learn from Section 2.4.3 that this is not a good idea if we want to get a strong disorder phase.

The diagrammatics for this model is exactly the same as for the interfering spring length and pinning disorder model explained in Section 2.7, except for the meaning of the triangle symbol. This now also includes a deterministic square root factor. Also the resulting SCE are similar to the ones discussed in Section 2.4.2, namely

$$\mathcal{M} = M_0 B_m(B_m + b_m) \tag{2.57a}$$

$$\mathcal{S} = S_0 B_s(B_s + b_s) \tag{2.57b}$$

$$gz = \frac{B_m(B_m + b_m - 1)}{b_m} = \frac{B_s(B_s + b_s - 1)}{b_s} \tag{2.57c}$$

$$g = \frac{1}{n}\operatorname{Tr}\frac{z}{z^2 + \mathcal{M}\mathcal{S}}\,. \tag{2.57d}$$

By construction, the coherent mass and springs are proportional to their deterministic values. As with the additive model, there is a duality of coherent masses and spring constants. The DOS will be discussed in the following, but we can already infer from the above mentioned duality between M and S sector that there will be a strong spring constant disorder phase.

2.6.2a Weak disorder

From Equation (2.57c) we can read off that for weak disorder ($b_m, b_s < 1$) we have $B_s(z=0) = 1 - b_s$ similar to B_m. Hence weak mass disorder rescales the inverse mass by $1 - b_m$, as before, and weak spring constant disorder does exactly the same, namely rescaling κ by $1 - b_s$. Therefore both types of disorder *decrease the speed of sound*,

$$\nu^2 \mapsto \nu^2(1 - b_s)(1 - b_m)\,. \tag{2.58}$$

In fact, as long as $b_s < 1$, we can apply the analysis of Section 2.4.2b. On the critical line, $b_m = 1$ for $b_s < 1$, the density of states shows the critical power law behaviour as discovered for the interfering mass disorder model, given in Equation (2.37). For strong mass, but weak spring constant disorder, $b_m > 1$ at $b_s < 1$, we find a finite density of states at zero. Its value is changed by a factor $(1 - b_s)^{-1/2}$ as compared to the interfering mass disorder model, see Equation (2.38). By the duality mentioned above, the $b_m < 1$ sector is the same as the $b_s < 1$ sector with the roles of b_m and b_s exchanged.

From now on, we restrict our attention to $d \geq 3$ dimensions. Here, summarising the above results, we have the following non-Debye phases:

- For $b_s < 1$ and $b_m > 1$, we have

$$\tilde{g}(z=0) = \frac{1}{\Omega b_m}\sqrt{\frac{b_m - 1}{1 - b_s}}\sqrt{\frac{d}{d-2}}\,. \tag{2.59a}$$

- For $b_m < 1$ and $b_s > 1$, roles are exchanged,

$$\tilde{g}(z=0) = \frac{1}{\Omega b_s}\sqrt{\frac{b_s - 1}{1 - b_m}}\sqrt{\frac{d}{d-2}}\,. \tag{2.59b}$$

- For $b_s < 1$ and $b_m = 1$, we have to leading order

$$\tilde{g} = \left(\frac{d}{(d-2)\Omega^2}\frac{1}{1-b_s}\right)^{\frac{2}{3}} \tilde{z}^{\frac{1}{3}}\,. \tag{2.60a}$$

- And for $b_s = 1$ and $b_m < 1$, again the same with exchanged roles

$$\tilde{g} = \left(\frac{d}{(d-2)\Omega^2}\frac{1}{1-b_m}\right)^{\frac{2}{3}} \tilde{z}^{\frac{1}{3}}\,. \tag{2.60b}$$

2.6.2b Critical disorder

For $b_s = b_m = 1$ there is a double-critical point in the phase diagram where the two critical lines intersect. Here, we have $B_m^2 = B_s^2 = gz$ and we find

$$\tilde{g}(z=0) = \frac{1}{\Omega}\sqrt{\frac{d}{d-2}} \tag{2.61}$$

in $d \geq 3$ dimensions. This is the continuation of Equation (2.59). For $b_s > 1$, $b_m = 1$, and $d \geq 3$ we find

$$\tilde{g} = \left(\frac{b_s - 1}{b_s^2 \Omega^2} \frac{d}{d-2}\right)^{\frac{2}{5}} \tilde{z}^{-\frac{1}{5}} \tag{2.62}$$

and similarly with b_s replaced by b_m for $b_s = 1$ and $b_m > 1$.

2.6.2c Strong disorder

The last regime to study is $b_m, b_s > 1$. Here, we find to leading order

$$\tilde{g} = \left(\frac{(b_s - 1)(b_m - 1)}{\Omega^2 b_s^2 b_m^2} \frac{d}{d-2}\right)^{\frac{1}{3}} \tilde{z}^{-\frac{1}{3}} \tag{2.63}$$

in $d \geq 3$ dimensions. This is the [LSZ06] phase and the only solution of the SCE that can be continuously connected across the dashed critical lines in Figure 2.14 to the phases of constant density of states. The solution with both $B_s(z=0) = 1 - b_s$ and $B_m(z=0) = 1 - b_m$ also leads to a positive (Debye-like) density of states, but the only way of reaching it continuously is through the double critical point.

2.6.3 Conclusions from the spring constant disorder models

The *interfering mass and spring constant disorder* (IMSC) model marks the point of culmination of this chapters model building efforts. It features disorder in the mass as well as in the springs sector, all realisations of disorder lead to stable dynamics and the physical symmetries, in particular time-reversal invariance and invariance under global translations, are preserved. Switching on disorder continuously modifies the clean density of states by decreasing the speed of sound up to a critical point. In the interesting critical and strong-disorder phases, the *coherent speed of sound*, $\mathcal{V}$, as a function of frequency vanishes at $\omega = 0$. The latter is defined to be the real part of coherent mass and springs, $-\mathcal{V}(\omega)\Delta := \Re(\mathcal{M}(\omega)\mathcal{S}(\omega))$, as a function of frequency. In the Debye phase, $\mathcal{V}$ determines the pre-factor of the Debye power law of the DOS. The phase diagram of the IMSC model is summarised in Figure 2.14.

In Figure 2.15 we speculate about the RG flow of the interfering internal disorder model. If the model is renormalisable with two couplings given by b_s and b_m, and

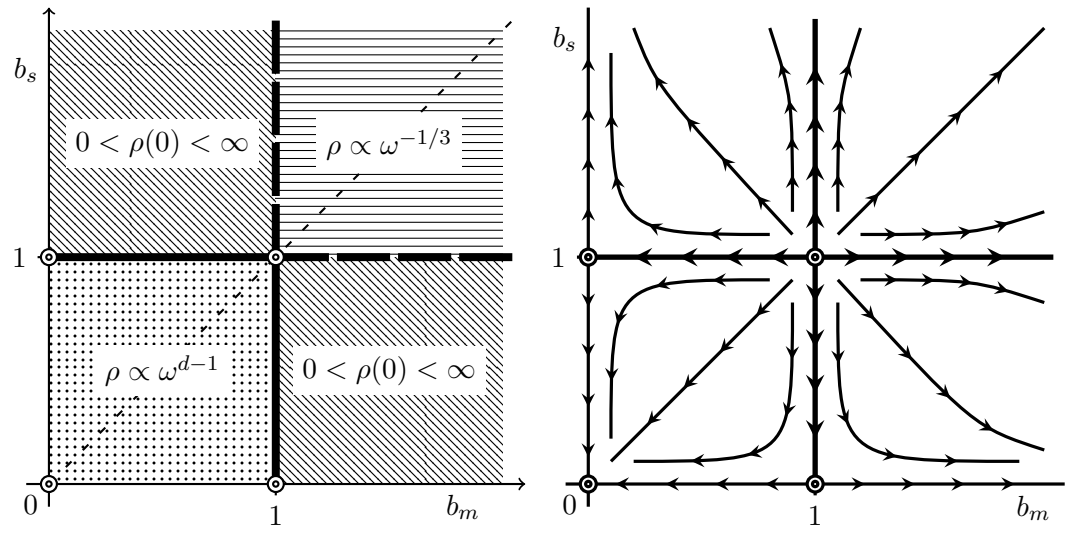

Figure 2.14: Left: Phase diagram of the IMSC model. There is an exact duality of exchanging b_m and b_s, i.e. upon reflecting the phase diagram at the diagonal. There are three extended phases: the Debye phase for $0 \leq b_m, b_s < 1$ marked with dots, the phase of finite DOS at zero frequency at $b_s < 1$ and $b_m > 1$, marked with diagonal lines, and the LSZ phase with $\rho \propto \omega^{-1/3}$ for $b_m, b_s > 1$, marked by horizontal lines. The weak disorder critical lines at $b_m = 1$ and $b_s < 1$ with $\rho \propto \omega^{1/3}$ are marked with bold solid lines and the strong disorder critical lines where $\rho \propto \omega^{-1/5}$ are marked with bold dashed lines. At the double-critical point at $b_m = b_s = 1$, the DOS at zero frequency is finite.

Figure 2.15: Right: Tentative RG flow diagram inferred from the positions of the four tentative critical points and the M-S-duality.

if the critical points have been correctly identified within our investigation of the mean-field density of states, then the flow diagram is strongly constrained. Assuming that changes the disorder strength are always relevant or irrelevant (but not marginal) only leaves two possibilities for the qualitative RG flow diagram, one of which is shown in Figure 2.15 and the other one is the same but with all arrows reversed. The decision which is the correct one boils down to whether the clean fixed point is stable or not. In both scenarios, a starting point in the $0 < \rho(0) < \infty$ phase will retain this property, either because it flows toward the double-critical point, or because it flows towards the interfering random mass model (or its dual) at strong disorder.

The computation of RG flow of the yet to be derived field theory remains a subject for future research. The first steps along this path up to the derivation of a suitable

Figure 2.16: Additional symbols for the square roots of the deterministic parts. The left one stands for D_m^T or D_{sp}^T and the right one for D_m or D_{sp}.

(super) lattice field theory will be presented in Chapter 3.

2.7 Interfering disorder diagrams

In this section we derive the self-consistency equations (SCE) for the interfering and combined mass, spring length, and pinning disorder models. The only constraint is that still spring length and pinning disorder must be of equal strength $b_s = b_p = b_{sp}$. In addition to the symbols used in Section 2.3 (see Figure 2.3), we also need a symbol for the deterministic square roots D. This is introduced in Figure 2.16.

Now the elementary contractions for our Gaussian integrals (as displayed in Figure 2.3) are:

$$\langle R_m^T R_m \rangle = (b_m^{\circledcirc} + b_m^{+})\mathbf{1}_N \quad \text{and} \quad \langle R_{sp}^T R_{sp} \rangle = d(b_{sp}^{\circledcirc} + b_{sp}^{+})\mathbf{1}_N \,. \tag{2.64}$$

At this elementary level, we can discriminate between the effects of spring length and pinning disorder:

$$\langle R_p^T R_p + R_s^T R_s \rangle \propto 2d\, b_p\, \mathbf{1} + \frac{1}{2}(b_p - b_s)\Delta \,. \tag{2.65}$$

This means that for $b_s = b_p$ we only see the effect of pinning, since the effect of spring constant disorder generating the Laplacian is precisely cancelled. For a more thorough discussion going beyond the perturbative level, see Section 3.2.

To calculate the Green's function g, the first steps of rewriting the resolvent operator and expanding the geometric series are the same as given in Section 2.3.1. Now the random part involves 15 terms:

$$\nu^{-2}\mathtt{R} := \nu^{-2}(MS - M_0S_0) = R_m^T R_m R_s^T R_s + D_m^T R_m R_s^T R_s + R_m^T D_m R_s^T R_s \tag{2.66}$$

$$+ R_m^T R_m D_s^T R_s + R_m^T R_m R_s^T D_s + D_m^T D_m R_s^T R_s + D_m^T R_m D_s^T R_s + \dots \,. \tag{2.67}$$

Note that $\mathtt{R}$ does *not* include $D_m^T D_m D_s^T D_s = M_0 S_0$.

To derive the rules of how to translate between diagrams and formulas, we will now examine a few diagrams in detail (given in Figure 2.17 to 2.19). The diagrammatic rules are then summarised in Section 2.7.1.

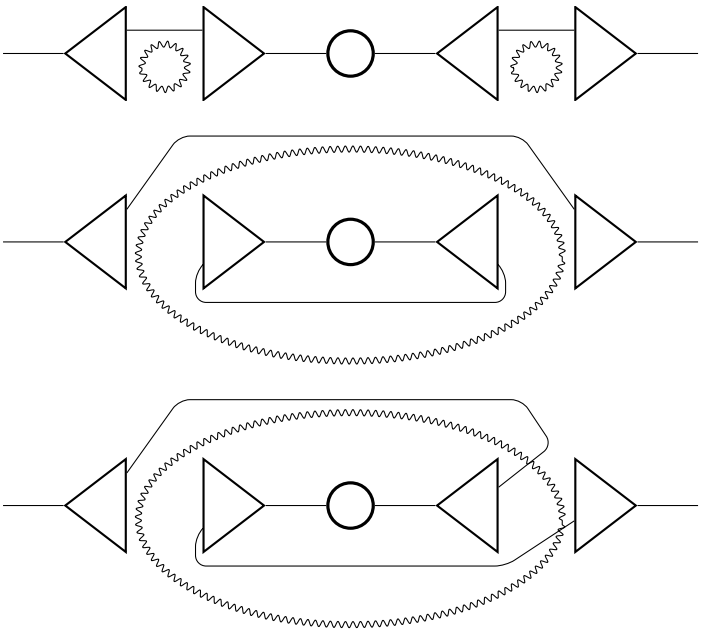

Figure 2.17: These diagrams represent the expansion of $\langle R_x^T R_x Y R_x^T R_x \rangle$, for $x \in \{m, sp\}$ and any deterministic matrix Y.

The contributions of the diagrams in Figure 2.17 for $x = m$ are (top to bottom)

$$\left(b_m^{\circledcirc} + b_m^{+}\right)^2 Y\,, \tag{2.68a}$$

$$\left((b_m^{\circledcirc})^2 + \frac{(b_m^{+})^2}{\alpha_m}\right) \frac{1}{n} \operatorname*{Tr}_{V(i)}(Y)\, 1_N\,, \tag{2.68b}$$

$$\text{and} \quad \left((b_m^{\circledcirc})^2 + \frac{(b_m^{+})^2}{\alpha_m}\right) \frac{1}{n} Y^T\,. \tag{2.68c}$$

For $x = sp$ in Figure 2.17 we have

$$\left(d(b_{sp}^{\circledcirc} + b_{sp}^{+})\right)^2 Y\,, \tag{2.69a}$$

$$d\left((b_{sp}^{\circledcirc})^2 + \frac{(b_{sp}^{+})^2}{\alpha_s}\right) \frac{1}{n} \operatorname*{Tr}_{V(i)}(Y) \mathbf{1}_N\,, \tag{2.69b}$$

$$\text{and} \quad \left((b_{sp}^{\circledcirc})^2 + \frac{(b_{sp}^{+})^2}{\alpha_s}\right) \frac{1}{4n}(4d + \Delta) Y^T\,. \tag{2.69c}$$

Notice that only the upper two diagrams are non-crossing and the third diagram is of

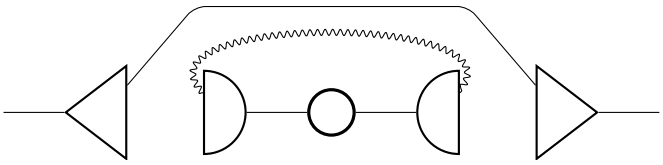

Figure 2.18: Diagram for $\langle R_x^T D_x Y D_x^T R_x \rangle$ (same notation as in Figure 2.17)

lower order in n.[8] The diagram in Figure 2.18 evaluates to

$$\frac{b_m^{\circledcirc}}{n} \operatorname{Tr}_{V(i)}(D_m^T D_m Y)\mathbf{1}_N \quad \text{for} \quad x = m \tag{2.70a}$$

$$\text{and} \quad \frac{b_s^{\circledcirc}}{n} \operatorname{Tr}_{V(i)}(D_s^T D_s Y)\mathbf{1}_N \quad \text{for} \quad x = sp\,. \tag{2.70b}$$

It might not be obvious which diagram comes with which geometric factor. To illustrate when the number of sites per link (2) or links per site ($2d$) comes in, we give a few instructive examples of more complicated diagrams involving R_{sp} in Figure 2.19. They evaluate to (top to bottom)

$$\left(\frac{b_{sp}^{\circledcirc}}{n}\right)^2 \operatorname*{Tr}_{V(i)}(Y) \operatorname*{Tr}_{V(i)}(D_S^T D_S Z)\mathbf{1}_N\,, \tag{2.71}$$

$$d\left(b_{sp}^{\circledcirc} + b_{sp}^{+}\right) \frac{b_{sp}^{\circledcirc}}{n} D_S^T D_S \operatorname*{Tr}_{V(i)}(YZ)\,, \tag{2.72}$$

$$\text{and} \quad \left(\frac{b_{sp}^{\circledcirc}}{n}\right)^2 \operatorname*{Tr}_{V(i)}(Y) \operatorname*{Tr}_{V(i)}(Z) D_S^T D_S\,. \tag{2.73}$$

These are also helpful for distinguishing b^{+} from $b^{\circledcirc}$ terms.

2.7.1 Diagrammatic rules

Starting from the diagrams explicitly evaluated in the last section, we derive the following rules for expanding $\langle g \rangle$ diagrammatically:

- All diagrams contributing to leading order (in n) are non-crossing.
- Each triangle has to be joined to a mirrored triangle with the same label by a vanilla line.
- Next to each vanilla line there runs a wiggly line (sometimes drawn elsewhere in the figures for aesthetic reasons).

[8] If we distinguish between pinning and spring constant disorder, the second diagram will produce terms proportional to $\sum_{i,j \in C_0} \Delta_{i,j} \operatorname{Tr}(\Delta_{i,j} Y)$, which are difficult to re-sum.

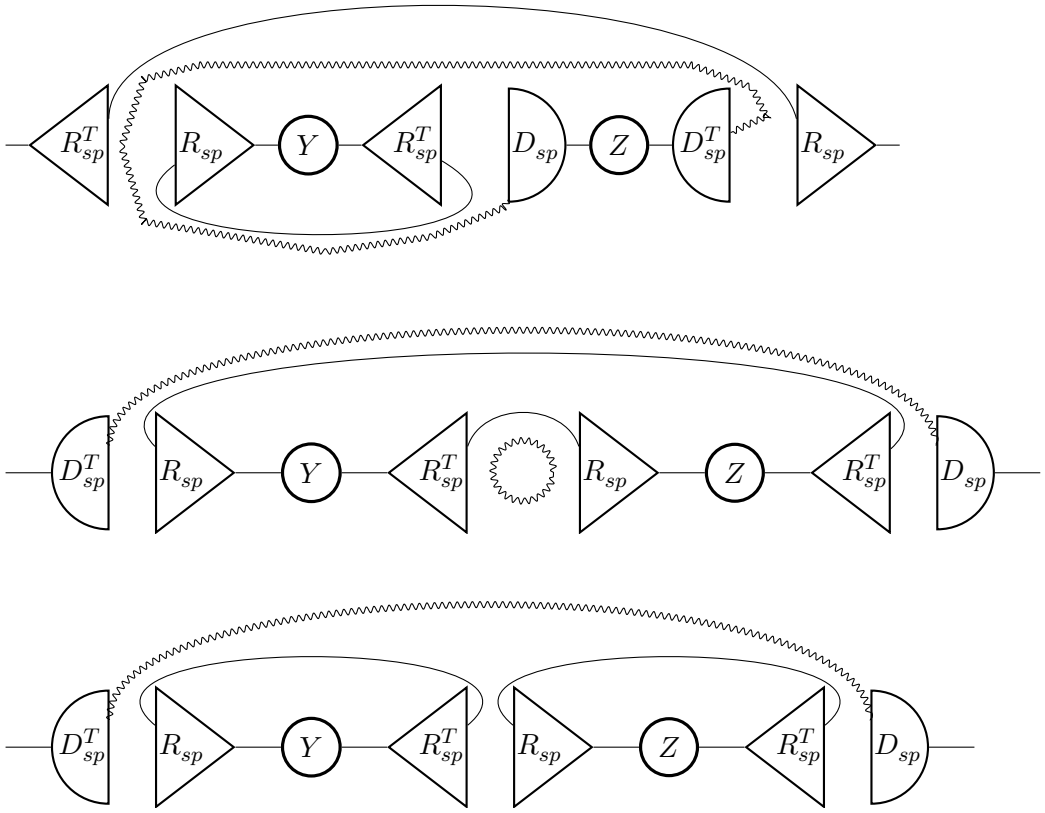

Figure 2.19: Here we depict examples of bigger diagrams which appear in the expansion of $\langle g \rangle$, where Y and Z are any matrices independent of R_{sp}.

- Round (deterministic) shapes have to be end points of the wiggly part of the double line.
- Triangles pass on wiggly lines (see Figure 2.19 and 2.20).
- For each pair of M triangles there is a factor $\mu^{-1} b_m^{\circledcirc}/n$.
- For each pair of S triangles there is a factor[9] $\kappa b_{sp}^{\circledcirc}/n$.
- Loops correspond to traces.
- If all shapes along a wiggly line are triangles then there is a free wiggly loop.

[9]Notice that there is a factor of two, which might stem from either of the geometric factors, 2 or $2d$. However, these factors are cancelled by each b_{sp} coming with a factor of $1/2$.

- Such free loops contribute an extra factor of n.
- If it is an S-type loop it contributes another factor of d.
- The factor of $(b_x^{\circledcirc})^k$ stemming from the triangles along the loop is replaced by $(b_x^{\circledcirc})^k + (b_x^{+})^k/\alpha_x^{k-1}$, for $x \in \{m, sp\}$.

Every time two non-neighbouring triangles are joined, a rainbow is created that spans over one or more *bubbles*. This is due to the non-crossing nature of all relevant diagrams. This is what implies that double lines (vanilla and wiggly) are to join pairs of shapes, which are mirror symmetric.

2.7.2 Self-consistency equation

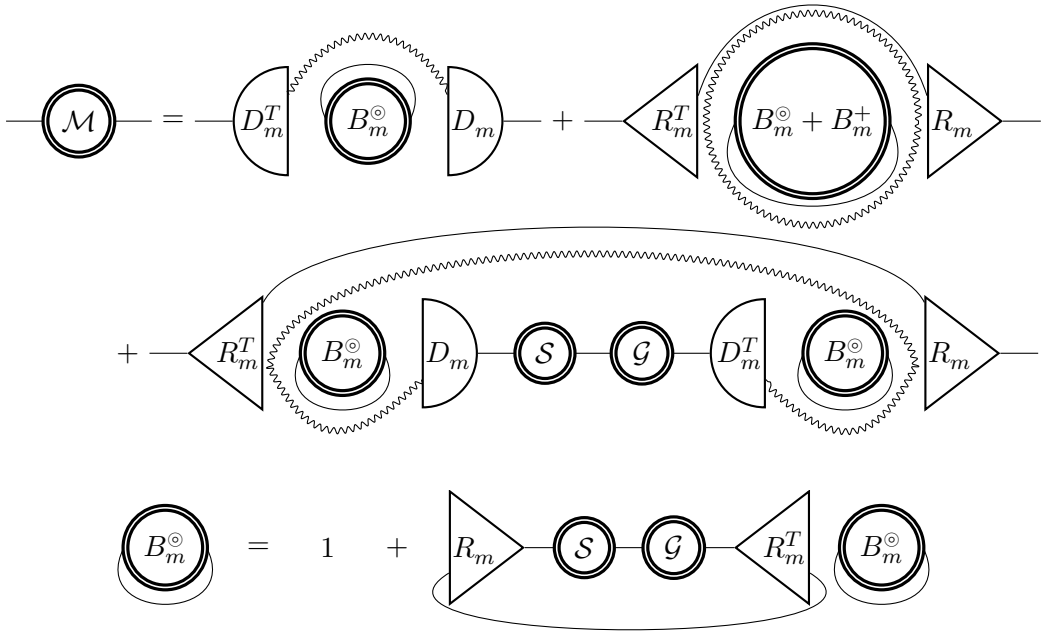

Figure 2.20: Diagrammatic derivation of the self-consistency equations for the coherent mass in the combined additive and interfering disorder model.

We can now translate pictures back into formulas to get the Green's function. Notice that $g = -z/N \operatorname{Tr}_N \mathcal{G} = -z/n \operatorname{Tr}_{V(i)} G$ for all $i \in C_0$ since the coherent mass $\mathcal{M}$ and coherent springs $\mathcal{S}$ are translation invariant. The diagrams in Figure 2.20 together with similar diagrams for the springs sector correspond to the following set of equations, determining $\mathcal{G} = (G_0^{-1} - \Sigma)^{-1} = -(z^2 + \mathcal{M}\mathcal{S})^{-1}$.

$$\mu\mathcal{M} = b_m^+ B_m^+ + B_m^\circledcirc \left(\mu M_0 + b_m^\circledcirc + b_m^\circledcirc B_m^\circledcirc \frac{1}{n} \operatorname{Tr}_{V(i)} (M_0 \mathcal{S}\mathcal{G})\right) \tag{2.74a}$$

$$\kappa^{-1}\mathcal{S} = d b_s^+ B_{sp}^+ + B_{sp}^\circledcirc \left(\kappa^{-1} S_0 + d b_{sp}^\circledcirc + b_{sp}^\circledcirc B_{sp}^\circledcirc \frac{1}{n} \operatorname{Tr}_{V(i)} (S_0 \mathcal{G}\mathcal{M})\right) \tag{2.74b}$$

$$(B_m^\circledcirc)^{-1} = 1 - \frac{b_m^\circledcirc}{\mu} \frac{1}{n} \operatorname{Tr}_{V(i)} (\mathcal{S}\mathcal{G}) \tag{2.74c}$$

$$(B_{sp}^\circledcirc)^{-1} = 1 - \kappa b_s^\circledcirc \frac{1}{n} \operatorname{Tr}_{V(i)} (\mathcal{G}\mathcal{M}) \tag{2.74d}$$

$$\left(B_m^+\right)^{-1} = 1 - \frac{b_m^+}{\mu\alpha_m} \frac{1}{n} \operatorname{Tr}_{V(i)} (\mathcal{S}\mathcal{G}) \tag{2.74e}$$

$$\left(B_{sp}^+\right)^{-1} = 1 - \kappa \frac{b_s^+}{\alpha_s} \frac{1}{n} \operatorname{Tr}_{V(i)} (\mathcal{G}\mathcal{M})\,. \tag{2.74f}$$

We have introduced B_x^+, which re-sums all irreducible diagrams containing b_x^+ terms. In terms of diagrams, this is the same sum over bubble diagrams as given for $B_m^\circledcirc$ in the lower part of Figure 2.20. Before we start investigating these equations, let us first change to natural units, $\tilde{z} := \frac{z}{\nu}$ and hence $\tilde{g} := \nu g$. We rewrite Equations (2.74) as

$$\mu\mathcal{M} = B_m^\circledcirc (b_m^\circledcirc + B_m^\circledcirc) + b_m^+ B_m^+ = \frac{1 - B_{sp}^\circledcirc}{b_{sp}^\circledcirc B_{sp}^\circledcirc} \frac{\tilde{z}}{\tilde{g}} = \alpha_s \frac{1 - B_{sp}^+}{b_{sp}^+ B_{sp}^+} \frac{\tilde{z}}{\tilde{g}} \tag{2.75a}$$

$$(B_m^+)^{-1} = 1 - \frac{b_m^+}{\alpha_m B_m^\circledcirc} \frac{B_m^\circledcirc - 1}{b_m^\circledcirc} \tag{2.75b}$$

$$b_m^\circledcirc \tilde{g}\tilde{z} = B_m^\circledcirc (B_m^\circledcirc + b_m^\circledcirc - 1) + b_m^+ \frac{B_m^+}{B_m^\circledcirc} (B_m^\circledcirc - 1) \tag{2.75c}$$

$$\text{and} \quad \tilde{g} = \frac{1}{n} \operatorname{Tr} \frac{\tilde{z}}{\tilde{z}^2 - \mu\mathcal{M} B_{sp}^\circledcirc \Delta + b_{sp}^\circledcirc \mu\mathcal{M}(d - 1 + \tilde{g}\tilde{z}) + d\, b_{sp}^+ \mu\mathcal{M} B_{sp}^+ (B_{sp}^\circledcirc)^{-1}}\,. \tag{2.75d}$$

Inserting Equations (2.75a) to (2.75c) into (2.75d) we obtain a single self-consistency equation that determines the complex parameter[10] $B_m^\circledcirc(z)$, which in turn determines all other parameters and in particular the Green's function, $g(z)$. For the discussion of the solutions of these equations, see Section 2.4.

2.7.3 Numerical solution of the self-consistency equation

In Section 2.4 and 2.6 we derived the leading order power law for $g(z)$ from the SCE (2.75). To verify our findings and to display the density of states at finite frequencies, we have also solved this self-consistency equation numerically.

[10] In the limit $b_m^\circledcirc \to 0$ one should rather use $(B_m^\circledcirc - 1)/b_m^\circledcirc$ as the one parameter to determine the rest.

The idea for the solver is to fix some $0 < \epsilon \ll \omega$ and a point $b = (b_m^\circledcirc, b_m^+, b_{sp}^\circledcirc, b_{sp}^+) \in (\mathbb{R}^+)^4$ very close to 0 and, using $(B_m^\circledcirc - 1)/b_m^\circledcirc$ as the relevant variable, search for a solution of Equation (2.34d). The deterministic solution is the initial starting point, then b is iteratively "increased" along a path towards the target point and the starting point for the search of the new solution is extrapolated from the solutions found in the last few steps. Concretely, to check whether the outcome is independent of the path, we have implemented a straight line from 0 to the target b and a path that is piecewise parallel to the axes, increasing the components one by one from 0 to their respective target values. The source code is available at [Sch14]. All numerical solutions of the SCE presented in this chapter were produced with this code.

2.8 Phase coherence length

Before concluding this chapter and turning our attention to the supersymmetry arguments in Chapter 3, we calculate the decay of the Green's function with spatial distance. Up to this point, we have only considered the space-diagonal components, $g(z) = G_{i,i}(z)$, where

$$\mathcal{G}_{i,j} = \frac{1}{n} \operatorname*{Tr}_{\mathbb{R}^n} \left\langle \pi_i \frac{z}{z^2 + MS} \pi_j \right\rangle_{\text{disorder}} . \tag{2.76}$$

Here π_i and π_j denote projectors onto $V(i)$ and $V(j)$, respectively.

We can read off the averaged resolvent operator, $\mathcal{G} = z(z^2 + \mathcal{MS})^{-1}$, from the self-consistency equations (2.74). In the strong disorder phase, $b_m^\circledcirc > 1$ with $g_0 := g(0) > 0$, its Fourier components to leading order in z are given by

$$\mathcal{G}_k(z) = \frac{z}{z^2 - cz\left(\sum_{i=1}^d \cos(k_i) - d\right)} . \tag{2.77}$$

For the interfering mass disorder model at strong disorder, we have $c = 2\nu^2 \frac{(b_m^\circledcirc)^2}{b_m^\circledcirc - 1} g_0$. Across all models, we find the extended strong disorder phase with a finite DOS at zero frequency as well as the double critical point of the interfering mass and spring constant disorder model to be characterised by Equation (2.77) with some $c > 0$ depending on the concrete model. Let us emphasise again that this is correct to leading order in z, i.e. for small frequencies. From here we can determine the phase coherence length by transforming back to $\mathcal{G}_x$. It is important that the Debye approximation for the momentum space integrals must *not* be used (or else smoothness of the integrand and the correct decay law for large $|x|$ is lost). Since x singles out one direction, we can use the complex analysis arguments given in Appendix A.1.2, namely

$$\mathcal{G}_x(z) = \int \frac{d^dk}{(2\pi)^d} \frac{e^{ik_d|x|}}{z - c\left(\sum_{i=1}^d \cos(k_i) - d\right)} \tag{2.78}$$

$$= \frac{1}{c} \int \frac{d^{d-1}k}{(2\pi)^{d-1}} \frac{\left(a_k \pm \sqrt{a_k^2 - 1}\right)^{-|x|}}{\pm\sqrt{a_k^2 - 1}}\,, \tag{2.79}$$

with $a_k := \frac{z}{c} + d - \sum_{i=1}^{d-1} \cos(k_i)$. Here we assume x to be parallel to the dth lattice vector, with no loss of generality (for large x). As mentioned in Equation (A.13b), the branch of the square root is to be chosen such that $\left|a_k \pm \sqrt{a_k^2 - 1}\right| > 1$, i.e. the integrand decays exponentially with $|x|$ everywhere (in k), as long as $\omega = \Im z \neq 0$. More precisely, for $0 < -i\hat{z} := -i\frac{z}{c} = \hat{\omega} \ll 1$ and $d > 1$, we have the following rough estimate

$$(2d)^{-|x|-1/2} < c\,|\mathcal{G}_x| < \frac{\left(1 + \sqrt{\hat{\omega}}\right)^{-|x|}}{\sqrt{\hat{\omega}}}\,, \tag{2.80}$$

which in particular yields a lower bound for $\rho(0) = \mathcal{G}_0(0)$ without using the Debye approximation. More importantly, phase correlations do decay exponentially with distance, if $\omega \neq 0$.

Since we are actually most interested in $\omega = 0$, we will now derive stronger estimates for this case. First using Equation (2.79) and then sending $\omega \to 0$, the integrand still has a pole at $k = 0$. It is integrable[11] if and only if $d > 2$, which hints at two being a critical dimension for the applicability of our coherent potential approximation. Assuming $d \geq 3$, we have the following estimate:

$$I_\varepsilon(c_1) < \tilde{c}|\mathcal{G}_x(0)| < I_\varepsilon(c_2) + c_3 d^{-x} \tag{2.81a}$$

$$\text{for} \quad I_\varepsilon(c) := c^{-1} \int_0^\varepsilon (1 + c|k|)^{-x}\, |k|^{d-3} d|k| \overset{d=3}{=} \frac{1 - \varepsilon c - (1 + \varepsilon c)^x}{c(1 - x)(1 + \varepsilon c)^x}\,, \tag{2.81b}$$

where $\tilde{c} = c(2\pi)^{d-1}/\operatorname{Vol}(S^{d-2}) > 0$, and we may choose $c_1 = 2$, $c_2 = (2d)^{-1}$, some irrelevant $c_3 > 0$, and a small enough $\varepsilon > 0$ for Equation (2.81a) to hold. In particular, $|\mathcal{G}_x(0)| \propto 1/|x|$ asymptotically for large x in three dimensions. In higher dimensions, similar expressions yield $|\mathcal{G}_x(0)| \propto 1/|x|^{d-2}$, asymptotically. Since $\mathcal{G}_x(0)$ does *not* decay exponentially, the phase coherence length must diverge for $\omega \to 0$.

Denoting this length by l, i.e. $|\mathcal{G}_x(i\omega)| \propto e^{-x/l(\omega)}$ asymptotically in x, we compute the integral in Equation (2.79) numerically for $d = 3$ to find $l(\omega) \propto \omega^\lambda$ for small ω with $\lambda = -1/2$. This is the result which one would guess from Equation (2.79), or

[11] This can also be seen in Equation (2.78), directly.

directly from Equation (2.78) with the denominator $i\omega \approx c|k|^2/2$ setting the scale for the exponent, ikx. In the critical phase with $\rho \propto \omega^{1/3}$, similar arguments yield $l \propto \omega^{-2/3}$ in $d = 3$ dimensions. Note that this decay of phase coherence does not imply localisation, nor is knowledge of $|\mathcal{G}|$ generally sufficient to make predictions about conduction. The point of this section is that the zero frequency modes are long-range correlated, even in the strong disorder phase where plenty of such modes exist.

3 Supersymmetric treatment

Similar to Chapter 2, the goal of this chapter is to compute the average density of eigenfrequencies (DOS) from the Green's function (as in Equation (2.2) and (2.3)) in coherent potential approximation (CPA). The supersymmetry technique is a little more involved than the diagrammatics used in Chapter 2, but it has the advantage that, apart from a substantial increase in mathematical rigour, we can now study the spring length disorder model without pinning. Furthermore, models of time-reversal invariance breaking disorder can be studied in order to compare to previous results. We re-derive the self-consistency equations (SCE) for the models studied in Chapter 2 and verify the validity of the series expansions and re-summations used above, which *a priori* might have been ill-defined. Further we also re-derive the SCE derived in [SZ10] and verify that the Hubbard-Stratonovich method used here yields the same results as the superbosonisation used there. A major conceptual advantage of supersymmetry is that the CPA is only the very last step in the derivation. Below we derive a lattice field theory, which exactly represents the Green's function for any number of bands. This may be used in future research to compute corrections to the CPA or proceed to a continuum theory of non-linear σ-model, or similar type, in order to study renormalisation.

The essential idea why supersymmetry might be helpful is

$$\mathrm{Tr}(z-X)^{-1} = \partial_{z_1}\big|_{z_1=z_2=z} \frac{\mathrm{Det}(z_1-X)}{\mathrm{Det}(z_2-X)} \tag{3.1a}$$

$$\text{and} \quad \frac{\mathrm{Det}(z_1-X)}{\mathrm{Det}(z_2-X)} = \underset{V\otimes\mathbb{C}^{1|1}}{\mathrm{SDet}} \left(\mathbf{1}_{2N}\otimes \mathrm{diag}(z_2|z_1) - X\otimes \mathbf{1}_{1|1}\right)^{-1}, \tag{3.1b}$$

where $\mathbb{C}^{p|q}$ denotes the super (i.e. $\mathbb{Z}_2$ graded) vector space $\mathbb{C}^p \oplus \mathbb{C}^q$, $\mathbf{1}_{p|q}$ the identity on this space and SDet the super determinant. Continuing from Equation (3.1b), one can rewrite the super determinant as a Gaussian super integral and then, paying close attention to convergence issues, interchange that integral with the Gaussian average over the random matrices. The details are explained in Section 3.3. An introduction to the relevant super calculus can be found in e.g. [Zuk94]. Some further details of the saddle-point (or "super Laplace") method are explained in Appendix A.2.

We will now introduce the time-reversal invariance breaking (TRIB) disorder model and present a *unified model* that encompasses TRIB, mass, spring length and pinning

disorder of arbitrary strength. Then we first discuss the resulting DOS for some sub-models before giving the details of the actual derivation in Section 3.3.

Since most disorder types are not introduced from scratch, the reader is advised to read Chapter 2 up to and including Section 2.2.1 before proceeding. Since neither spring length nor band mixing disorder is considered in this chapter, the time evolution generator will always be of the form $X = J(D+R)^T(D+R)$ where, as before, $J = i\sigma_2 \otimes \mathbf{1}_N$ denotes the symplectic unit, D is a deterministic (sparse) matrix which reproduces the clean limit (see Section 2.1.1), and R is a (sparse) matrix of Gaussian distributed random variables. In this chapter, it will be convenient to incorporate the factors of μ^{-1} and κ (see Equation 2.4) into D and R.

3.1 Time-reversal invariance breaking disorder

As explained in Chapter 2, we are primarily interested in time-reversal invariance *preserving* disorder. Nevertheless, we will also introduce time-reversal invariance *breaking* (TRIB) disorder types in this section. This will allow us to compare to our results obtained in [SZ10]. Within the supersymmetry method, the calculations for the TRIB model can be done along the way.

For this purpose, we use the mass, spring length and pinning disorder model of Section 2.4 for $(2-\beta) \in [0,1]$ of the phonon bands and a similar but time-reversal invariance breaking model for the remaining $\beta - 1$ bands. More precisely, we keep

$$W_s(l) \simeq \mathbb{R}^{(1+\alpha)(2-\beta)n} \qquad \text{located on the edges, } l \in C_1\,, \tag{3.2a}$$

$$\text{and} \quad W_m(i) \simeq \mathbb{R}^{(1+\alpha)(2-\beta)n} \qquad \text{located on the sites, } i \in C_0\,, \tag{3.2b}$$

both with slightly changed dimensions. We refrain from using different $\alpha \geq 0$ in the different sectors, since these turned out to be (qualitatively) irrelevant in Chapter 2. Instead we have introduced the parameter $\beta \in [1,2]$ to tune from the *time-reversal invariant model* at $\beta = 1$ to the TRIB model at $\beta = 2$. The larger β, the more of the disorder will be realised using a new auxiliary space,

$$W_{ms}(l) \simeq \mathbb{R}^{2(1+\alpha)(\beta-1)n}\,, \qquad \text{located on the edges, } l \in C_1\,. \tag{3.2c}$$

This new space serves as the target for $R_{ms} : V_m \oplus V_s \to W_{ms}$, which is constrained to map from a given site only to adjacent links. Further, the block of R_{ms} mapping from $V_m(i)$ to $W_{ms}(l)$ is non-zero only if i is the *starting* point of the directed link l. These locality constraints again ensure that mass disorder is site diagonal and random spring constants and pinning only couple nearest neighbours. Denoting the space of operators with these locality constraints, which are invariant under global displacements (see Section 2.2.1) by L_{ms} and the pinning-like complement by L_{mp}, we again use a Gaussian distribution of random variables,

$$\left\langle f\left(R^{\circledcirc}_{ms}+R^{+}_{ms}\right)\right\rangle \propto \int\limits_{L_{ms}} f\left(R^{\circledcirc}_{ms}+R^{+}_{ms}\right) e^{-\frac{\beta n}{\kappa b^{\circledcirc}_{ms}}\mathrm{Tr}(R^{\circledcirc}_{ms})^T R^{\circledcirc}_{ms}}\, dR^{\circledcirc}_{ms} \\ e^{-\frac{\alpha\beta n}{\kappa b^{+}_{ms}}\mathrm{Tr}(R^{+}_{ms})^T R^{+}_{ms}}\, dR^{+}_{ms}\,, \tag{3.3}$$

normalised to $\langle 1\rangle = 1$ and similarly for R_{mp}, to model TRIB disorder. We keep the old disorder types to be distributed as in Equation (2.10) and (2.12), apart from the minor modification of setting $\alpha_s = \alpha_m = \alpha$ and replacing b_m by $\mu^{-1}b_m/\beta$ and the other b_x by $\kappa b_x/\beta$.

The square roots of the deterministic part need to gradually change their target space in line with R as β increases. The factor 2 in the dimension of W_{ms} (see Equation (3.2c)) ensures that there is room for D_m and D_s to map into W_{ms} without their images intersecting. While D_s only changes target from $W_s(l)$ to the S subspace in $W_{ms}(l)$, D_m is now additionally distributed over $D_m : V_m(i) \to \sum_{(i,j)\in C_1} W_s(l)$ and all non zero matrix entries of D_m are changed[1] to $1/\sqrt{\mu d}$ in order to maintain $D_m^T D_m = M$. As opposed to the previous chapter, see Equation (2.5), D_m now has some structural importance in coupling positions and momenta in the interfering TRIB model.

3.1.1 Comparison of the TRIB model with [SZ10]

The saddle-point equations for the TRIB ($\beta = 2$) model, which ignores the difference between springs and pinning ($b_{ms} = b_{mp}$), are given in Equation (3.70). For the additive model, $b^{\circledcirc} = 0$, we can relabel $\hat{p} := 2p_1^+$, $\hat{b}_+ := \frac{4b^+}{\alpha}$ and $\hat{\alpha} := \alpha d$ to obtain

$$\frac{1}{\hat{b}^+} = \frac{\hat{\alpha}}{\hat{p}} - \frac{\hat{g}}{\hat{z}}\frac{\hat{p}+\mu^{-1}}{2} + \frac{gz-1}{2(\hat{p}+\mu^{-1})} \tag{3.4}$$

$$g = \int \frac{d^dk}{(2\pi)^d}\frac{z}{z^2+(\hat{p}+\mu^{-1})(\hat{p}-\kappa\Delta_k)}\,. \tag{3.5}$$

This is exactly the saddle-point equation and expression for the Green's function which we computed in [SZ10] by means of superbosonisation.

This model features a gap for all $0 < \hat{b}^+ < \infty$ as can be seen from the additive term in the denominator of the Green's function, which is caused by the presence of pinning disorder in the Debye phase (compare to Section 2.4.2d). Furthermore, there is no transition to a strong-disorder phase. In this thesis, we found the same phenomenology for all additive models with pinning, independent of time-reversal invariance being broken or not.

The strong-disorder phase, which we found in the *interfering* mass, spring length and pinning disorder model in Section 2.4.2, is absent in the interfering TRIB model.

[1] This splitting of D_m leads to a convenient separation of the additive and multiplicative sector in the time-reversal invariance breaking case, but is of no conceptual importance. One could as well choose one of the links at each vertex to host all of D_m.

The latter shows very similar behaviour to the additive TRIB model in that pinning in the Debye phase causes a gap for all $0 \leq b^{\circledcirc} < \infty$. We did not find any TRIB model with a strong-disorder phase.

3.2 Spring length disorder without pinning

We restore the differentiation between spring constant and pinning disorder, which was originally introduced in Section 2.2.1, Equation (2.12) but never used in Chapter 2 due to the technical difficulties that it causes for the diagrammatics. The supersymmetry method presented in this chapter can handle this additional feature with ease. We specialise the saddle-point equations derived for the unified model in Section 3.3.6 to $\beta = 1$ and $b_p = 0$. This leads to the following set of SCE for the (time-reversal invariant) *mass and spring length disorder* model:

$$g = \int \frac{d^d k}{(2\pi)^d} \frac{z}{z^2 - \mathcal{M}\mathcal{S}\Delta_k} \tag{3.6a}$$

$$\mu\mathcal{M} := \frac{1}{1+\tilde{p}_2^{m,\circledcirc}} + \mu\tilde{p}_1^m \qquad \kappa^{-1}\mathcal{S} := \kappa^{-1}\frac{p_1^s}{2d} + \frac{1}{1+p_2^{s,\circledcirc}} \tag{3.6b}$$

$$= \frac{b_m^{\circledcirc}(1-gz)}{\tilde{p}_2^{m,\circledcirc}} \qquad = \frac{b_s^{\circledcirc}(1-gz)}{dp_2^{s,\circledcirc}} \tag{3.6c}$$

$$\mu\tilde{p}_1^{m,\circledcirc} = \frac{1}{1+\tilde{p}_2^{m,\circledcirc}}\left(b_m^{\circledcirc} - \frac{\tilde{p}_2^{m\circledcirc}}{1+\tilde{p}_2^{m,\circledcirc}}\right) \quad \kappa^{-1}\tilde{p}_1^{s,\circledcirc} = \frac{2d}{1+\tilde{p}_2^{s,\circledcirc}}\left(b_s^{\circledcirc} - \frac{\tilde{p}_2^{s\circledcirc}}{1+\tilde{p}_2^{s,\circledcirc}}\right) \tag{3.6d}$$

$$\mu\tilde{p}_1^{m,+} = \frac{b_m^+}{1+\tilde{p}_2^{m,+}} \qquad \kappa^{-1}\tilde{p}_1^{s,+} = \frac{2db_s^+}{1+\tilde{p}_2^{s,+}} \tag{3.6e}$$

$$\tilde{p}_2^{m,+} = \frac{b_m^+}{\alpha b_m^{\circledcirc}}\tilde{p}_2^{m,\circledcirc} \qquad \tilde{p}_2^{s,+} = \frac{b_s^+}{\alpha b_s^{\circledcirc}}\tilde{p}_2^{s,\circledcirc} \tag{3.6f}$$

Notably, the M and S sector are almost decoupled. The two sets of equations describing the two sectors are similar, but this should not be thought of as a "duality", like the one that we found for the interfering internal disorder model in Section 2.6.2. The reason is that the various factors of d in the S sector make a matching impossible. More precisely, the above equations for the M sector lead to

$$b_m^{\circledcirc} gz = \frac{b_m^{\circledcirc} + p_2^{m,\circledcirc}(b_m^{\circledcirc}-1)}{(1+p_2^{m,\circledcirc})^2} - \frac{b_m^+ p_2^{m,\circledcirc}}{1+p_2^{m,+}}\,, \tag{3.7}$$

which is well known from Section 2.4. For $z \to 0$ at $b_m^+ = 0$, this equation has two solutions, namely $\tilde{\mu}p_2^{m,\circledcirc} = \frac{b_m^{\circledcirc}}{1-b_m^{\circledcirc}}$ leading to $\mathcal{M} = \mu^{-1}(1-b_m^{\circledcirc})$ and $\tilde{p}_2^{m,\circledcirc} \to \infty$ leading to $\mathcal{M} = 0$. The phase transition to a strong-disorder phase occurs as the two solutions

meet at $b_m^\circledcirc = 1$, as discussed in Section 2.4.2. The corresponding equation in the S sector reads

$$b_s^\circledcirc gz = \frac{b_s^\circledcirc + p_2^{s,\circledcirc}(2b_s^\circledcirc - d(b_s^\circledcirc + 1)) + (1-d)b_s^\circledcirc(\tilde{p}_2^{s,\circledcirc})^2}{(1+p_2^{s,\circledcirc})^2} - \frac{db_s^+ p_2^{s,\circledcirc}}{1+p_2^{s,+}}\,. \tag{3.8}$$

It has three solutions in the interfering, i.e. $b_s^+ = 0$, as well as in the additive, i.e. $b_s^\circledcirc = 0$, case, none of which meet for any disorder strength. The situation is similar to the one in the M sector for the additive or combined disorder model, described in Sections 2.4.1 and 2.4.3. namely, $\mathcal{S}(z=0)$ stays finite everywhere in parameter space and there is no transition out of the Debye phase.

The phase diagram of the interfering mass and spring disorder model is the same as the one of the interfering mass disorder model discussed in Section 2.4.2b, i.e. there is a Debye phase at low mass disorder, terminated by a critical point for $b_m^\circledcirc = 1$ and a strong disorder phase with a finite CPA DOS at zero frequency in $d \geq 3$ dimensions. Spring length disorder of any strength rescales the speed of sound but has no qualitative effect in any of these phases. This is in accordance with the findings of [JSS83]. Similarly, the additive scenario is qualitatively the same as the one with only mass disorder described in Section 2.4.1, i.e. there is no phase transition and the system stays in the Debye phase. Also the random matrix limits of the additive and interfering models, $\mu^{-1} \to 0$ and $\kappa \to 0$, are qualitatively the same as for the models with mass disorder only.

We will now present the supersymmetric derivation of the saddle-point equations in detail. Further conclusions from the unified model are mentioned in the summary in Chapter 4.

3.3 Supersymmetry for the unified model

In this section we will present the derivation of the super lattice field theory and the saddle-point equations. It will be convenient to combine $D = D_s \oplus D_m = D_s\pi_s^V + D_m\pi_m^V$, where π_x^V projects onto the x sector in V. Similarly $R = R_m \oplus (R_s + R_p) \oplus (R_{ms} + R_{mp})$ denotes the (Hilbert-Schmidt) orthogonal sum over all types of disorder. For $\beta = 1$ and $b_m = b_s = b_{sp}$ we get the same model as in Chapter 2 (see Equation (2.13)), due to $2R_s := R - \Pi(R)$.

3.3.1 Linear super fields

Instead of using Equation (3.1b) directly, we take the following "detour".[2]

[2]For the additive disorder (sub-)model this enlarging of the determinant is not necessary. There one can use Equation (3.1b) directly and proceed by superbosonisation. Instead, since interfering disorder is present, we will instead invoke a Hubbard-Stratonovich transformation, for which it is convenient, if not essential, that the exponents in Equation (3.9c) and (3.10) are linear in R.

$$\underset{V}{\mathrm{Det}}^{-1}(z-X) = \underset{V}{\mathrm{Det}}^{-1}\left(z - J(R+D)^\dagger(R+D)\right) \tag{3.9a}$$

$$= z^{-\Delta\,\mathrm{dim}} \underset{W\oplus V}{\mathrm{Det}} \begin{pmatrix} z\,\mathbf{1}_W & i(R+D) \\ i(R+D)^T & J \end{pmatrix}^{-1} \tag{3.9b}$$

$$= z^{-\Delta\,\mathrm{dim}} \int\limits_{(W\oplus V)\otimes\mathbb{R}^2} \prod_{j=1}^{2} d(w_j, v_j)\; e^{-z w_j^T w_j - v_j^T J v_j - i(w_j^\dagger (R+D) v_j + v_j^\dagger (R+D)^\dagger w_j)} \tag{3.9c}$$

$$\text{with} \quad \Delta\,\mathrm{dim} := \mathrm{dim}(V) - \mathrm{dim}(W) = L^d n(2 - (2 - \beta + \beta d)(1+\alpha))\,. \tag{3.9d}$$

The integral converges[3] because the spectrum of the matrix in (3.9b) is a subset of $i\mathbb{R} + \mathbb{R}^+$, i.e. $\Re(z) \in \mathbb{R}^+$ and R and D are real matrices.[4] Notice that we could have introduced complex integration variables v and w to conveniently get the correct power of the determinant. Instead the integration domain is written as $\mathbb{C} \simeq \mathbb{R}^2$ and the exponent in Equation (3.9c) as a bi-linear (instead of sesqui-linear) form. This point of view will be more convenient in the odd sector and crucial in Sections 3.3.3 and 3.3.4 below. The numerator is written as a Grassmann integral

$$\underset{V}{\mathrm{Det}}(z-X) = z^{\Delta\,\mathrm{dim}} \int\limits_{(W\oplus V)\otimes\mathbb{R}^{0|2}} d(\xi, \bar{\xi}, \chi, \bar{\chi})\; e^{z\bar{\xi}^T\xi + \bar{\chi}^T J \chi + i(\bar{\xi}^T (R+D)\chi + \bar{\chi}^T (R+D)^T \xi)}\,. \tag{3.10}$$

Notice that there is no convergence issue for Grassmann integration, however the sign in the exponent depends on the chosen order of differentials in the Berezin form, i.e. on the order of differentiation.

The next step is to gather the integration variables into the following super matrices:

$$\Psi := \begin{pmatrix} v_1^T \\ v_2^T \\ \frac{1}{2}\left(\bar{\chi}^T - \chi^T\right) \\ \frac{1}{2}\left(\chi^T + \bar{\chi}^T\right) \end{pmatrix} \qquad : V \to T_1 \simeq \mathbb{R}^{2|2}\,, \tag{3.11a}$$

[3] For oscillatory integrals, i.e. if the covariance matrix of a Gaussian integral has purely imaginary eigenvalues, convergence here and in the following is meant in the weak sense.

[4] To translate the endomorphism in Equation (3.9b) into a bi-linear form in Equation (3.9c), we choose the isomorphisms $V \simeq V^*$ given by the basis of position and momentum operators used throughout. Further we have introduced $W \simeq W^*$ to come with a Euclidean structure from the beginning.

$$\Phi := \begin{pmatrix} w_1^T \\ w_2^T \\ \frac{1}{2}\left(\bar{\xi}^T - \xi^T\right) \\ \frac{1}{2}\left(\xi^T + \bar{\xi}^T\right) \end{pmatrix} \qquad : W \to T_2 \simeq \mathbb{R}^{2|2}\,, \tag{3.11b}$$

$$\Psi^\dagger := \Psi^T \varsigma_{12} = \left(v_1, v_2, \frac{\chi + \bar{\chi}}{2}, \frac{\chi - \bar{\chi}}{2}\right) \qquad : T_2 \to V\,, \tag{3.11c}$$

$$\text{and} \quad \Phi^\dagger := \Phi^T \varsigma_{21} = \left(w_1, w_2, \frac{\xi + \bar{\xi}}{2}, \frac{\xi - \bar{\xi}}{2}\right) \qquad : T_1 \to W\,. \tag{3.11d}$$

Here the target spaces of Φ and Ψ are considered as two *different*[5] real linear super spaces $T_1 \simeq T_2 \simeq \mathbb{R}^{2|2}$. From this point of view, we use isomorphisms $\varsigma_{ij} : T_j \xrightarrow{\sim} T_i$, $Z : T_2 \xrightarrow{\sim} T_1$, and $\tau : T_1 \xrightarrow{\sim} T_2$ to express "Grassmann conjugation" and the original matrices in Equation (3.9c) and (3.10) in terms of the new super matrices,

$$-\operatorname*{STr}_{T_1}\left(Z\Phi\Phi^\dagger\right) = -z_2(w_1^T w_1 + w_2^T w_2) + z_1 \bar{\xi}^T \xi\,, \tag{3.12}$$

$$2\operatorname*{STr}_{T_2}\left(\Phi D \Psi^\dagger\right) = 2\operatorname*{STr}_{T_1}\left(\Psi D^T \Phi^\dagger\right) \tag{3.13}$$

$$= \sum_{j=1}^{2}\left(w_j^T D v_j + v_j^T D^T w_j\right) - \xi^\dagger D \chi - \chi^\dagger D^T \xi\,, \tag{3.14}$$

$$\text{and} \quad \operatorname*{STr}_{T_2}\left(-\tau \Psi J \Psi^\dagger\right) = v_1^T J v_1 + v_2^T J v_2 - \chi^\dagger J \chi\,. \tag{3.15}$$

In the bases introduced along with the T_i and fixed from here on, ς_{12} and ς_{21} have the same matrix form, ς. With this notation, the matrices of the isomorphisms are

$$\varsigma := \operatorname{diag}(\mathbf{1}_2 \,|\, -i\sigma_2), \quad \tau := \operatorname{diag}(\sigma_2|\sigma_1), \quad \text{and} \quad Z := \operatorname{diag}(z_2|z_1) \otimes \mathbf{1}_2\,. \tag{3.16}$$

Notice that both, Ψ and Φ, live in *real* linear super spaces.

3.3.2 Disorder average

To calculate the disorder average, we will need to complete squares similar to

$$\begin{aligned} \sum_t \operatorname{Tr} R_t^T R_t \xmapsto{R_t \mapsto R_t + \Phi_t^\dagger \Psi_t} \sum_t \operatorname{Tr} R_t^T R_t + \sum_{j=1}^{2}\left(w_j^T R v_j + v_j^T R^T w_j\right) \\ - \xi^\dagger R \chi - \chi^\dagger R^T \xi + \sum_{t \in T} \operatorname{STr} \Phi_t \Phi_t^\dagger \Psi_t \Psi_t^\dagger\,. \end{aligned} \tag{3.17}$$

[5]The distinction between T_1 and T_2 might seem artificial at present, but will become very natural in the Hubbard-Stratonovich transformation in Section 3.3.3.

The important point here is that R can only be shifted by local operators in the appropriate space, L_t. In particular, also time-reversal invariance, if present, and the disorder type are passed on. In order to maintain a unified notation, we will use a combined label

$$t \in T := T_m \times C_0 \cup T_s \times C_1 \,, \tag{3.18}$$

$$\text{where} \quad T_s := \{s, p, ms, mp\} \times \{+, \circledcirc\} \tag{3.19}$$

$$\text{and} \quad T_m := \{m\} \times \{+, \circledcirc\} \,. \tag{3.20}$$

The meaning of most of these labels should be clear, like $\Psi_{i,m} := \Psi \pi_m^V \pi_i^V$ where $\pi_i^V : V \twoheadrightarrow V(i)$ for $i \in C_0$ and $\pi_m^V : V \twoheadrightarrow V_m$ project out the rest of the direct sum in the definition of V. I.e. $\Psi_{i,m}$ is obtained from the matrix Ψ by replacing most blocks with zeros. To keep track of the difference between spring length and pinning, we have further introduced $\Psi_{p/s,(i,j)}$. Here we need to swap blocks, as can be seen from Equation (2.11). More precisely, $\Psi_{p/s,(i,j)}$ has two non-vanishing blocks, $\Psi_{p/s,(i,j)} = \Psi_{p/s,(i,j)}(\pi_i^V + \pi_j^V)$. The blocks are either the same, given by the sum of the original blocks, or the negative of each other, given by the difference,

$$\Psi_{p/s,(i,j)} = \frac{1}{2}(\Psi \pm \Pi_{i,j}(\Psi))\pi_s^V(\pi_i^V + \pi_j^V) \,. \tag{3.21}$$

The definitions for the time-reversal invariance breaking sectors, mp and ms, are the same without projecting onto the s sector. Since not all spaces have different sectors for every disorder type, some labels are ignored, like $\Phi_p = \Phi_s$, $\Phi_{mp} = \Phi_{ms}$, and $\Psi^+ = \Psi^\circledcirc = \Psi$. All of the above definitions for the daggered versions are similar.

With this notation in place, we can write the actual disorder average compactly as

$$\begin{aligned} \prod_{t \in T_m \cup T_s} \int_{L_t} & e^{-\frac{\alpha_t \beta n}{2b_t} \operatorname{Tr} R_t^T R_t} e^{-i(v^\dagger R_t w + w^\dagger R_t^T v) + i(\xi^\dagger R_t \chi + \chi^\dagger R_t^T \xi)} \, dR_t \\ &= \prod_{t \in T} e^{-\frac{2b_t}{\alpha_t \beta n} \operatorname{STr} \Phi_t \Phi_t^\dagger \Psi_t \Psi_t^\dagger} \,, \end{aligned} \tag{3.22}$$

where spatial labels on α and b are ignored and we denote $\alpha_m^+ := \mu\alpha$, $\alpha_{s/p/ms/mp}^+ := 2\alpha/\kappa$, $\alpha_m^\circledcirc := \mu$, and $\alpha_{s/p/ms/mp}^\circledcirc := 2/\kappa$ to unify the notation.

Collecting the terms from Equation (3.12) to (3.15) and (3.22), we arrive at the intermediate result

$$\left\langle \frac{\operatorname{Det}(z_1 - X)}{\operatorname{Det}(z_2 - X)} \right\rangle \propto \left(\frac{z_1}{z_2}\right)^{\Delta \dim} \iint_{(W \oplus V) \otimes \mathbb{C}^{1|1}} d(\Phi, \Psi) e^{-\operatorname{STr} L(\Phi, \Psi)} \tag{3.23a}$$

$$\text{with} \quad L(\Phi, \Psi) := Z \Phi \Phi^\dagger + i(\Phi D \Psi^\dagger + \Psi D^T \Phi^\dagger) + \tau \Psi J \Psi^\dagger \tag{3.23b}$$

$$+ \sum_{t \in T} \frac{2b_t}{\beta \alpha_t n} \Phi_t \Phi_t^\dagger \Psi_t \Psi_t^\dagger \,. \tag{3.23c}$$

Here the integration is over the original variables, $(V \oplus W) \otimes \mathbb{R}^{2|2}$, introduced in Equations (3.9c) and (3.10), or, equivalently, over the linear super fields $(\Phi, \Psi) : W \oplus V \to \mathbb{R}^{2|2}$.

3.3.3 Schäfer-Wegner Hubbard-Stratonovich transformation

As long as only additive disorder is considered, as in [SZ10], no square roots of the deterministic part are needed. In this case, $b^{\circledcirc} = 0$, the $\Phi^{\circledcirc}$ fields in Equation (3.23) can be integrated out and the resulting action for the additive sector will only depend on Φ^+ through the combination $\Phi\Phi^\dagger$, which is invariant under the action of the orthogonal group of W. This case is ideally suited to apply superbosonisation (see [LSZ07]), but $\Phi D \Psi^\dagger$ breaks this symmetry in the interfering sector. If $b^{\circledcirc} > 0$ and the corresponding quartic terms are present, we need to adapt the Schäfer-Wegner version (see [SW80]), as used in [Zir98], of the Hubbard-Stratonovich transformation to the symmetries of our model in order to reduce the dimension of the domain of integration.

We will carefully explain how the transformation works in the boson-boson sector, for which matters of convergence are non-trivial. The fermion-fermion sector turns out to be less problematic and, as usual, there are no convergence issues in the odd sectors.

To concisely phrase the symmetries of our model, let $\tilde{\gamma}_B := i\sigma_2 \otimes \mathbf{1}_2$ and $\eta := \sigma_1 \otimes \mathbf{1}_2$, i.e. $\tilde{\gamma}_B^\dagger = \tilde{\gamma}_B^T = \tilde{\gamma}_B^{-1}$ is a symplectic unit and $\eta^\dagger = \eta^T = \eta = \eta^{-1}$ a symmetric swap. Then, for each $t \in T$, we assemble

$$\psi_t := \begin{pmatrix} (\Psi_t^\dagger)_B & 0 \\ 0 & (\Phi_t^\dagger)_B \end{pmatrix} \tag{3.24}$$

to write the term whose dual we are looking for as

$$\tilde{\psi}_t \psi_t := \eta \psi_t^\dagger \psi_t = \begin{pmatrix} 0 & \left(\Phi_t \Phi_t^\dagger\right)_{BB} \\ \left(\Psi_t \Psi_t^\dagger\right)_{BB} & 0 \end{pmatrix} \tag{3.25}$$

$$= -\operatorname{Ad}(\tilde{\gamma}_B)(\tilde{\psi}_t \psi_t)^T = \operatorname{Ad}(\eta)(\tilde{\psi}_t \psi_t)^\dagger. \tag{3.26}$$

Notice that, depending on t, ψ_t either lives on the sites or the links and either Ψ_t or Φ_t is a sum over the adjacent links/sites.

The above symmetries can be concisely phrased as $\tilde{\psi}_t \psi_t \in i\mathfrak{g}_{\mathbb{R}}$ once we have introduced the *complex* Lie algebra

$$\mathfrak{g} = \mathfrak{k} \oplus \mathfrak{p} := \{x = -\operatorname{Ad}(\tilde{\gamma}_B) x^T\} = \mathfrak{sp}(4) \tag{3.27}$$

with (non-standard but still non-compact) *real form*

$$\mathfrak{g}_{\mathbb{R}} := \{x \in \mathfrak{g} \mid x = -\operatorname{Ad}(\eta) x^\dagger\} \tag{3.28}$$

and corresponding Cartan decomposition

$$\mathfrak{k} := \{x \in \mathfrak{g} \mid x = \mathrm{Ad}(\eta)x\}, \quad \mathfrak{p} := \{y \in \mathfrak{g} \mid y = -\mathrm{Ad}(\eta)y\}, \tag{3.29}$$

which means $\eta \in i\mathfrak{k}_{\mathbb{R}}$. By construction $\tilde{\psi}_t\psi_t = -\mathrm{Ad}(\sigma_3 \otimes \mathbf{1})(\tilde{\psi}_t\psi_t)$ is an additional symmetry (i.e. $\tilde{\psi}_t\psi_t$ is block off-diagonal), which we do not incorporate into $\mathfrak{g}$ explicitly for the sake of clarity of the following calculations.

We will now explain the Hubbard Stratonovich transformation given in Equation (3.46) below. See Section 3.3.3d for a summary.

3.3.3a Embedding

There is an embedding of smooth manifolds

$$\iota_B : \mathfrak{k}_{\mathbb{R}} \oplus \mathfrak{p}_{\mathbb{R}} \hookrightarrow \mathfrak{g} \ : x \oplus y \mapsto x - \mathrm{Ad}(e^y)\eta\,. \tag{3.30}$$

Whilst smoothness of ι_B is clear, injectivity requires some elaboration. We rewrite

$$\mathrm{Ad}(e^y)\eta = \cosh(\mathrm{ad}(y))\eta \oplus \sinh(\mathrm{ad}(y))\eta \in i\mathfrak{k}_{\mathbb{R}} \oplus i\mathfrak{p}_{\mathbb{R}}. \tag{3.31}$$

Since $y \in \mathfrak{p}_{\mathbb{R}}$, we have $\mathrm{ad}(y)\eta = 0$ only if $y = 0$. So ι_B is an immersion. Further, since y is hermitian, so is $\mathrm{ad}(y)$, with respect to the Hilbert-Schmidt scalar product. Hence $\sinh \circ \mathrm{ad}\,|_{\mathfrak{p}_{\mathbb{R}}}$ is injective.

3.3.3b Hubbard-Stratonovich integral

The following integral converges for any $\upsilon \in \mathbb{R}^+$ and $\Upsilon \in \mathbb{C}$:

$$\int\limits_{\mathfrak{g}_{\mathbb{R}}} e^{\upsilon \,\mathrm{Tr}(\iota_B(g))^2} dg = \int\limits_{\mathfrak{g}_{\mathbb{R}}} e^{\upsilon \,\mathrm{Tr}(\iota_B(g) + \Upsilon \tilde{\psi}_{i,k}\psi_{i,k})^2} dg\,. \tag{3.32}$$

$$\text{Here} \quad \mathrm{Tr}(\iota_B(g))^2 = -\mathrm{Tr}(xx^\dagger) - 2\,\mathrm{Tr}\,(x\cosh(\mathrm{ad}(y))\eta) + \mathrm{Tr}\,\eta^2 \tag{3.33}$$

due to $\mathfrak{k}_{\mathbb{R}} \perp \mathfrak{p}_{\mathbb{R}}$, where $\mathrm{Tr}(xx^\dagger) \in \mathbb{R}^+$ amounts to a standard real Gaussian integral on $\mathfrak{k}_{\mathbb{R}}$ and $\mathrm{Tr}\,(x\cosh(\mathrm{ad}(y))\eta) \in i\mathbb{R}$ is oscillatory. Further, as stated in Equation (3.32), Stokes' theorem applies. Using Section 3.3.3a, we can consider the push forward through ι as an integral over a smooth sub-manifold of $\mathfrak{g}$ without boundary. Since the integrand is non-singular, we can freely shift that contour.

We rewrite Equation (3.32) with appropriately normalised measure as

$$e^{-\frac{2b_t}{\beta\alpha_t n}\operatorname{Tr}\left(\Phi_t\Phi_t^\dagger\Psi_t\Psi_t^\dagger\right)_{BB}} = e^{-\frac{b_t}{\beta\alpha_t n}\operatorname{Tr}(\tilde{\psi}_t\psi_t)^2} \tag{3.34}$$

$$= \int_{\mathfrak{g}_\mathbb{R}} e^{\frac{\beta\alpha_t n}{4b_t}\operatorname{Tr}\iota_B(g)^2+\operatorname{Tr}(\iota_B(g)\tilde{\psi}_t\psi_t)}dg\,, \tag{3.35}$$

$$\text{where}\quad \operatorname{Tr}(\iota_B(g)\tilde{\psi}\psi) = \operatorname{Tr}(x\tilde{\psi}\psi) - \operatorname{Tr}\left((\operatorname{Ad}(e^y)\eta)\eta\psi^\dagger\psi\right) \tag{3.36}$$

$$= \operatorname{Tr}(x\tilde{\psi}\psi) - \operatorname{Tr}(\psi e^{2y}\psi^\dagger) \in i\mathbb{R}+\mathbb{R}^-, \tag{3.37}$$

because $\tilde{\psi}\psi \in i\mathfrak{g}_\mathbb{R}$, $x \in \mathfrak{g}_\mathbb{R}$ and $y = y^\dagger$. We can exchange the integration over g with those over Φ and Ψ without encountering ill-defined integrals.

For the fermion-fermion sector the situation is much simpler. Here, the Lie algebra under consideration is

$$\mathfrak{o}_\mathbb{R} := \{h : \mathbb{R}^4 \to \mathbb{R}^4 | h = -\operatorname{Ad}(\tilde{\gamma}_F)h^T = -h^\dagger\}, \tag{3.38}$$

defined by $\tilde{\gamma}_F := \sigma_2 \otimes \sigma_2$. It is compact and the trivial embedding $\iota_F : \mathfrak{o}_\mathbb{R} \hookrightarrow \mathfrak{o}$ does not cause convergence issues. Now, we assemble boson-boson and fermion-fermion parts into the full super picture. Thus let $\tilde{\gamma} = \operatorname{diag}(\tilde{\gamma}_B, \tilde{\gamma}_F)$ and $\iota : \mathfrak{spo}_\mathbb{R}(4|4) \hookrightarrow \mathfrak{spo}(4|4)$ with $\iota_0 = (\iota_B, \iota_F)$ and trivial embedding of the odd part. Here $\mathfrak{spo}(4|4)$ denotes the *complex* ortho-symplectic Lie super algebra with even part $\mathfrak{spo}_0(4|4) = \mathfrak{sp}(4) \oplus \mathfrak{o}(4)$ and standard representation acting on $\mathbb{C}^{4|4}$.

3.3.3c Full supersymmetric transformation

Using the notation

$$P^t := -i\,\iota(g) =: \left(\begin{array}{cc|cc} \bar{P} & (P_1^t)_{BB} & \bar{P} & (P_1^t)_{BF} \\ (P_2^t)_{BB} & \bar{P} & (P_2^t)_{BF} & \bar{P} \\ \hline \bar{P} & (P_1^t)_{FB} & \bar{P} & (P_1^t)_{FF} \\ (P_2^t)_{FB} & \bar{P} & (P_2^t)_{FF} & \bar{P} \end{array}\right) \in \mathfrak{spo}(4|4) \quad \text{and} \tag{3.39}$$

$$\Xi^t := \left(\begin{array}{cc|cc} 0 & (\Phi_t\Phi_t^\dagger)_{BB} & 0 & (\Phi_t\Phi_t^\dagger)_{BF} \\ (\Psi_t\Psi_t^\dagger)_{BB} & 0 & (\Psi_t\Psi_t^\dagger)_{BF} & 0 \\ \hline 0 & (\Phi_t\Phi_t^\dagger)_{FB} & 0 & (\Phi_t\Phi_t^\dagger)_{FF} \\ (\Psi_t\Psi_t^\dagger)_{FB} & 0 & (\Psi_t\Psi_t^\dagger)_{FF} & 0 \end{array}\right) \in i\mathfrak{spo}_\mathbb{R}(4|4), \tag{3.40}$$

we finally arrive at the full super version of the Schäfer-Wegner Hubbard-Stratonovich transformation:

$$\prod_{t\in T} e^{-\frac{2b_t}{\beta\alpha_t n}\operatorname{STr}\Phi_t\Phi_t^\dagger\Psi_t\Psi_t^\dagger} \propto \prod_{t\in T}\int dP^t e^{-\frac{\alpha_t\beta n}{4b_t}\operatorname{STr}\left(P^t\right)^2+i\operatorname{STr}P^t\Xi^t}, \tag{3.41}$$

where $dP = \iota_*(dg)$ is the push forward measure onto the domain $-i\,\iota(\mathfrak{spo}_{\mathbb{R}})$. To get back to the original notation, we rewrite

$$\operatorname{STr} P^t \Xi^t = \operatorname{STr} P_1^t \Psi_t \Psi_t^\dagger + \operatorname{STr} P_2^t \Phi_t \Phi_t^\dagger \tag{3.42}$$

$$\operatorname{STr} \left(P^t\right)^2 = \operatorname{STr} \left(\bar{P}^t\right)^2 + 2 \operatorname{STr} P_1^t P_2^t \tag{3.43}$$

with the important symmetry

$$P \in \mathfrak{spo} = \{P = -\operatorname{Ad}(\tilde{\gamma}) P^T\}, \quad \text{where} \quad \tilde{\gamma} = -i\sigma_2 \otimes \varsigma\,, \tag{3.44}$$

$$\text{and hence} \quad P_i = \operatorname{Ad}(\varsigma) P_i^T \Rightarrow P_i = \operatorname{Ad}(\varsigma^{-1}) P_i^T\,. \tag{3.45}$$

Notice that the appearance of the $\bar{P}$ component, which is not coupled to the original fields and can be integrated out immediately, is due to our ignorance of the additional symmetry $\tilde{\psi}\psi = -\operatorname{Ad}(\sigma_3)\tilde{\psi}\psi$, as mentioned above.

3.3.3d Summary of the Hubbard-Stratonovich transformation

Summing up the results of this section, we have introduced a non-linear field P with values in $-i\iota(\mathfrak{spo}_{\mathbb{R}}(4|4)) \subset \mathfrak{spo}(4|4)$ to decouple the quartic $\Phi\Phi^\dagger\Psi\Psi^\dagger$ interaction. Denoting the target spaces of Ψ and Φ by $T_1 \simeq T_2 \simeq \mathbb{R}^{2|2}$ as above, the two relevant components of P take values in $\operatorname{Hom}^{\mathbb{C}}(T_1, T_2)$ and $\operatorname{Hom}^{\mathbb{C}}(T_2, T_1)$, respectively. The mass type fields live on the sites, the spring, pinning, and time-reversal invariance breaking types live on the links. This means that for each site/link of our original lattice we have two classes of super matrices coupling the old linear super fields, as shown in Figure 3.1. The advantage gained is that we can now carry out the Gaussian integrals over Φ and Ψ and replace a large number ($\propto n$) of linear super fields by a small number (independent of n) of non-linear super fields, P_i.

The transformation formula to be used in the following is

$$\prod_{t\in T} e^{-\frac{2b_t}{\beta\alpha_t n} \operatorname{STr} \Phi_t \Phi_t^\dagger \Psi_t \Psi_t^\dagger} \tag{3.46a}$$

$$\propto \int DP\, e^{\sum_{t\in T}\left(-\frac{\alpha_t\beta n}{2b_t} \operatorname{STr}\left(P_1^t P_2^t\right) + i \operatorname{STr} P_1^t \Psi_t \Psi_t^\dagger + i \operatorname{STr} P_2^t \Phi_t \Phi_t^\dagger\right)}\,, \tag{3.46b}$$

where $DP := \prod_t dP_1^t dP_2^t$.

3.3.4 Integrals over linear fields

3.3.4a Links

Collecting the terms from Equations (3.23) and (3.46), we can now compute the integrals over Φ. Convergence is assured by Equation (3.37). We will do the computation

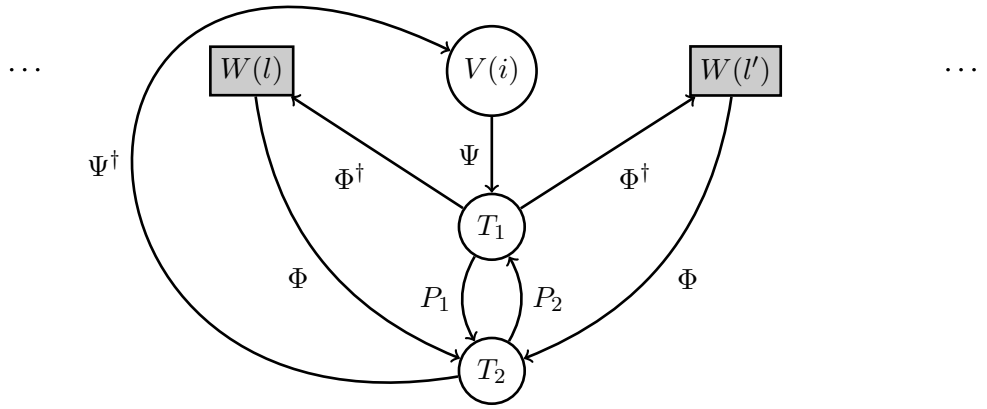

Figure 3.1: The Hubbard-Stratonovich transformation introduces new super fields, P_i.

for the three (m, s, and ms) sectors in W one by one. The simplest case is the additive mass sector,[6] but the interfering mass sector is not much more complicated.[7]

$$\int\limits_{i\in C_0, t\in\{+,\circledcirc\}} \prod e^{-\operatorname{STr}\left(-i(P_2^{i,m,t})\Phi_{i,m,t}\Phi^\dagger_{i,m,t}+Z\Phi_{i,m,t}\Phi^\dagger_{i,m,t}+i\Phi_{i,m,t}D\Psi^\dagger+i\Psi D^T\Phi^\dagger_{i,m,t}\right)} d\Phi_m \tag{3.47a}$$

$$= \prod_{i\in C_0} \frac{\operatorname{SDet}_{\mathbb{C}^{2|2}}\left(Z-iP_2^{i,m,+}\right)^{\alpha(\beta-2)n/2}}{\operatorname{SDet}_{\mathbb{C}^{2|2}}\left(Z-iP_2^{(i,m,\circledcirc)}\right)^{(2-\beta)n/2}} e^{-\operatorname{STr}\left(Z-iP_2^{i,m,\circledcirc}\right)^{-1}\Psi D^T_{m,i}D_{m,i}\Psi^\dagger}. \tag{3.47b}$$

For the springs and pinning sectors we should stress that $\Phi_s = \Phi_p = \Phi\pi_s^W$. Hence

$$\int\limits_{l\in C_1, t\in\{+,\circledcirc\}} \prod e^{-\operatorname{STr}\left(-i(P_2^{l,s,t}+P_2^{l,p,t})\Phi_{l,s,t}\Phi^\dagger_{l,s,t}+Z\Phi_{l,s,t}\Phi^\dagger_{l,s,t}+i\Phi_{l,s,t}D\Psi^\dagger+i\Psi D^T\Phi^\dagger_{l,s,t}\right)} d\Phi_s \tag{3.48a}$$

$$= \prod_{l\in C_1} \operatorname*{SDet}_{\mathbb{C}^{2|2}}\left(Z-iP_2^{l,s,+}-iP_2^{l,p,+}\right)^{\alpha(\beta-2)n/2} \tag{3.48b}$$

$$\times \prod_{l\in C_1} \frac{e^{-\operatorname{STr}\left(Z-iP_2^{(l,s,\circledcirc)}-iP_2^{(l,p,\circledcirc)}\right)^{-1}\Psi D^T_{l,s}D_{l,s}\Psi^\dagger}}{\operatorname{SDet}_{\mathbb{C}^{2|2}}\left(Z-iP_2^{(l,s,\circledcirc)}-iP_2^{(l,p,\circledcirc)}\right)^{(2-\beta)n/2}}. \tag{3.48c}$$

[6] To verify the power counting, Equation (3.11d) and (3.2) are helpful.

[7] Here we used Equation (3.11b) and (3.45) to remove all dagger notation and completed the square as a bi-linear (as opposed to a sesqui-linear) form.

Finally, the new time-reversal breaking disorder type, ms, is very similar to s, but for the deterministic part not being projected onto the m or s sector and the dimension of W_{ms}. The corresponding factors are

$$\int \prod_{l\in C_1, t\in\{+,\circledcirc\}} e^{-\operatorname{STr}\left((Z-iP_2^{l,ms,t}-iP_2^{l,mp,t})\Phi_{l,ms,t}\Phi^\dagger_{l,ms,t}+i\Phi_{l,ms,t}D\Psi^\dagger+i\Psi D^T\Phi^\dagger_{l,ms,t}\right)} d\Phi_{ms} \tag{3.49a}$$

$$= \prod_{l\in C_1} \underset{\mathbb{C}^{2|2}}{\operatorname{SDet}} \left(Z - iP_2^{l,ms,+} - iP_2^{l,mp,+}\right)^{\alpha(1-\beta)n} \tag{3.49b}$$

$$\times \prod_{l\in C_1} \frac{e^{-\operatorname{STr}\left(Z-iP_2^{(i,ms,\circledcirc)}-iP_2^{(i,mp,\circledcirc)}\right)^{-1}\Psi D_l^T D_l \Psi^\dagger}}{\operatorname{SDet}_{\mathbb{C}^{2|2}}\left(Z - iP_2^{(i,ms,\circledcirc)} - iP_2^{(i,mp,\circledcirc)}\right)^{(\beta-1)n}} \,. \tag{3.49c}$$

3.3.4b Sites

Collecting the terms in the exponent that involve Ψ from Equations (3.23), (3.46), (3.47), (3.48) and (3.49) we get

$$L_\Psi(\Psi) := \sum_{i\in C_0} \left(Z - iP_2^{i,m,\circledcirc}\right)^{-1} \Psi D_{i,m}^T D_{i,m} \Psi^\dagger + \tau \Psi J \Psi^\dagger \tag{3.50a}$$

$$+ \sum_{l\in C_1} \left(Z - iP_2^{l,s,\circledcirc} - iP_2^{l,p,\circledcirc}\right)^{-1} \Psi D_{l,s}^T D_{l,s} \Psi^\dagger - i\sum_{t\in T} P_1^t \Psi_t \Psi_t^\dagger \tag{3.50b}$$

$$+ \sum_{l\in C_1} \left(Z - iP_2^{l,ms,\circledcirc} - iP_2^{l,mp,\circledcirc}\right)^{-1} \Psi D_{l,ms}^T D_{l,ms} \Psi^\dagger \,. \tag{3.50c}$$

The remaining Gaussian integral involves no linear terms,

$$\int d\Psi\, e^{-\operatorname{STr} L_\Psi(\Psi)} = \underset{\mathbb{C}^{2|2}\otimes V}{\operatorname{SDet}}{}^{-1/2} \Bigg(i\tau\otimes\sigma_2\otimes\mathbf{1} - i\sum_{i\in C_0, t\in\{m\}\times\{+,\circledcirc\}} P_1^{i,t}\otimes\pi_{i,t}^V \tag{3.51a}$$

$$- \frac{i}{2}\sum_{l=(i,j)\in C_1, t\in\{p,mp\}\times\{+,\circledcirc\}} P_1^{l,t}\otimes\left(2(\pi_i^V+\pi_j^V)+\Delta_l\right)\pi_t^V + \frac{i}{2}\sum_{l\in C_1, t\in\{s,ms\}\times\{+,\circledcirc\}} P_1^{l,t}\otimes\Delta_l\pi_t^V \tag{3.51b}$$

$$+ \sum_{i\in C_0}\left(Z - iP_2^{i,m,\circledcirc}\right)^{-1}\otimes D_{i,m}^T D_{i,m} \tag{3.51c}$$

$$+ \sum_{l\in C_1}\left(Z - iP_2^{l,s,\circledcirc} - iP_2^{l,p,\circledcirc}\right)^{-1}\otimes D_{l,s}^T D_{l,s} \tag{3.51d}$$

$$+ \sum_{l\in C_1}\left(Z - iP_2^{l,ms,\circledcirc} - iP_2^{l,mp,\circledcirc}\right)^{-1}\otimes D_{l,ms}^T D_{l,ms}\Bigg) \,. \tag{3.51e}$$

Here $\Delta_{i,j}$ denotes the component of the Laplace operator[8] connecting i and j, i.e. Δ_l acts by ± 1 and $\sum_{l\in C_1}\Delta_l = \Delta$. Further we are using projectors[9] $\pi_{i,t} : V \twoheadrightarrow V_t(i)$. The operator under the determinant is not overall a pure tensor, but there is a trivial tensor factor over the phonon bands, which can be taken out.

$$\int d\Psi\, e^{-\operatorname{STr} L_\Psi(\Psi)} = \operatorname*{SDet}_{\mathbb{C}^{2|2}\otimes\mathbb{R}^2\otimes\mathbb{R}^{L^d}} \Bigg(\tau\otimes i\sigma_2\otimes \mathbf{1} \tag{3.52a}$$

$$- i\sum_{i\in C_0}(P_1^{i,m,\circledcirc}+P_1^{i,m,+})\otimes\pi_m\otimes\pi_i \tag{3.52b}$$

$$+ \frac{1}{\mu}\sum_{i\in C_0}(Z-iP_2^{i,m,\circledcirc})^{-1}\otimes\pi_m\otimes\pi_i \tag{3.52c}$$

$$+ \frac{i}{2}\sum_{l\in C_1}(P_1^{l,s,\circledcirc}+P_1^{l,s,+})\otimes\pi_s\otimes\Delta_l \tag{3.52d}$$

$$- \frac{i}{2}\sum_{l=(i,j)\in C_1}(P_1^{l,p,\circledcirc}+P_1^{l,p,+})\otimes\pi_s\otimes(2(\pi_i+\pi_j)+\Delta_l) \tag{3.52e}$$

$$- \kappa\sum_{l\in C_1}(Z-iP_2^{l,s,\circledcirc}-iP_2^{l,p,\circledcirc})^{-1}\otimes\pi_s\otimes\Delta_l\Bigg)^{-\frac{(2-\beta)n}{2}} \tag{3.52f}$$

$$\operatorname*{SDet}_{\mathbb{C}^{2|2}\otimes\mathbb{R}^2\otimes\mathbb{R}^{L^d}} \Bigg(\tau\otimes i\sigma_2\otimes\mathbf{1} + \frac{i}{2}\sum_{l\in C_1}(P_1^{l,ms,\circledcirc}+P_1^{l,ms,+})\otimes\mathbf{1}_2\otimes\Delta_l \tag{3.52g}$$

$$- \frac{i}{2}\sum_{l=(i,j)\in C_1}(P_1^{l,mp,\circledcirc}+P_1^{l,mp,+})\otimes\mathbf{1}_2\otimes(2(\pi_i+\pi_j)+\Delta_l) \tag{3.52h}$$

$$\sum_{l\in C_1,}(Z-iP_2^{l,ms,\circledcirc}-iP_2^{l,mp,\circledcirc})^{-1}\left(\frac{1}{\mu}\pi_m\otimes\mathbf{1}-\kappa\pi_s\otimes\Delta_l\right)\Bigg)^{-\frac{(\beta-1)n}{2}}. \tag{3.52i}$$

3.3.5 Field theory

No approximations have been made in this chapter so far. The full super lattice field theory for the density of states reads

[8] Recall that we use the sign convention $\Delta_{i,i} = -2d$. The spatial structure of spring constants leads to terms $\propto -\Delta_l$. The other term, $\Delta_{i,j} + 2(\pi_i + \pi_j)$, has the same non-vanishing matrix elements as Δ, but with all signs changed to $+$.

[9] Recall that the spaces on the left hand side of the projectors are introduced as direct sums. The kernels are given by the terms not appearing on the right hand side.

$$\left\langle \frac{\mathrm{Det}(z_1 - X)}{\mathrm{Det}(z_2 - X)} \right\rangle \propto \int dP_1 dP_2 \, e^{-\sum_{t\in T} \frac{\alpha_t \beta n}{2b_t} \mathrm{STr}_{\mathbb{C}^{2|2}}\left(P_1^t P_2^t\right)} \tag{3.53a}$$

$$\left(\frac{z_1}{z_2}\right)^{\Delta \dim} \times (3.52) \times e^{-\mathrm{STr}_{\mathbb{C}^{2|2}}\left(\frac{n(2-\beta)}{2} L_T(P_2) + n(\beta-1) L_{\mathcal{T}}(P_2)\right)} \tag{3.53b}$$

where we have gathered Equation (3.47) to (3.49) in

$$L_T(P_2) = \alpha \left(\sum_{i\in C_0} \ln\left(Z - iP_2^{i,m,+}\right) + \sum_{l\in C_1,} \ln\left(Z - iP_2^{l,s,+} - iP_2^{l,p,+}\right) \right) \tag{3.54a}$$

$$+ \sum_{i\in C_0} \ln\left(Z - iP_2^{i,m,\circledcirc}\right) + \sum_{l\in C_1} \ln\left(Z - iP_2^{l,s,\circledcirc} - iP_2^{l,p,\circledcirc}\right) \tag{3.54b}$$

$$L_{\mathcal{T}}(P_2) = \alpha \sum_{l\in C_1,} \ln\left(Z - iP_2^{l,ms,+} - iP_2^{l,mp,+}\right) \tag{3.54c}$$

$$+ \sum_{l\in C_1} \ln\left(Z - iP_2^{l,ms,\circledcirc} - iP_2^{l,mp,\circledcirc}\right) \tag{3.54d}$$

3.3.6 Saddle-point equations for the interfering disorder model

After producing a field theory, which exactly represents the Green's function for a rather big class of different models, we will now examine the $n \to \infty$ coherent potential approximation (CPA) for the various sub-models. Technically, this means that we study the saddle points (see Appendix A.2) of the action in Equation (3.53) for a constant field configuration. We anticipate that the saddle points will feature maximal supersymmetry, i.e. we assume that $P_j^t = p_j^t \otimes \mathbf{1}_2$.

Due to the CPA, the spatial dependence of the terms in Equation (3.52) is only in the $\mathbb{R}^{L^d}$ factor, which can therefore be diagonalised by Fourier transformation. The remaining factors in $\mathbb{C}^{2|2} \otimes \mathbb{R}^2$ are almost diagonal, so the corresponding super determinants can be written down explicitly as

$$(3.52) =: e^{-n\sum_k \mathrm{STr}_{\mathbb{C}^{1|1}}\left((2-\beta)L_T^D(k,p_1,\tilde{p}_2) + (\beta-1)L_{\mathcal{T}}^D(k,p_1,\tilde{p}_2) - 2\ln(z)\right)}, \tag{3.55}$$

$$L_T^D(k,\tilde{p}_1,\tilde{p}_2) = \ln\left(z^2 + \left(\frac{\mu^{-1}}{1+\tilde{p}_2^{m,\circledcirc}} + \tilde{p}_1^m \right) \right. \tag{3.56}$$

$$\left. \times \left(2\tilde{p}_1^p + \left(\frac{\tilde{p}_1^p - \tilde{p}_1^s}{2d} - \frac{\kappa}{1 + \tilde{p}_2^{s,\circledcirc} + \tilde{p}_2^{p,\circledcirc}} \right) \Delta_k \right) \right), \tag{3.57}$$

$$L_{\mathcal{T}}^D(k,\tilde{p}_1,\tilde{p}_2) = \ln\left(z^2 + \left(\frac{\mu^{-1}}{1 + \tilde{p}_2^{ms,\circledcirc} + \tilde{p}_2^{mp,\circledcirc}} + \frac{\tilde{p}_1^{mp} - \tilde{p}_1^{ms}}{2d} \Delta_k + 2\tilde{p}_1^{mp} \right) \right. \tag{3.58}$$

$$\left. \times \left(2\tilde{p}_1^{mp} + \left(\frac{\tilde{p}_1^{mp} - \tilde{p}_1^{ms}}{2d} - \frac{\kappa}{1 + \tilde{p}_2^{ms,\circledcirc} + \tilde{p}_2^{mp,\circledcirc}} \right) \Delta_k \right) \right), \tag{3.59}$$

where $\tilde{p}_1^m := -izp_1^{m,\circledcirc} - izp_1^{m,+}$, $\tilde{p}_1^s = -idzp_1^{m,\circledcirc} - idzp_1^{m,+}$ and similarly for $\tilde{p}_1^{ms}$, $\tilde{p}_1^p$, and $\tilde{p}_1^{mp}$ and further $z\tilde{p}_2 := -ip_2$. Notice that this rescaling of the integration variables does not change the measure.

We combine Equation (3.53) with (3.55) and take the limit of large lattice size $\sum_k \mapsto L^d \int Dk := L^d \int_{[0,2\pi]^d} \frac{d^dk}{(2\pi)^d}$ as in Chapter 2. The resulting action is

$$\left\langle \frac{\mathrm{Det}(z_1 - X)}{\mathrm{Det}(z_2 - X)} \right\rangle \propto \int d\tilde{p}_1 d\tilde{p}_2 e^{-nL^d S(z,\tilde{p}_1,\tilde{p}_2)} \tag{3.60a}$$

$$S(z,\tilde{p}_1,\tilde{p}_2) = \int Dk \operatorname*{STr}_{\mathbb{C}^{1|1}} \left((2-\beta) L_T^k(\tilde{p}_1,\tilde{p}_2) + (\beta-1) L_{\not T}^k(\tilde{p}_1,\tilde{p}_2) \right) \tag{3.60b}$$

$$L_T^k(\tilde{p}_1,\tilde{p}_2) = -\beta \sum_{t\in\{m,s,p\}\times\{+,\circledcirc\}} \alpha_t b_t^{-1} \tilde{p}_1^t \tilde{p}_2^t + \alpha \ln\left(1+\tilde{p}_2^{m+}\right) + \ln\left(1+\tilde{p}_2^{m,\circledcirc}\right) \tag{3.60c}$$

$$+ \alpha d \ln\left(1+\tilde{p}_2^{s,+}+\tilde{p}_2^{p,+}\right) + d\ln\left(1+\tilde{p}_2^{s,\circledcirc}+\tilde{p}_2^{p,\circledcirc}\right) \tag{3.60d}$$

$$+ L_T^D(k,\tilde{p}_1,\tilde{p}_2) \tag{3.60e}$$

$$L_{\not T}^k(\tilde{p}_1,\tilde{p}_2) = -\beta \sum_{t\in\{ms,mp\}\times\{+,\circledcirc\}} \alpha_t b_t^{-1} \tilde{p}_1^t \tilde{p}_2^t + 2\alpha d \ln\left(1+\tilde{p}_2^{ms,+}+\tilde{p}_2^{mp,+}\right) \tag{3.60f}$$

$$+ 2d \ln\left(1+\tilde{p}_2^{ms,\circledcirc}+\tilde{p}_2^{mp,\circledcirc}\right) + L_{\not T}^D(k,\tilde{p}_1,\tilde{p}_2) \tag{3.60g}$$

The correct normalisation is $\int d\tilde{p}_1 \tilde{d}p_2 e^{-nL^d S(\mathbf{1}_{1|1},\tilde{p}_1,\tilde{p}_2)} = 1$. Notice that all terms $\propto \ln(z)$, which arise in the action due to the rescaling precisely cancel with the $\Delta \dim \ln(z)$ term in Equation (3.53).

3.3.6a Green's function and clean limit

Recall (from Equation (2.3) and (3.1a)) that we are actually interested in the derivative of Equation (3.60a) with respect to z. At super symmetric saddle points, $p \propto \mathbf{1}_{1|1}$ and $z \propto \mathbf{1}_{1|1}$, the action is exactly zero and using the saddle point method (also known as Laplace method, see Appendix A.2), we obtain the Green's function

$$\frac{g(z)}{z} = (2-\beta) \int \frac{d^dk}{(2\pi)^d} \left(z^2 + \left(\frac{\mu^{-1}}{1+\tilde{p}_2^{m,\circledcirc}} + \tilde{p}_1^m \right) \right. \tag{3.61a}$$

$$\left. \times \left(2\tilde{p}_1^p + \left(\frac{\tilde{p}_1^p - \tilde{p}_1^s}{2d} - \frac{\kappa}{1+\tilde{p}_2^{s,\circledcirc}+\tilde{p}_2^{p,\circledcirc}} \right) \Delta_k \right) \right)^{-1} \tag{3.61b}$$

$$+ (\beta-1) \int \frac{d^dk}{(2\pi)^d} \left(z^2 + \left(\frac{\mu^{-1}}{1+\tilde{p}_2^{ms,\circledcirc}+\tilde{p}_2^{mp,\circledcirc}} + \frac{\tilde{p}_1^{mp} - \tilde{p}_1^{ms}}{2d} \Delta_k + 2\tilde{p}_1^{mp} \right) \right. \tag{3.61c}$$

$$\left. \times \left(2\tilde{p}_1^{mp} + \left(\frac{\tilde{p}_1^{mp} - \tilde{p}_1^{ms}}{2d} - \frac{\kappa}{1+\tilde{p}_2^{ms,\circledcirc}+\tilde{p}_2^{mp,\circledcirc}} \right) \Delta_k \right) \right)^{-1}, \tag{3.61d}$$

where p_i^t here are understood to be the saddle-point values (of the boson-boson part of the fields). The first observation is that the clean limit (see Equation (1.12)) is reproduced correctly by Equation (3.61) for $b_t \to 0$, leading to $p_i^t \to 0$.

In Section 2.7, Equation (2.65), we have mentioned that pinning cancels the spring constant disorder effect and is responsible for the gap, perturbatively. Now we can verify in Equation (3.61) that this is indeed the case on the coherent level. Furthermore, comparing Equation (3.61) (for $\beta = 1$ and $b_s = b_p$) to (2.75d) gives strong hints for how to match saddle-point to self-consistency parameters, as is done in Section 3.3.6c.

3.3.6b Time-reversal invariant sector

We will first calculate the partial derivatives of the action with respect to the parameters from the time-reversal invariant sector (i.e. $t \in \{m, s, p\} \times \{+, \circledcirc\}$) to compare to the SCE from Section 2.7.2. Therefore let $\beta = 1$ for the rest of this section. Then, using Equation (A.6) and (3.61), we can replace all appearing integrals over the deterministic spectrum by appropriate functions of g. We find:

$$\mu\tilde{p}_1^{m,\circledcirc} = \frac{b_m^\circledcirc(1-gz)}{\tilde{p}_2^{m,\circledcirc}} - \frac{1}{1+\tilde{p}_2^{m\circledcirc}} - \mu\tilde{p}_1^{m,+} \tag{3.62a}$$

$$\mu\tilde{p}_1^{m,\circledcirc} = \frac{1}{1+\tilde{p}_2^{m,\circledcirc}}\left(b_m^\circledcirc - \frac{1}{1+\tilde{p}_2^{m,\circledcirc}}\tilde{p}_2^{m\circledcirc}\right) \tag{3.62b}$$

$$\mu\tilde{p}_1^{m,+} = \frac{b_m^+}{1+\tilde{p}_2^{m,+}} \tag{3.62c}$$

$$\tilde{p}_2^{m,+} = \frac{b_m^+}{\alpha b_m^\circledcirc}\tilde{p}_2^{m,\circledcirc} \tag{3.62d}$$

$$\frac{2\tilde{p}_1^{s,+}}{\kappa b_s^+} = \frac{2\tilde{p}_1^{p,+}}{\kappa b_p^+} = \frac{d}{1+\tilde{p}_2^{s,+}+\tilde{p}_2^{p,+}} \tag{3.62e}$$

$$\alpha\frac{\tilde{p}_2^{s,+}}{b_s^+} = \frac{\tilde{p}_2^{s,\circledcirc}}{b_s^\circledcirc} = \frac{1+\tilde{p}_2^{s,\circledcirc}+p_2^{p,\circledcirc}}{4d}\frac{1-gz-\frac{b_m^\circledcirc(1-gz)}{\tilde{p}_2^{m,\circledcirc}}2p_1^p\frac{g}{z}}{1-\frac{1+\tilde{p}_2^{s,\circledcirc}+p_2^{p,\circledcirc}}{\kappa}\frac{\tilde{p}_1^p-\tilde{p}_1^s}{2d}} \tag{3.62f}$$

$$\alpha\frac{\tilde{p}_2^{p,+}}{b_p^+} = \frac{\tilde{p}_2^{p,\circledcirc}}{b_p^\circledcirc} = \nu^2\left(\frac{1}{1+p_2^{m,\circledcirc}}+\mu p_1^m\right)\frac{g}{z} - \frac{\tilde{p}_2^{s,\circledcirc}}{b_s^\circledcirc} \tag{3.62g}$$

$$\frac{2\tilde{p}_1^{s,\circledcirc}}{\kappa b_s^\circledcirc} = \frac{2\tilde{p}_1^{p,\circledcirc}}{\kappa b_p^\circledcirc} = \frac{d}{1+\tilde{p}_2^{s,\circledcirc}+p_2^{p,\circledcirc}}\left(1-\frac{4\tilde{p}_2^{s,\circledcirc}}{b_s^\circledcirc(1+\tilde{p}_2^{s,\circledcirc}+p_2^{p,\circledcirc})}\right). \tag{3.62h}$$

Using Equation (3.61) (for $\beta = 1$), and (3.62) yields two equations for the two parameters, $p_2^{m,\circledcirc}(z)$ and $p_2^{s,\circledcirc}(z)$, which in turn determine all others, in particular $g(z)$.

3.3.6c Consistency with diagrammatics

In this section we check the diagrammatic results. The first step is to note that for $b_p = b_s$ (as assumed throughout Chapter 2) we have $p_i^{s,t} = p_i^{p,t}$ for $i \in \{1,2\}$ and $t \in \{+, \circledcirc\}$. We can now identify the self-consistency parameters in Equation (2.75) with the saddle-point parameters in Equation (3.62). The dictionary is

$$\mu\mathcal{M} = \frac{1}{1+\tilde{p}_2^{m,\circledcirc}} + \mu\tilde{p}_1^m = \frac{b_m^{\circledcirc}(1-gz)}{\tilde{p}_2^{m,\circledcirc}} \tag{3.63}$$

$$B_s^{-1} = 1 + \tilde{p}_2^{s,\circledcirc} + \tilde{p}_2^{p,\circledcirc} \tag{3.64}$$

$$(B_s^+)^{-1} = 1 + \tilde{p}_2^{s,+} + \tilde{p}_2^{p,+} \tag{3.65}$$

$$B_m^{-1} = 1 + \tilde{p}_2^{m,\circledcirc} \tag{3.66}$$

$$(B_m^+)^{-1} = 1 + \tilde{p}_2^{m,+} \tag{3.67}$$

where we have used Equation (3.62a) in Equation (3.63). With this relabeling

$$(3.62\text{g}) \Leftrightarrow \mu\mathcal{M} = \frac{1-B_s}{B_s}\frac{\tilde{z}}{\tilde{g}}\frac{1}{b_s^{\circledcirc}} = \alpha\frac{1-B_s^+}{B_s^+}\frac{\tilde{z}}{\tilde{g}}\frac{1}{b_s^+}\,. \tag{3.68}$$

This is (part of) Equation (2.75a), where $b_p = b_s = b_{sp}$. Using Equation (3.62h) together with (3.62f), (3.68), and (3.62e) we get

$$\tilde{p}_1^p = \tilde{p}_1^s = \tilde{p}_1^{s,\circledcirc} + \tilde{p}_1^{s,+} = \kappa b_s^{\circledcirc}(d-1+gz) + \kappa d b_s^+\frac{B_s^+}{B_s} \tag{3.69}$$

which, together with Equation (3.63) and (3.64) identifies the expressions for the Green's function, (3.61) $\Leftrightarrow$ (2.75d). Finally, inserting Equation (3.66) and (3.67) into Equation (3.7) yields Equation (2.75c). Together with Equation (3.63) this also leads the last missing equation in (2.75a).

We have shown that the saddle-point equations for the mass, spring length and pinning disorder model in particular confirm the validity of the SCE derived in Section 2.7.

3.3.6d Breaking time-reversal invariance

For the maximally time-reversal invariance breaking (TRIB) model, $\beta = 2$, Equation (A.6) is in general not sufficient to replace by functions of g the two algebraically independent integrals appearing in the saddle-point equations. The numerator and the denominator of the integrand are now generically of second order in Δ_k. In the spirit of the Debye approximation, we could ignore the $\Delta_k^2 \propto |k|^4 + O(|k|^6)$ terms, but this would disregard a very prominent effect of TRIB, namely the spring-like coupling

of momenta. Instead we specialise to $b_{ms} = b_{mp}$ in order to compare to [SZ10]. In this case, we can drop the ms and mp labels, since $\tilde{p}^{ms} = \tilde{p}^{mp}$ and find:

$$\frac{\tilde{p}_1^+}{\kappa b^+} = \frac{d}{1+2\tilde{p}_2^+} \tag{3.70a}$$

$$\mu\mathcal{M} := \frac{1}{1+2\tilde{p}_2^\circledcirc} + 2\mu\tilde{p}_1 \tag{3.70b}$$

$$\frac{\tilde{p}_1^\circledcirc}{\kappa b^\circledcirc} = \frac{d}{1+2\tilde{p}_2^\circledcirc} + \tilde{p}_1\frac{g}{z}(1+2\tilde{p}_1) + \frac{1+\mathcal{M}}{\mathcal{M}}(gz-1) \tag{3.70c}$$

$$\alpha\frac{\tilde{p}_2^+}{b^+} = \frac{\tilde{p}_2^\circledcirc}{b^\circledcirc} \tag{3.70d}$$

$$1-gz = \left(\frac{2\tilde{p}_2^\circledcirc}{\kappa b^\circledcirc} - \mathcal{M}\frac{g}{z}\right)\mathcal{M} \tag{3.70e}$$

$$g(z) = \int \frac{d^dk}{(2\pi)^d}\frac{z}{z^2+\mathcal{M}\left(2\tilde{p}_1 - \frac{\kappa}{1+2\tilde{p}_2^\circledcirc}\Delta_k\right)}\,. \tag{3.70f}$$

As discussed in Section 3.1.1, these can be rephrased as the SCE found in [SZ10] by superbosonisation instead of the Hubbard-Stratonovich transform used here.

4 Summary and outlook

We have discovered four extended and three critical phases of our harmonic models of disordered phonons. The observable that we calculated in order to distinguish between these phases is the power law of the density of eigenfrequencies (DOS) in the coherent potential approximation (CPA), $\rho \propto \omega^{\chi-1}$, which determines the law of the temperature dependence of the heat capacity $C \propto T^{\chi}$. The validity of the CPA has been checked to be correct by comparison to exact numerical diagonalisation. To the best of our knowledge, only three of these phases were known before. One is the Debye phase ($\chi = d$ in d spatial dimensions), which is represented by the clean harmonic crystal and whose localisation properties due to disorder have been studied in [JSS83]. The Debye phase is, by construction, present in all our models. Whether or not the other phases are present depends on which types of disorder are used and in particular on how they are implemented. The other phase that was known before is the [LSZ06] phase ($\chi = 2/3$), which can be realised by a zero dimensional (i.e. non-local) random matrix model. Both of these phases are extended and so is the gapped phase ($C(T < T_c) = 0$ as discovered in [SZ10]), which occurs whenever pinning disorder is added to a model in the Debye phase. In view of the experimentally observed linear temperature dependence of the heat capacity of vitreous solids, the most interesting phase is the fourth extended one, which encompasses $\chi = 1$. We have found it for strong enough *interfering mass* as well as for the physically more relevant *interfering spring constant* disorder. In Figure 4.2 we show some examples of the CPA DOS of this phase in the same coordinates usually used in experimental data plots, such as shown in Figure 1.1. The phase diagram of the IMSC model is depicted in Figure 2.14. This is the model that combines both disorder types leading to the $\chi = 1$ phase. It comprises all of the above mentioned phases at finite disorder strength. The gapped phase is not in the picture but may be introduced by adding pinning disorder.

We classify the models constructed in this thesis by the physical quantity being disordered. There is only one physical type of *mass* disorder, but the pair potentials can be blended with *spring constant*, *spring length*, *pinning*, or *band mixing* disorder. Further we constructed *spring-like* and *pinning-like time-reversal invariance breaking* (TRIB) disorder models (see Figure 4.1 for an overview). Each of these disorder types can be implemented as *interfering* or *additive* disorder and in principle all of these 14 types can be combined. We stress that all resulting models are Lyapunov-stable, i.e. there are no runaway dynamics.

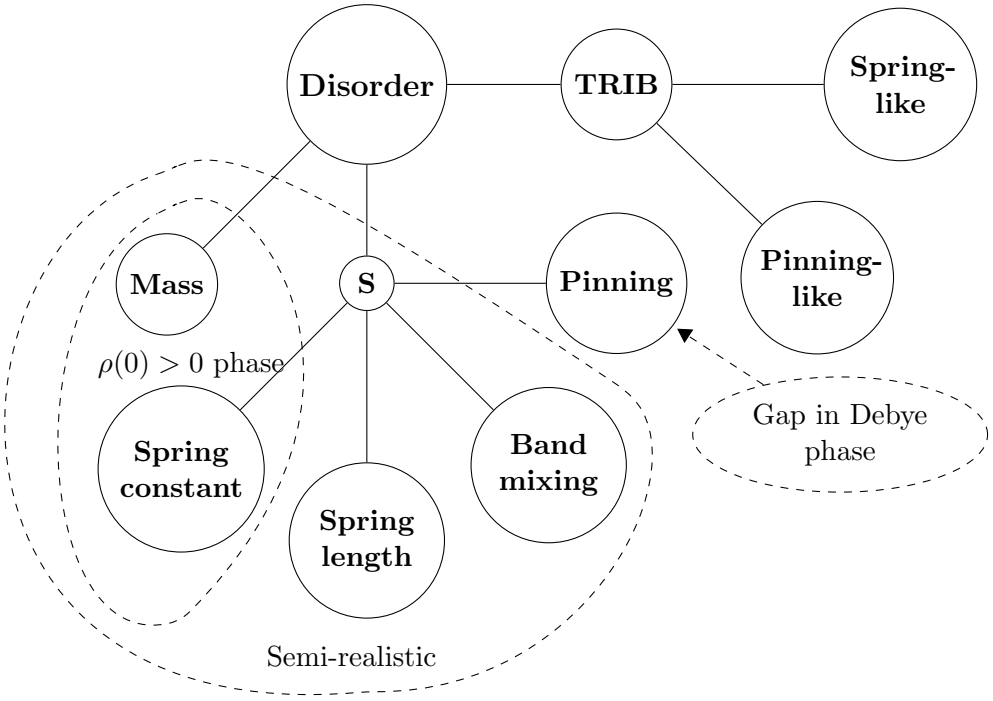

Figure 4.1: Overview over the physically different types of disorder.

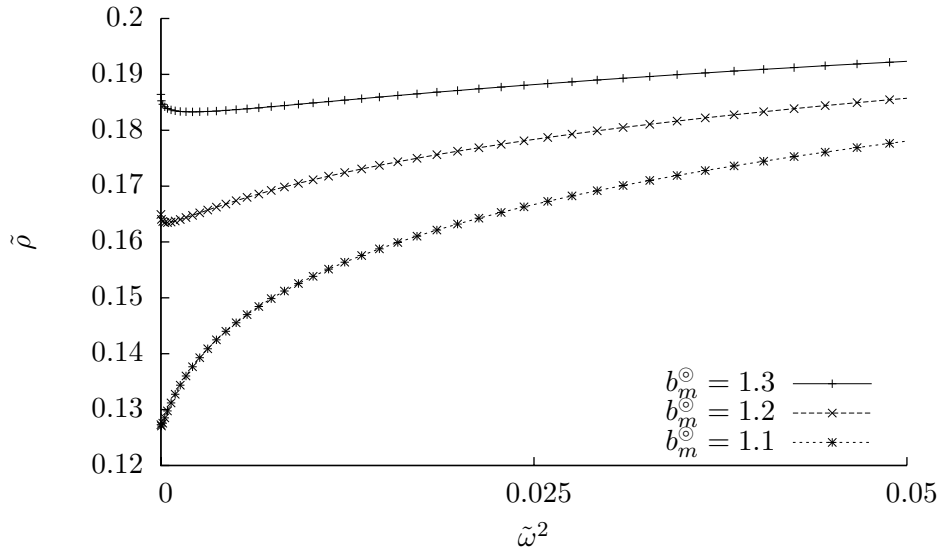

Figure 4.2: DOS of the interfering mass disorder model at strong disorder $b_m^{\circledcirc} > 1$.

We found that random *pinning* does not only remove the Goldstone modes of broken translation invariance. In the Debye phase, it leads to a gap in the frequency spectrum, i.e. there are no states at very low energies. Since this type of disorder lacks a microscopic motivation, at least in three dimensions, and a gap of finite size is *not* observed experimentally, we conclude that this type of disorder should be excluded for the model to be realistic. *Band mixing* is a rather generic type of disorder. However, it necessarily leads to pinning (if it is implemented locally). This type of disorder should hence be abandoned together with pinning disorder.

Spring length disorder is microscopically well motivated. The relaxed lengths of the springs are disordered, which leads to random local differentiation of longitudinal and transverse waves. The inter-constituent forces in the relaxed crystal are purely attractive, which is not ultimately realistic. Spring length disorder improves this model by adding random short range repulsion. As we mentioned when the harmonic crystal was introduced in Section 1.3.1, terms of this type should in principle already be included in the clean model. However, we found spring length disorder to be irrelevant in the sense that arbitrarily strong disorder does *not* lead to a phase transition (see Section 3.2). This adds *a posteriori* to the justification of using the stressed crystal and ignoring the difference between longitudinal and transverse modes in the clean case.

Spring *constant* disorder, on the other hand, is found to be relevant and exactly dual to *mass* disorder on the level of the DOS (see Section 2.2, in particular Figure 2.2). As mentioned above, *interfering mass and spring constant* (IMSC) disorder are the two types of disorder that lead to phase transitions. Spring constant disorder has an indirect structural effect by effectively removing springs from the model if very low spring constants are randomly assigned. Fluctuations in the strength of the restoring forces are anyway a type of disorder to be included in a realistic model of disordered solids. Our findings confirm the common belief that structural disorder is the relevant type of disorder to drive the crystal-glass transition.

The situation in the *mass* sector is much simpler than in the spring sector. Since M_0 is scalar, there is no distinction like the one between spring length, spring constant and band mixing disorder. Mass disorder is microscopically well motivated. However, [JSS83] found that taking the mass to fluctuate down to zero locally does not lead to a phase transition, although this kind of disorder is experimentally found to be more relevant, at least for conduction, than random changes in the equilibrium positions (see [HW70]). Instead, we take the *inverse* mass to fluctuate. In the interfering mass disorder models it might even fluctuate down to zero. This produces a model which is easier to formulate than the model of fluctuating spring constants since no square root of the Laplace operator is needed. On the level of the DOS the two models are exactly dual, although very heavy local masses are less realistic.

Interfering mass disorder can be combined with any type of spring constant or spring length disorder for the resulting model to feature a phase with a finite DOS at zero

frequency. The same is true for interfering spring constant disorder in combination with any type of mass disorder. Based on the assumption of the IMSC model being renormalisable with the two coupling constants given by the disorder strengths and assuming further that the critical points are correctly identified from the CPA DOS, we show a tentative RG flow diagram in Figure 2.15. According to this flow diagram, the $\rho(0) > 0$ phase is also stable under renormalisation. The same arguments apply to the phase and flow diagram of the *interfering mass and spring length* (IMSL) disorder model. They are the same as those of the IMSC, except for the critical line at $b_s = 1$ being moved up to $b_s = \infty$.

The CPA DOS for the IMSC model was derived by accessible diagrammatic means. We did not develop the diagrammatics to include momentum exchange, hence the IMSL model is not treated diagrammatically. Instead we use the supersymmetry technique, which also provides a more rigorous verification of the diagrammatic self-consistency equations (SCE). More precisely, the SCE for the CPA DOS for the models of additive or interfering spring length disorder and random pinning of equal strength (possibly combined with mass disorder) have been derived with both techniques in order to demonstrate that they indeed yield the same results.

Time-reversal invariance breaking (TRIB) disorder is hardly motivated in a model of disordered phonons. Nevertheless, we have studied it for the sake of the greater picture of bosonic universality classes, as well as to compare to our earlier results. We found that it makes a difference whether time-reversal invariance is being preserved or not, in that the TRIB variant of the IMSL disorder model does *not* lead to a strong disorder phase. The SCE of the additive TRIB model of equal pinning-like and spring-like disorder strength computed via the Hubbard-Stratonovich transformation in Chapter 3 is equivalent to the one derived by superbosonisation for the same model in [SZ10].

As mentioned above, we can also sort our models into two classes in terms of how disorder is implemented, namely as *additive*, or *interfering*, disorder. In the additive models, the inverse mass and spring constants only fluctuate to larger values, where the interfering model also allows them to fluctuate down to zero. Consequently, none of the additive models feature a phase transition nor a strong disorder phase at finite disorder strength. Here the perturbative effect of disorder at low energies is an effective *increase* of the coherent speed of sound, as opposed to the overall *decrease* caused by interfering disorder.

In the interfering case, the transition to the strong disorder phase happens as the fluctuations become strong enough to outweigh the deterministic part and hence lead to a vanishing local speed of sound with non-negligible probability. The *coherent* speed of sound $\mathcal{V}$ is defined by $\mathcal{V} M_0 S_0 := \nu \mathcal{M} \mathcal{S}$ for the models where this is possible. It is complex and energy dependent and the phase transition happens as $\mathcal{V}(\omega = 0)$ reaches zero. For the additive and combined models, $\mathcal{V}(0)$ increases indefinitely and in particular stays positive. Consequently, these models stay in the Debye phase (or in

the gapped phase, if pinning is present) for any finite amount of disorder. We stress that, if interfering and additive disorder are combined, the additive phenomenology wins over the more interesting interfering one. Hence disorder is to be implemented as purely *interfering* disorder for the resulting model to possess a strong disorder phase (see Section 2.4.3). On the microscopic level, combined additive and interfering disorder leads to the local speed of sound to be non-vanishing almost surely, since the sum of two positive semi definite operators has almost surely no zero modes if the two are free.

The model considered in [JSS83] can in our terminology also be called additive. We confirm the authors statement that a model similar to theirs but excluding negative masses, such as our additive mass disorder model, shows the same phenomenology, at least on the level of the CPA DOS. As a representative of the class of additive models, it always stays in the Debye phase. We also confirm that additional spring length disorder has no qualitative effect. However, our models exclude the possibility of the mass fluctuating down to zero locally, which did not lead to a phase transition in the model studied by [JSS83].

We did not yet address the question of localisation studied in [JSS83]. There a mobility edge was found in their additive mass disorder model in the Debye phase. Investigating the question of localisation in our model remains an interesting direction for future research. Starting from the lattice field theory derived in Section 3.3.5, we are planing to advance to a continuum field theory of the non-linear σ-model (or similar) type. Then the RG flow of this theory is to be studied in order to test our tentative considerations and shed some light on the degree of universality of the phases discovered in this work.

Before turning to localisation, however, the most interesting question to us is whether the IMSC model can also explain the experimentally observed anomalous temperature dependence of the heat conductivity $\Lambda \propto T^2$. The corresponding calculation of the four-point function is being done.

A Appendix

A.1 Debye approximation (details)

The idea of the Debye approximation is given in Section 1.3.3. The main point is that the averages over the spectrum of Δ are approximated by

$$\int_{[0,2\pi]^d} \frac{d^d k}{(2\pi)^d} f(\Delta_k) \approx \frac{d}{\Omega^d} \int_0^\Omega f\left(-k^2\right) k^{d-1} dk \tag{A.1}$$

and in particular:

$$g(z) = \int \frac{d^d k}{(2\pi)^d} \frac{z}{z^2 - \nu^2 \Delta_k} \approx z \frac{d}{\Omega^d} \int_0^\Omega \frac{k^{d-1} dk}{z^2 + \nu^2 k^2} \,. \tag{A.2}$$

where the cutoff Ω is to be determined such that Equation (1.12) is correctly reproduced to first order in z. Using the integrals computed in Appendix A.1.1 the deterministic density of states in Debye approximation is

$$\rho(\omega) = |\omega|^{d-1} \frac{d}{2(\nu\Omega)^d} \Theta\left(\sqrt{\frac{\nu^2\Omega^2}{\omega^2}} - 1\right), \tag{A.3}$$

where Θ denotes the Heaviside function with $\Theta(x) = 1$ for $\Re(x) > 0$ and $\Theta(x) = 0$ otherwise. By definition, the density of states is normalised to $\int \rho(\omega) d\omega = 1$, which is still true for our approximation with any cutoff since we chose the normalisation in Equation (A.1) accordingly.

Since $\rho \propto \omega^{d-1}$ is the correct power law for the full deterministic density of states, we can tune Ω such that our approximation is correct to leading order at low frequencies. In the following, we compute this leading order pre-factor.[1]

[1] The calculation also shows that the range of applicability of the Debye approximation (for the clean system) is $0 < |\omega| \ll \nu/a$. We consider the lattice spacing to be fixed at $a = 1$, but still, in the low-energy sector we are interested in, the Debye approximation is justified.

$$\int \frac{d^d k}{(2\pi)^d} \lim_{\epsilon\to 0} \Re \frac{z}{z^2 - \nu^2 \Delta_k} \tag{A.4a}$$

$$= \frac{1}{2} \int \frac{d^d k}{(2\pi)^d} \lim_{\epsilon\to 0} \frac{\epsilon}{\epsilon^2 + x^2} \tag{A.4b}$$

$$\approx \frac{\pi \operatorname{Vol}(S^{d-1})}{4(2\pi)^d} \int \delta\left(x(k^2)\right) \left(k^2\right)^{\frac{d-2}{2}} d(k^2) \tag{A.4c}$$

$$= \frac{\pi \operatorname{Vol}(S^{d-1})}{2(2\pi)^d} \left(\frac{|\omega|}{\nu}\right)^{d-1}, \tag{A.4d}$$

where we have changed coordinates to

$$2x^2 = \frac{\left(\omega^2 + \nu^2 \Delta_k\right)^2}{\omega^2 - \nu^2 \Delta_k} \approx \frac{\left(\omega^2 - \nu^2 k^2\right)^2}{\omega^2 + \nu^2 k^2}. \tag{A.4e}$$

Albeit being an expansion in k, the approximation in (A.4e) is correct to leading order[2] in ω due to the δ factor in (A.4c), which localises the integral at $k^2 = \omega^2/\nu^2$.

Comparing (A.3) with (A.4d) we find

$$\Omega = 2\pi \left(\frac{d}{\nu \operatorname{Vol}(S^{d-1})}\right)^{\frac{1}{d}} = \begin{cases} 2\sqrt{\pi} \left(\frac{d}{2\nu} \left(\frac{d}{2}\right)!\right)^{\frac{1}{d}} & d \text{ even} \\ \frac{1}{2} \pi^{\frac{d+1}{2d}} \left(\frac{d!}{\nu \left(\frac{d-1}{2}\right)!}\right)^{\frac{1}{d}} & d \text{ odd}\,. \end{cases} \tag{A.5}$$

Inserting this cutoff into (A.1) completes the Debye approximation.

A.1.1 Integrals over the deterministic spectrum

The integrals encountered above are of the form

$$\int \frac{a + bf(k)}{c + df(k)} g(k) dk = \frac{b}{d} + \frac{ad - bc}{d^2} \int \frac{g(k) dk}{c/d + f(k)}\,. \tag{A.6}$$

The integral over the exact spectrum of the Laplacian in one dimension is

$$\int_0^{2\pi} \frac{dk}{2\pi} \frac{1}{a + \cos(k)} = \frac{1}{\sqrt{a^2 - 1}}\,, \tag{A.7}$$

where the branch of the square root has to be chosen such that $|a \pm \sqrt{a^2 - 1}| > 1$ (see Appendix A.1.2).

[2] Notice that $\operatorname{Vol}(S^0) = 2$.

The integrals over the spectrum in Debye approximation in higher dimensions are given by

$$\frac{2\Omega}{(-a)^n}\int_0^\Omega \frac{k^{2n}dk}{a+k^2} = \sqrt{x}\log\left(\frac{1-\sqrt{x}}{1+\sqrt{x}}\right) + \sum_{k=1}^{n}\frac{2x^k}{2k-1}\,, \tag{A.8}$$

for $d = 2n+1$ odd, or

$$\frac{2}{(-a)^n}\int_0^\Omega \frac{k^{2n+1}dk}{a+k^2} = \log(1-x) + \sum_{k=1}^{n}\frac{x^k}{k}\,, \tag{A.9}$$

for $d = 2n+2$ even. In both cases we used the abbreviation $x := -\Omega^2/a$. Notice that in both cases the arising power series exactly cancels the leading order terms for $x \to 0$, i.e. $a \to \infty$, hence in this limit the leading order term in any dimension is $\Omega^d/(ad)$. In the opposite limit, $a \to 0$, the leading order term is the constant one, namely $\Omega^{d-2}/(d-2)$, if $d \geq 2$. In one or two dimensions, the leading order term is the logarithmic one.

Both series can be extracted from the generating function

$$2i\int_0^\Omega \frac{e^{iyk}dk}{1+k^2} = e^{-y}(\mathcal{E}(y(i\Omega+1)) - \mathcal{E}(y)) - e^{y}(\mathcal{E}(y(i\Omega-1)) - \mathcal{E}(-y)) \tag{A.10}$$

where

$$\mathcal{E}(x) = -\int_{-x}^{\infty}\frac{e^{-t}}{t}dt = \gamma + \log(x) + \sum_{n=1}^{\infty}\frac{x^n}{n!n} \tag{A.11}$$

is the exponential integral.

A.1.2 Some complex analysis

A particular integral needed several times in this thesis is

$$\int_0^{2\pi}\frac{e^{ikx}}{a-cos(k)}\frac{dk}{2\pi}\,, \tag{A.12}$$

for some $x \in \mathbb{N}$ and $a \in \mathbb{C}\setminus[-1,1]$. Since $\cos(z) = \cos(z+2\pi)$ for all $z \in \mathbb{C}$, we can shift the contour in the $i\mathbb{R}$ direction using Cauchy's (or Stokes') theorem and a rectangular closed path in which the vertical contributions cancel, see FigureA.1.

Picking up the additional contribution from the single first order pole in the upper half plain, the contour can then be moved to $+i\infty + [0, 2\pi]$. The cosh contribution from the denominator renders the integrand to be constantly zero on this contour, even if $x = 0$, hence we find the above integral to be given by the residue alone, i.e.

$$\int_0^{2\pi} \frac{e^{ikx}}{a - cos(k)} \frac{dk}{2\pi} = \pm \frac{e^{\pm ix \arccos(a)}}{i\sqrt{1-a^2}} = \frac{\left(a \pm \sqrt{a^2-1}\right)^{-x}}{\pm\sqrt{a^2-1}}\,, \tag{A.13a}$$

where we used that $\arccos(a) = i \ln(a \pm \sqrt{a^2-1}) = \pm i \ln(a + i\sqrt{1-a^2})$. The correct sign is determined by the pole lying in the upper half plain,[3]

$$\Im \arccos(a) > 0 \Leftrightarrow \left|a \pm \sqrt{a^2-1}\right| > 1\,, \tag{A.13b}$$

where $a \notin [-1, 1]$ guarantees that exactly one of the two branches of the square root fulfils Equation (A.13b).

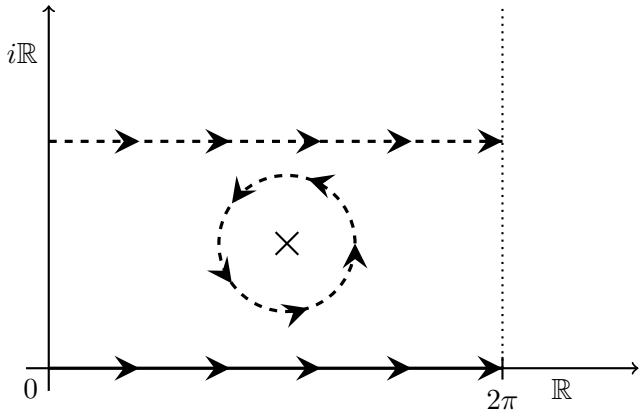

Figure A.1: The contour of the integral $\int_0^{2\pi} f(k)dk$ over a meromorphic periodic function, $f(z) = f(z + 2\pi)$, with a single pole at the marked position may be shifted. Integration over the original black contour yields the same result as integration over the dashed contour, picking up the residue.

A.2 Super Laplace method

Lemma A.1. *Let $S : \mathbb{R}^{m|2n} \to \mathbb{R}^{1|1}$ be an even smooth super function with positive numerical part S_0 and a unique singular point x_S of the numerical part, which is*

[3]For $x = 0$ we may choose to move the contour towards $-i\infty$, which means choosing the other pole, but the additional sign is then compensated by the pole being encircled clockwise.

to be non degenerate, i.e. $\partial_{x_i} S_0(x_S) = 0$ *and* $\operatorname{Det}\left(\partial_{x_i}\partial_{x_j} S_0\right)(x_S) \neq 0$. *Let further* $\operatorname{Pf}\left(\partial_{\xi_i}\partial_{\xi_j} S\right)(x_S) \neq 0$ *and let* $f : \mathbb{R}^{m|2n} \to \mathbb{R}^{1|1}$ *be a smooth super function with numerical part* f_0 *non vanishing at* x_S. *Then we have the asymptotic behaviour*

$$\frac{1}{N^n} \int\limits_{\mathbb{R}^{m|2n}} f(x,\xi) e^{-NS(x,\xi)} D(x,\xi) = (-2)^n \frac{f_0(x_S) e^{-NS_0(x_S)}}{\sqrt{\operatorname{SDet}(S'')_0(x_S)}} \left(1 + O(\frac{1}{\sqrt{N}})\right) \tag{A.14}$$

where

$$\sqrt{\operatorname{SDet}(S'')_0(x_S)} = \frac{\sqrt{\left|\operatorname{Det}\left(\partial_{x_i}\partial_{x_j} S_0\right)(x_S)\right|}}{\operatorname{Pf}\left(\partial_{\xi_i}\partial_{\xi_j} S\right)_0(x_S)}$$

Proof. We compute

$$\int\limits_{\mathbb{R}^{m|2n}} f(x,\xi) e^{-NS(x,\xi)} D(x,\xi) \tag{A.15a}$$

$$= \int\limits_{\mathbb{R}^m} D^m x e^{-NS_0(x)} \partial_\xi^{2n} \left(\sum_I f_I(x)\xi^I\right) \left(\sum_{k=0}^{n} \frac{(-N)^k}{k!} \left(\sum_{I\neq 0} S_I(x)\xi^I\right)^k\right) \tag{A.15b}$$

$$= \left(1 + O\left(\frac{1}{\sqrt{N}}\right)\right) \frac{e^{-NS_0(x)}}{\sqrt{\left|\operatorname{Det}(\partial_{x_i}\partial_{x_j} S_0)(x_S)\right|}} f_0(x_S) \frac{(-N)^n}{n!} \tag{A.15c}$$

$$\times \sum_{\sigma\in\Sigma_{2n}} \operatorname{sign}(\sigma) \prod_{i=1}^{n} S_{\sigma(2i-1)\sigma(2i)}(x_S) \tag{A.15d}$$

$$= (-2)^n N^n \frac{f_0(x_S) e^{-NS_0(x_S)}}{\sqrt{\operatorname{SDet}(S'')_0(x_S)}} \left(1 + O(\frac{1}{\sqrt{N}})\right) \tag{A.15e}$$

where we used the ordinary Laplace method in Equation (A.15d), ignoring lower order contributions in N. Note that the appearing sums are finite, hence interchanging them with the integration is of no concern. The absolute value is due to the fact that one has to deform the contour such as to run through the saddle-point in the direction of steepest descent. Further we used the formula for the Pfaffian

$$\operatorname{Pf}(X) = \frac{1}{2^n\, n!} \sum_{\sigma\in\Sigma_{2n}} \operatorname{sign}(\sigma) \prod_{i=1}^{n} X_{\sigma(2i-1)\sigma(2i)}(x_S) = \sqrt{\operatorname{Det}(X)}$$

□

Corollary A.2. *From the above proof we see that we can use the generalisations of Lemma A.1 for multiple saddle points or saddle point manifolds known from the ordinary Laplace method, provided* $\operatorname{Pf}\left(\partial_{\xi_i}\partial_{\xi_j} S\right)(x_S) \neq 0$ *and* $f_0(x_S) \neq 0$ *for all saddle points. If one of the two vanishes, lower order contributions will become dominant.*

Bibliography

[ABDF11] G. Akemann, J. Baik, and P. Di Francesco, editors. The Oxford Handbook of Random Matrix Theory. *Oxford Handbooks in Mathematics*. Oxford University Press, 2011.

[AHV72] P. W. Anderson, B. I. Halperin, and C. M. Varma. Anomalous low-temperature thermal properties of glasses and spin glasses. *Philosophical Magazine*, 25(1):1, 1972.

[AM76] N. W. Ashcroft and D. N. Mermin. Solid state physics. Thomson Learning, 1976.

[CKR+10] A. Chaudhuri, A. Kundu, D. Roy, A. Dhar, J. L. Lebowitz, and H. Spohn. Heat transport and phonon localization in mass-disordered harmonic crystals. *Physical Review B*, 81(6):064301, 2010.

[FA86] J. J. Freeman and A. C. Anderson. Thermal conductivity of amorphous solids. *Physical Review B*, 34(8):5684, 1986.

[HRK+12] M. Hassaine, M. A. Ramos, A. I. Krivchikov, I. V. Sharapova, O. A. Korolyuk, and R. J. Jiménez-Riobóo. Low-temperature thermal and elastoacoustic properties of butanol glasses: Study of position isomerism effects around the boson peak. *Physical Review B*, 85(10):104206, 2012.

[HW70] J. Harrington and C. Walker. Phonon Scattering by Point Defects in CaF_2, SrF_2, and BaF_2. *Physical Review B*, 1(2):882, 1970.

[JM73] W. Jones and N. H. March. Theoretical solid state physics, volume 1 and 2. Wiley-Interscience New York, 1973.

[JSS83] S. John, H. Sompolinsky, and M. Stephen. Localization in a disordered elastic medium near two dimensions. *Physical Review B*, 27(9):5592, 1983.

[LSZ06] T. Lück, H. J. Sommers, and M. R. Zirnbauer. Energy correlations for a random matrix model of disordered bosons. *Journal of Mathematical Physics*, 47:103304, 2006. arXiv:cond-mat/0607243.

[LSZ07] P. Littelmann, H. -J Sommers, and M. R Zirnbauer. Superbosonization of invariant random matrix ensembles. Commun. Math. Phys. 283 (2008) 343. arXiv:0707.2929.

[Lüc09] T. Lück. *Random Matrix Models for Disordered Bosons.* PhD thesis, Mathematisch-Naturwissenschaftliche Fakultät der Universität zu Köln, 2009.

[LV13] A. J. Leggett and D. C. Vural. "Tunneling two-level systems" model of the low-temperature properties of glasses: are "smoking-gun" tests possible? *The journal of physical chemistry. B*, 117(42):12966–71, 2013. arXiv:1310.3387.

[LW03] V. Lubchenko and P. G. Wolynes. The origin of the boson peak and thermal conductivity plateau in low-temperature glasses. *Proceedings of the National Academy of Sciences of the United States of America*, 100(4):1515, 2003. arXiv:cond-mat/0206194.

[Par94] D. Parshin. Interactions of soft atomic potentials and universality of low-temperature properties of glasses. *Physical Review B*, 49(14):9400, 1994.

[Phi72] W. A. Phillips. Tunneling states in amorphous solids. *Journal of Low Temperature Physics*, 7(3-4):351, 1972.

[Phi87] W. A. Phillips. Two-level states in glasses. *Reports on Progress in Physics*, 50(12):1657, 1987.

[PLT02] R. O. Pohl, X. Liu, and E. Thompson. Low-temperature thermal conductivity and acoustic attenuation in amorphous solids. *Reviews of Modern Physics*, 74(4):991, 2002.

[Sch14] S. E. Schmittner. An adaptive high precision solver for complex non-linear equations. github:Echsecutor/rootSolver, 2014.

[Sov67] P. Soven. Coherent-Potential Model of Substitutional Disordered Alloys. *Physical Review*, 156(3):809, 1967.

[SS09] M. Schechter and P. C. E. Stamp. Low temperature universality in disordered solids. Physical Review B 88, 174202, 2013

[Ste73] R. B. Stephens. Low-temperature specific heat and thermal conductivity of noncrystalline dielectric solids. *Physical Review B*, 8:2896, 1973.

[Ste76] R. B. Stephens. Intrinsic low-temperature thermal properties of glasses. *Physical Review B*, 13(2):852, 1976.

[SW80] L. Schäfer and F. Wegner. Disordered system with n orbitals per site: Lagrange formulation, hyperbolic symmetry, and goldstone modes. *Zeitschrift für Physik B Condensed Matter*, 38(2):113, 1980.

[SZ10] S. E. Schmittner and M. R. Zirnbauer. Coherent potential approximation for disordered bosons. *arXiv:1012.5283*, 2010.

[tH74] G. 't Hooft. A planar diagram theory for strong interactions. *Nuclear Physics B*, 72(3):461, 1974.

[TRV02] C. Talón, M. Ramos, and S. Vieira. Low-temperature specific heat of amorphous, orientational glass, and crystal phases of ethanol. *Physical Review B*, 66(1):012201, 2002.

[Tur04] M. Turlakov. Universal Sound Absorption in Low-Temperature Amorphous Solids. *Physical Review Letters*, 93(3), 2004. arXiv:cond-mat/0309097.

[Van53] L. Van Hove. The Occurrence of Singularities in the Elastic Frequency Distribution of a Crystal. *Physical Review*, 89(6):1189, 1953.

[Weg79] F. Wegner. Disordered system with n orbitals per site: $n = \infty$ limit. *Physical Review B*, 19(2):783, 1979.

[YM73] F. Yonezawa and K. Morigaki. Coherent Potential Approximation. *Progress of Theoretical Physics Supplement*, 53:1, 1973.

[Zir98] M. R. Zirnbauer. Riemannian symmetric superspaces and their origin in random matrix theory. *Journal of Mathematics and Physics* 37:4986, 1998. arXiv:math-ph/9808012

[ZP71] R. C. Zeller and R. O. Pohl. Thermal Conductivity and Specific Heat of Noncrystalline Solids. *Physical Review B*, 4(6):2029, 1971.

[Zuk94] J. A. Zuk. Introduction to the Supersymmetry Method for the Gaussian Random-Matrix Ensembles. arXiv:cond-mat/9412060, 1994.

Index

Danksagung

Ich möchte mich ganz herzlich bei allen bedanken die mir in den letzten Jahren freundschaftlich, mit Rat und Tat, konkret, finanziell oder allgemein moralisch zur Seite standen. Studium und Forschung haben mir viel Freude bereitet, nicht nur aufgrund der interessanten Inhalte, sondern auch aufgrund der sehr angenehmen Rahmenbedingungen.

Konkret möchte ich mich zuerst bei meiner Frau Catrin bedanken. Sie stand mir während Studium und Promotion immer zur Seite, hat mir in anstrengenden Phasen den Rücken gestärkt und mich zusammen mit unseren beiden Töchtern Ronja und Merle immer wieder aufgemuntert, wenn erfreuliche Fortschritte in der Forschung auf sich warten ließen. Ihre unbedingte Unterstützung war gerade in der Endphase der Promotion essentiell.

Besonderer Dank gilt natürlich meinem Doktorvater, Martin Zirnbauer, der mich seit Jahren in Studium und Forschung unterstützt, der während der Promotion immer ein offenes Ohr für mich hatte und der viele der wesentlichen Ideen zu dieser Arbeit beigetragen hat. Ich hoffe, dass wir unsere gemeinsame Forschung in Zukunft mit ähnlicher Intensität fortführen können wie in den letzten Wochen der Promotion.

Ganz herzlicher Dank gilt auch der Deutsche Telekom Stiftung die meine Forschungsarbeit in den letzten Jahren maßgeblich finanziert hat und insbesondere meinem Mentor, Klaus Kinkel. Die Treffen mit ihm sowie den Mitstipendiaten stellen eine Bereicherung weit jenseits der finanziellen Aspekte dar.

Für die finanzielle Förderung während meines Diplomstudiums und der Promotion, sowie die deutliche Verbesserung der Studienbedingungen möchte ich mich bei der Bonn Cologne Graduate School of Physics and Astronomy bedanken.

Ich danke Alexander Alldridge für die sehr anregende und fruchtbare Zusammenarbeit zur Darstellungstheorie von Lie Superalgebren und für Verbesserungsvorschläge zu diesem Manuskript. Weiterhin danke ich Artur Swiech für die Zusammenarbeit bei den Monte Carlo Simulationen und viele hilfreiche Gespräche, sowie für die angenehme Arbeitsatmosphäre in unserem Büro und für Anmerkungen zur Verbesserung einer frühen Version dieser Arbeit.

Für letzteres möchte ich mich auch bei Karin Everschor-Sitte und Matthias Sitte, Tobias Lück, Wolfgang Palzer, Dominik Ostermayer und Sebastian Sahler herzlich bedanken.

Vielen Dank!

Erklärung

Ich versichere, dass ich die von mir vorgelegte Dissertation selbständig angefertigt, die benutzten Quellen und Hilfsmittel vollständig angegeben und die Stellen der Arbeit – einschließlich Tabellen, Karten und Abbildungen –, die anderen Werken im Wortlaut oder dem Sinn nach entnommen sind, in jedem Einzelfall als Entlehnung kenntlich gemacht habe; dass diese Dissertation noch keiner anderen Fakultät oder Universität zur Prüfung vorgelegen hat; dass sie – abgesehen von unten angegebenen Teilpublikationen – noch nicht veröffentlicht worden ist, sowie, dass ich eine solche Veröffentlichung vor Abschluss des Promotionsverfahrens nicht vornehmen werde. Die Bestimmungen der Promotionsordnung sind mir bekannt. Die von mir vorgelegte Dissertation ist von Prof. Dr. Martin R. Zirnbauer betreut worden.

Köln, 23. Januar 2015 Sebastian Schmittner

Teilpublikationen

[SZ10] S. E. Schmittner and M. R. Zirnbauer. Coherent potential approximation for disordered bosons. *arXiv:1012.5283*, December 2010.

[SSZ15] S. E. Schmittner, A. Swiech, and M. R. Zirnbauer. Coherent mass and springs approximation for disordered phonons. *in preparation*, 2015.